Université de Montréal

Heterogeneous Structural Organization of Polystyrene Fibers Prepared by Electrospinning

présenté par

Anna Gittsegrad

Département de chimie

Faculté des arts et des sciences

Mémoire présenté à la Faculté des études supérieures et postdoctorales en vue de l'obtention du grade de maître ès sciences (M.Sc.) en chimie

Janvier 2018

RÉSUMÉ

L'électrofilage est une technique utilisée pour la préparation de fibres avec des diamètres allant de quelques micromètres jusqu'à des centaines de nanomètres à partir d'une solution polymère enchevêtrée dans un solvant volatil. Les fibres électrofilées sont formées sous l'influence de grandes forces d'étirement, qui contribuent à une évaporation extrêmement rapide du solvant, une orientation moléculaire élevée et une structure moléculaire hors d'équilibre. Il a été démontré que ces matériaux présentent des propriétés distinctes par rapport aux matériaux massiques. Dans ce travail, le comportement thermique des fibres polystyrène (PS) électrofilées à partir de différents solvants a été étudié à l'aide de calorimétrie différentielle à balayage (DSC) modulée en température. Une analyse détaillée du système PS/$CHCl_3$ ainsi que l'utilisation de trois masses moléculaires et de différentes concentrations a révélé la présence de deux phases dans les fibres de PS avec une phase secondaire moins dense que la phase normale. Ces résultats ont été corrélés au modèle précédemment proposé de l'organisation de la chaîne « cœur-couronne » avec la couronne mince partiellement désenchevêtrée et un cœur enchevêtré en masse. Des mesures supplémentaires de spectroscopie par une technique qui combine la spectroscopie infrarouge avec le microscope à force atomique (AFM-IR) à l'échelle de fibre unique ont démontré que les bandes IR associées à un désenchevêtrement partiel dans des chaînes sont situées essentiellement au bord de la fibre. Différents solvants, le tétrahydrofurane (THF), la méthyléthylcétone (MEK) et le diméthylformamide (DMF) ayant des points d'ébullition différents ont été utilisés pour électrofiler les fibres de PS et ont généré un comportement à deux phases pour toutes les masses moléculaires et concentrations. La morphologie des fibres PS électrofilées provenant de différents solvants a également été étudiée. De plus, le recuit thermique des fibres de PS dans de multiples conditions a été effectué qui a permis de mieux comprendre le comportement thermique inhabituel et une organisation en deux phases des fibres PS. Enfin, ces résultats ont été corrélés avec le modèle « cœur-couronne » pour l'organisation des chaînes au sein des fibres et les hypothèses de ce modèle ont été révisées.

Mots-clés: Électrofilage, fibres polymères, polystyrène, morphologie, comportement termique.

ABSTRACT

Electrospinning is a common technique used for preparing fibers with diameters ranging from a few micrometers down to hundreds of nanometers from an entangled polymeric solution in a volatile solvent. Electrospun fibers are formed under the influence of large stretching forces, therefore contributing to extremely fast solvent evaporation, high molecular orientation and out-of-equilibrium structure. These materials have been shown to exhibit distinct properties when compared to bulk materials. In this work, the thermal behavior of polystyrene (PS) fibers electrospun from different solvents as well as using three molecular weights and different concentrations was studied using temperature modulated differential scanning calorimetry (DSC). A detailed analysis of the PS/$CHCl_3$ system revealed the presence of two phases within PS fibers with a secondary phase being less dense than the normal phase. The observations were correlated to the previously proposed model of core-shell chain organization with a partially disentangled thin shell and a bulk entangled core. Additional spectroscopic measurements by atomic force microscopy infrared spectroscopy (AFM-IR) at the single fiber scale demonstrated that IR bands associated with partial disentanglement in chains are located mainly at the edge of the fiber. Different solvents, tetrahydrofuran (THF), methyl ethyl ketone (MEK) and dimethylformamide (DMF) having different boiling points were used to electrospin PS fibers that featured two-phase behavior at all molecular weights and concentrations. The morphology of PS fibers electrospun from different solvents was also studied. Moreover, the thermal annealing of PS fibers under multiple conditions was performed that shed light on the unusual thermal behavior and a better understanding of the two-phase organization of the PS fibers. Finally, these results were correlated with the core-shell model for the chain organization within fibers and the hypotheses of this model were revised.

Keywords: Electrospinning, polymer fibers, polystyrene, morphology, thermal behavior, annealing.

TABLE OF CONTENTS

LIST OF FIGURES

LIST OF TABLES

LIST OF ABBREVIATIONS

AFM	atomic force microscopy
ATR-IR	attenuated total reflection infrared spectroscopy
c	concentration
c^*	limiting concentration
c_e	critical entanglement concentration
DMF	dimethylformamide
DSC	differential scanning calorimetry
EID	excess of isotropic intensity
M_c	critical molecular weight
MEK	methyl ethyl ketone
Mw	molecular weight
PCL	poly(ε-caprolactone)
PDI	polydispersity index
PGS	poly(glycerol sebacate)
PHBHx	poly[(R)-3-hydroxybutyrate-co-(R)-3-hydroxyhexanoate]
PPO	poly(propylene oxide)
PS	polystyrene
PVA	poly(vinyl alcohol)
PVC	poly(vinyl chloride)
PVDF	poly(vinylidenefluoride)
PVDF-PHFP	poly(vinylidene fluoride-hexafluoropropylene)
PVME	poly(vinyl methyl ether)
SEM	scanning electron microscopy
T_c	crystallization temperature
T_g	glass transition temperature
THF	tetrahydrofuran
T_m	melting temperature

TMDSC	temperature modulated differential scanning calorimetry
V_c	critical potential
ΔC_p	specific heat capacity
ΔH	enthalpy

ACKNOWLEDGEMENTS

First and foremost, I would like to thank my thesis advisors, Prof. Christian Pellerin and Prof. C. Geraldine Bazuin. I would like to express my gratitude to them for their patience, motivation, enthusiasm and immense knowledge, and for allowing this thesis to be my own work, but steering me in the right the direction whenever they thought I needed it. I am grateful for all of the opportunities I was given to conduct my research on a variety of projects.

Besides my advisors, I would like to thank Prof. Robert E. Prud'homme for his support, guidance and collaborative work.

A very special thanks goes out to Marie Richard-Lacroix and Elise Siurdyban for their substantial contribution to our collaborative work, ideas and energy that led our joint project to good results.

I would like to specifically thank Sylvain Essiembre for his time, training and help with DSC instruments, providing me with necessary information to succeed in my project and deepen my instrumental knowledge.

I am grateful to all current and previous members of Pellerin, Bazuin and Prud'homme research groups that have contributed immensely to my personal and professional time at Université de Montréal.

Chapter 1

INTRODUCTION

1.1 Electrospinning of polymer fibers

Synthetic and natural polymers are being increasingly employed as structural materials and active functional systems. This technological development has often aimed to miniaturize commonly used systems and components to the micro- and nano-scale and to generate polymeric materials with superior performance that are improvements over the existing ones. At the same time, the development of characterization methods with enhanced spatial resolution allows studying complex systems, such as membranes, ultrathin polymer films and carbon nanotubes with unprecedented detail. Among these materials are polymeric fibers prepared by the electrospinning method. While the process of fiber preparation by electrospinning is relatively simple, the study of the out-of-equilibrium molecular organization within these fibers, which results in unique properties, is an active area of research.

Generally speaking, spinning of polymer fibers involves the extrusion of a polymer melt, solution or gel through a spinneret to generate continuous filaments.[1] The oldest process is *wet spinning*, where a dissolved polymer is pushed through a spinneret submerged in a chemical bath filled with non-solvent. When extruded, fibers precipitate from solution and solidify. A variation of wet spinning is *dry jet-wet spinning*. In this technique, the polymer solution is extruded into an air gap under heat and pressure before entering the coagulation bath. It is often used to produce high performance fibers possessing a liquid crystalline structure. Another solution-based fiber-forming method is *dry spinning,* in which fibers solidify through solvent evaporation with hot air or inert gas. It is simpler, since the drying and solvent recovery steps are eliminated. In *melt spinning*, thermoplastic polymer granules are melted and extruded through the spin head.

A thin stream of liquid then drops onto a spinning wheel and is cooled, resulting in rapid solidification. This process generates fibers with a variety of cross-sectional shapes.[1]

Electrospinning is another method that allows preparing ultrathin polymer fibers that has become popular since the mid-1990s. It is based on the uniaxial stretching and fast solvent evaporation of the jet derived from a semi-dilute polymer solution.[2] Unlike other spinning processes, it employs electrostatic repulsion between surface charges and attraction to an oppositely charged collector under a large electric field instead of mechanical forces in order to generate filaments, leading to a reduction in diameter of the jet and the resulting fibers. In fact, fibers with much smaller diameter, down to micrometer range or even tens of nanometers, can be readily obtained.[3] High-volume production of fibers with relatively long length and with either solid or hollow/porous interiors can be achieved because electrospinning represents a continuous process in which the elongation is attained through the application of an external electric field.

Electrospinning is in fact an old technique and its development has originated in the 18th century. The first studies were performed in 1745 by Bose, who was able to produce aerosol by applying high electric potentials to drops of fluids.[4] In 1882, Lord Rayleigh has quantified the amount of charges that are necessary to overcome the surface tension of a drop.[5] Later, in 1902, Cooley and Morton were issued the first patent for devices that allowed spraying a liquid by applying electrical fields.[6-7] The term electrospinning or "electrostatic spinning" was commonly used only at the end of 20th century. However, its origins lay in a crucial patent published by Formhals in 1934, describing for the first time the setup for the electrospinning of polymeric filaments.[8] In the 1960s, Taylor has demonstrated that under an electric field, a conical interface between two fluids can exist in equilibrium, with a semi-vertical angle of around 49.3^{o}.[9] He then proposed a theory of electrically driven jets establishing that the fluid at the end of a needle, when subjected to a sufficiently large electric field, gets ejected from vertices of the cone in fine jets.[10] In the literature, it is now commonly referred to as the "Taylor cone".

It is in 1990s that this technique became of high interest through the work of the Reneker group at University of Akron, who popularized the term "electrospinning" instead of "electrostatic spinning".[11] Their research was not only oriented towards the study of fundamental parameters but also focused on several potential applications. In particular, they have investigated the effects of experimental parameters, such as solution concentration and applied voltage, on the diameter of the resulting fibers. Most importantly, the group demonstrated the spiral trajectory of the jet with stretching forces acting upon it due to electrostatic forces. Moreover, they have studied the stability of the jet in order to be able to produce fibers under controlled conditions for a broad range of natural and synthetic polymers.[12] A wide range of polymers can be electrospun and allow tailoring a number of properties, for instance strength, surface functionality, porosity, etc.[13]

In general, electrospinning is based on the same principle as electrospraying, since in both methods the liquid jet is formed through the application of a high voltage. The main difference lies in the chain entanglement density of the polymer solution, which is intrinsically related to the viscosity of the solution.[14] In electrospray, which is a process of liquid atomization by electrical forces, small, self-dispersed droplets are generated from a solution of low (or absent) chain entanglement density due to Rayleigh break-up of the jet. On the other hand, fibers are obtained by electrospinning for a solution of higher entanglement density as a result of electrostatic repulsions between the surface charges and the evaporation of the solvent, leading to a continuous stretching and thinning of the electrified jet. Thus, polymer chain entanglements essentially stabilize the jet.[15] Even though electrospinning and electrospraying inherently produce different materials, they are considered "sister" technologies.[16] Moreover, a combined material can be obtained, consisting of fibers containing droplets, or beaded fibers. A specific concentration, or more precisely a minimum amount of entanglements, is required to produce purely fibrous filaments. In fact, completely stable fiber formation was reported to occur above 2.5 entanglements per chain.[17] A number of parameters have a direct influence on fiber production, for instance, the concentration, molecular weight of the

polymer, and the solvent used, which all influence chain entanglement. These parameters will be closely examined in this thesis. Furthermore, electrospinning is not only used to produce free-standing fibrous materials but also as part of hybrid products. It is possible to produce fibers from polymer blend solutions in order to tune the properties and morphology of the resulting material.[18] Fibers can also be combined with other materials, resulting in functionalized carriers for organic or inorganic molecules, metals and composite materials.[19]

This work focuses on the electrospinning of polystyrene (PS) fibers with the objective of investigating the heterogeneity in the radial density distribution, more explicitly the core-shell microstructural organization within the fibers, as a function of concentration and molecular weight of the polymer. The effect of the boiling point of the solvent on the electrospun PS fibers is also studied.

1.2 Theoretical basis and experimental aspects of electrospinning

Electrospinning is a highly versatile and easily controlled technique for producing continuous fibers from polymer solutions with small diameters and a large surface area. The approach is essentially based on electrostatic repulsion that is much stronger than weak surface tension forces present in the charged polymer solution. It should be noted that electrospinning can be conducted at room temperature under atmospheric conditions. A typical laboratory setup used for electrospinning is depicted in figure 1.1. The three main components are the high voltage power supply, a spinneret and a grounded or oppositely charged collector. A syringe pump is often used to ensure a constant solution feed to the Taylor cone in order to stabilize the process. In effect, the process consists of applying high voltage in the range of s few tens of kV on the polymer solution at the end of the capillary tube, held by its surface tension. When the electrical forces are much stronger than the surface tension, a charged solution is ejected from the tip of the Taylor cone in form of the jet. It is then accelerated towards the collector first

in a straight manner, which then transforms into a rapid whipping trajectory leading to thinning and solidification of the jet due to fast evaporation of the solvent and elongation forces.[20] The processes observed in electrospinning can be addressed by three main theories: fluid charging theory, Taylor cone theory and instability theory and jet thinning.

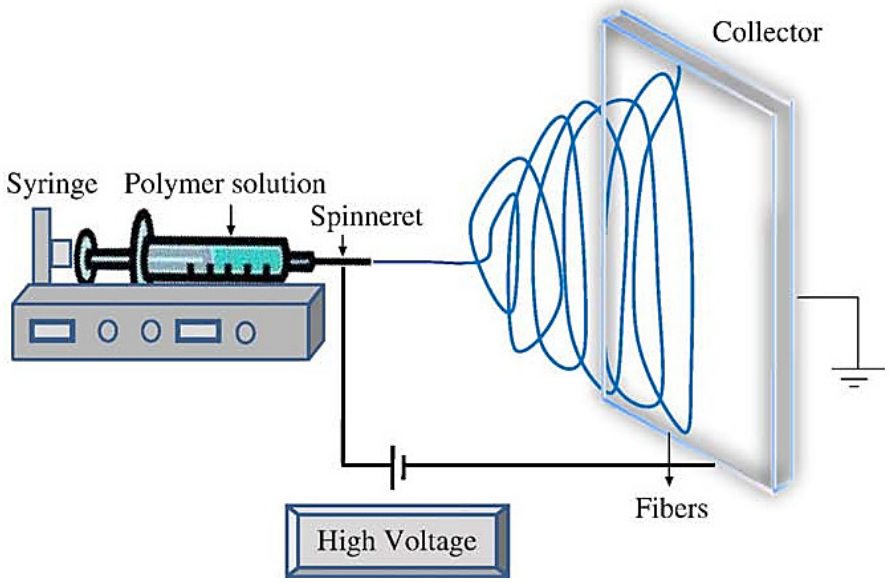

Figure 1.1 Typical setup for an electrospinning experiment. Reproduced with permission from ref 20 © Elsevier Inc. 2010.

Fluid charging theory

For polymer solutions, which are generally nonconductive fluids, the charges on the fluid within the syringe are generated through high electric field polarization between the positive and negative potentials. The process is therefore referred to as induction charging.[21] More precisely, a positive potential applied in electrospinning causes the accumulation of positive charges in the solution at the tip of the needle. At the same time, a negative potential applied on the collector attracts a positively charged solution creating a high electric field polarization. Overall, the charged solution in the drop is under the influence of two electrostatic forces, namely the mutual repulsion of positive charges within the solution and the Coulombic attraction generated by the electrical field and, when in equilibrium, adopts the form of the Taylor cone.[22]

Taylor cone theory

Normally, the surface tension dictates the shape of a volume of fluid. However, the surface of the droplet deforms under the high electric field from a spherical shape into the conical shape due to repulsion between charges at the free surface that work against the fluid elasticity and its surface tension. It results in a sharp point at the tip of the cone, where the concentration of electric stress results in the ejection of the jet due to the increased electrical attraction at the tip. This form of the drop is described by the Taylor cone theory established by Taylor in 1964.[23] As the equilibrium between electric forces and surface tension of the small volume of charged liquid exposed to electric field is reached, a stable shape is acquired. Therefore, Taylor cone characterizes the conical shape of a liquid body with a half angle of 49.3°[24] (figure 1.2).

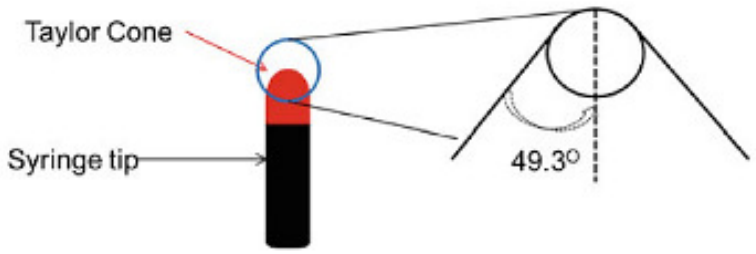

Figure 1.2 Schematic representation of the Taylor cone. Reproduced with permission from ref 23 © Springer 2013.

Taylor has shown that the shape of the cone approaches the theoretical model preceding the jet formation in electrospraying and electrospinning processes, which is based on two assumptions: the surface of the cone is an equipotential surface and the cone exists in steady state equilibrium based on:

$$U_c^2 = 4\frac{H^2}{L^2}\left(\ln\frac{2L}{R} - \frac{3}{2}\right)(0.117\pi\gamma R) \qquad (1.1)$$

where U_c is voltage, H is the distance between the tip of the needle and the collector, L is the length of needle, R is diameter of the tip of the needle and γ is the surface tension of the solution.[24]

The Taylor cone theory has been modified by Yarin and Reneker in 2001 based on experimental data.[25] They have established that the first assumption of Taylor cone theory was not completely correct. It was previously thought that the stable shape of the cone tends towards the sphere as the potential increases and reaches a critical Rayleigh value. Conversely, they have demonstrated, both experimentally and theoretically using hyperboloidal approximation, that with increasing potential and attaining a critical value (V_c) the drop becomes more prolate and hence adopts a critical shape with a half angle of 33.5° rather than 49.3°.

Jet thinning and instability theory

As the Taylor cone forms in the presence of a large electric field, a charged jet is ejected and follows a straight trajectory where the elongation and stretching of the jet along its axis is driven by the repulsive Coulombic forces between the charges, generating a high velocity at the leading end of the straight jet.[22] After a short flight time, typically over the distance of 10 mm, the jet becomes susceptible to a number of instabilities. For instance, the Plateau-Rayleigh instability, where the surface tension enhances small perturbations in a fluid, results in the breaking of the jet into small droplets. It is therefore responsible for the atomization in the electrospraying process, and needs to be avoided in electrospinning.[26-27]

The off axis bending instability takes place because of small perturbations in the straight portion of the jet resulting in bending of the straight segment of the jet into spiraling loops of increasing diameter with each turn. This perturbation results in a loss of perfect symmetry due to self-repulsion of the charged jet resulting in a force perpendicular to the primary axis of the jet. In the early stages, this force is resisted by the viscoelastic nature of the solution. As the bending instability progresses and becomes significant, the perturbation exceeds the damping in the jet.[28] This bending and stretching of the jet is caused by a rapid growth of a non-axisymmetric or whipping instability, which is the most important factor in reduction of diameter of the traveling jet. After several coils, an additional electrical bending instability can force smaller

loops to be formed on the turn of a large coil, which is further transitioned into even smaller coils. This process continues until the elongation ceases due to the solvent having evaporated and the jet having solidified (figure 1.3).[25, 29]

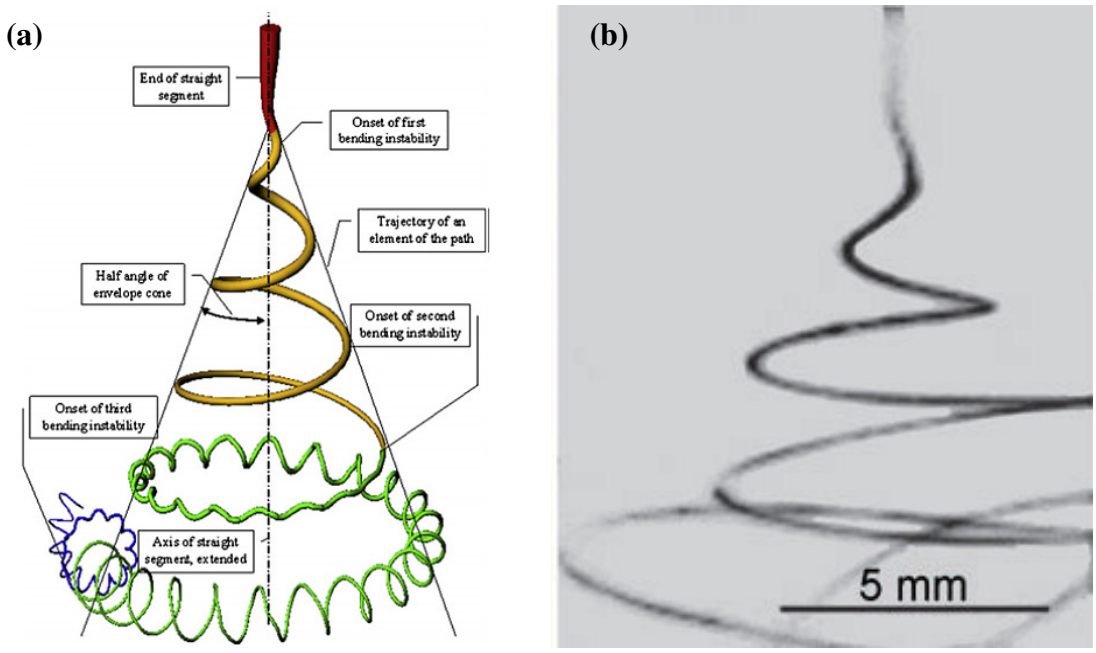

Figure 1.3 (a) Diagram representing the onset and development of bending instabilities and (b) image of the bending instability near the end of the straight part of the jet. Image (a) reproduced with permission from ref 28 © Elsevier Inc. 2010. Image (b) reproduced with permission from ref 29 © AIP Publishing LLC 2001.

In addition to bending instability, other fluid instabilities occur as the liquid jet travels. For instance, they can lead to splitting of the jet into droplets or branching into multiple smaller jets. In essence, jet elongation and rapid solvent evaporation provoke changes in the shape and charge per unit area of the jet. Consequently, the balance between the surface tension and the electrical forces shift, creating instabilities in the jet. Therefore, ejecting smaller jets from the main jet surface allows reducing local charge per unit surface area. Generally, this effect is mostly observed for more viscous or concentrated solutions as well as at electric fields much higher than the minimum field required to produce a single jet.[30-31] Moreover, there exists another type of instability, namely the capillary instability. It is characterized by the collapse of the cylindrical liquid jet into separate droplets due to decrease in excess electrical charge carried by the

jet. However, if the solution viscosity is high enough to prevent complete separation of the jet into droplets, beaded fibers are obtained. In other words, it is the stretching of entangled molecules in the strong elongational flow between the growing droplets that produces beads-on-string structure.[32] Beads or branches are very commonly observed on the coil formed by the bending instability, but rarely on the same segment of the jet.[29]

In order to obtain a continuous liquid jet during electrospinning, it is important to optimize experimental parameters that will in turn influence the resulting fibers, their structure, morphology and properties. For each system, experimental parameters will be unique and must be controlled. These can be divided into two categories, i.e. processing parameters and solution parameters.

Effects of processing parameters on electrospinnability

During electrospinning, various external parameters are exerted on the solution in order to produce the liquid jet and ultimately generate continuous fibers. These are the processing parameters inherent to the electrospinning setup that include the applied voltage, feedrate, type of collector and distance between the tip of the needle and the collector.

Applied voltage

The applied voltage is the most important processing parameter. It initiates the electrospinning process by inducing charges on the solution. Basically, the Coulombic repulsive forces present in the jet stretch the viscoelastic solution and the electric field generated by the potential difference guides the acceleration and elongation of the charged jet towards the collector. In order to generate a sufficient number of charges to overcome the viscoelastic forces and the surface tension of the solution, a critical voltage must be reached. The schematic representation of the effect of applied voltage is depicted in figure 1.4. If the applied voltage is too low, the Taylor cone forms at the tip of the pendant drop.[33] As a result, electrospray will be generated since there are not enough charges to overcome the surface tension instability. With increasing potential,

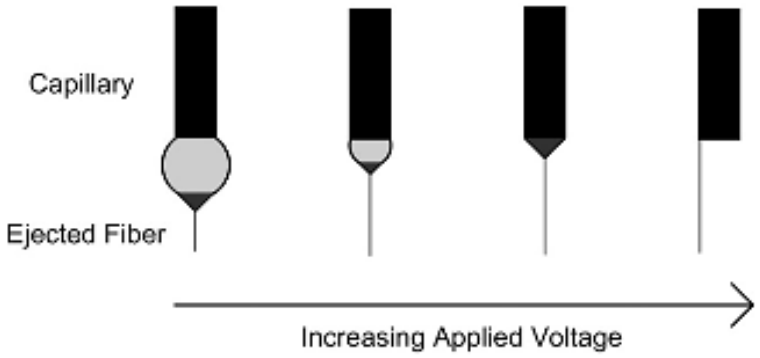

Figure 1.4 Effect of the applied voltage on the formation of the Taylor cone. Reproduced with permission from ref 33 © Elsevier Inc. 2008.

the volume of the drop decreases leading to the formation of the Taylor cone at the tip of the capillary. On the other hand, if the applied voltage is too high, more charges are produced leading to a faster acceleration of the jet. In this case, more solution volume is drawn from the needle, producing a smaller and less stable Taylor cone, which is associated with an increase in beads on the fibers.[33]

The voltage supplied also has a certain influence on the morphology of the fibers. The diameter of the resulting fibers is affected by the applied voltage based on the relationship between three major forces: Coulombic forces, surface tension and viscoelastic forces. The fibers electrospun at low potentials tend to have large diameters with the presence of beads since the Coulombic forces are less important than the surface tension and viscoelastic forces. Moderate applied voltage will generate unbeaded fibers with narrow diameter distribution because of the balance between all three forces. Finally, if a high potential is applied, an increase in fiber diameter is observed since the Coulombic forces are much greater than viscoelastic forces. Under much high potential, the fibers will reach the collector much faster, which in turn reduces the solvent evaporation process and effect on bending instability. Moreover, retraction of the jet can occur, resulting in large but irregular fibers.[34-35]

Feedrate

The feedrate or injection rate determines the amount of the solution that is pushed out of the tip of the needle and therefore available for electrospinning. In order to maintain a stable Taylor cone, a specific and constant feedrate must be selected depending on the applied voltage used. If the injection rate is too slow, electrospinning is much faster than the solution feed and therefore the Taylor cone recedes into the needle. On the other hand, a high feedrate will destabilize the Taylor cone and the solution will leak from the needle.[34] The most conventional method of preparing electrospun fibers is using the needle as the spinneret. However, there are other techniques that have been developed such as needleless or multiple needle electrospinning. In the needleless process, the fibers are electrospun directly from an open liquid surface, leading to the generation of numerous jets simultaneously. In this case, there is no influence of capillary effect and the fibers can be produced on a larger scale. Yet, this process is hard to control with respect to fiber quality and productivity.[36-37] Another way to increase throughput is by using multiple needle electrospinning.[38] It also allows preparing mixed fibers by ejecting different polymer solutions from the needles, where the mixing ratio can be controlled by adjusting the number of needles containing different solution components.[39]

Effect of collector

In electrospinning, the collector is used to recuperate the resulting fibers and to maintain an electric field between the source and the collector. Therefore, it is made of a conducting material, which is grounded or on which an opposite potential is applied, allowing a stable difference in potential to be maintained. A conducting collector allows dissipation of the charges on the fibers and an increase in the attraction of the fibers towards the collector. [34]

There are different types of collectors that can be used in electrospinning. The simplest type of collector is an aluminum foil or metal plate on which the fibers accumulate randomly resulting in a bulk nonwoven sample. Several collectors can be used to produce aligned fibers,.[40] A rotary collector, for instance, can consist of a rotating drum with a principal axis parallel to the ground. It can have a metal ring in the middle to localize the fiber accumulation or consist of a disk where the fibers are accumulated on the whole surface (figure 1.5a). Depending on the linear velocity of the rotation of the drum, it is possible to tailor the alignment of the fibers as well as their molecular orientation.[41] Another way to collect aligned electrospun fibers is by using a two electrodes collector (figure 1.5b). Essentially, it allows uniaxially aligned fibers to be obtained over a large area between the two parallel electrodes through electrostatic interactions. The fibers are therefore stretched across the gap in parallel arrays.[42]

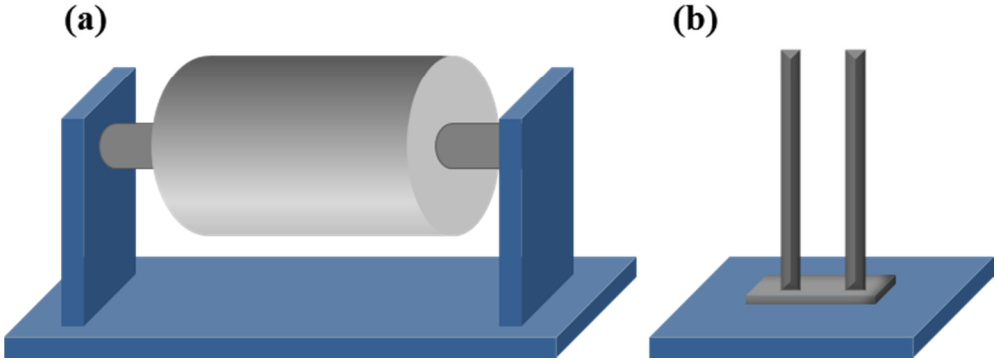

Figure 1.5 Schematic representation of rotating drum collector (a) and a parallel rods collector for electrospinning.

Working distance

The working distance, representative of the distance between the tip of the needle and the collector, also affects the diameter and the morphology of electrospun fibers. Basically, at short working distance, the fibers reach the collector too fast, reducing the time for solvent evaporation and fiber solidification. In contrast, when the distance is too long, the electric field is not strong enough to pull the jet towards the collector.[43]

Overall, in order to obtain continuous fibers, all parameters outlined above must be carefully selected and optimized. Since all of these are interdependent, a balance between the applied voltage, feedrate and the working distance is necessary to generate fibers with a uniform distribution of diameter and without beadlike defects.

Effects of solution parameters on electrospinnability

Processing parameters play an important role in fiber formation and their morphology. However, the most important parameters that will predominantly influence the electrospinnability, morphology, diameter and diameter distribution are the solution parameters. These include the molecular weight of the polymer, the solution concentration, viscosity, conductivity, the nature of the solvent (boiling point, affinity for the polymer, etc.), surface tension, etc.

Concentration and molecular weight

Chain entanglement is one of the most significant parameters that influence the formation of fibers and the resulting structure during the electrospinning process. Generally speaking, chain entanglement in solution represents the physical interlock of polymer chains, which is directly related to chain overlap. The concept of chain entanglement can be characterized as physical cross-linking, where the chains can slide past one another.[44] The number of entanglements per chain depends on the solution concentration and polymer molecular weight, which can be correlated to the zero shear melt viscosity, η_0. In fact, for unentangled solutions and for polymer melts at low molecular weights, η_0 is directly proportional to molecular weight. With increasing M_w, the entanglement of the chains increases and another parameter must be taken into consideration, namely the critical molecular weight, M_c, which represents the minimum molecular weight for which there is one entanglement per chain. It is therefore the onset of entanglement behavior as a function of M_w. Above M_c, the viscosity dependence on M_w changes from $\eta_0 \propto M_w$ to $M_w^{3.4}$.[45]

Furthermore, for a polymer solution to have chain entanglements, a dimensionless product between intrinsic viscosity and concentration, [η]c, must be greater than 1. In dilute solutions there is no chain overlap and therefore [η]c < 1 (figure 1.6a). The intrinsic viscosity can be related to the molecular weight of a linear polymer through the Mark–Houwink–Sakurada equation:

$$[\eta] = KM_w^a \tag{1.2}$$

where M_w is the molecular weight and K and a are constants dependent on the polymer, solvent and temperature.[46-47]

In the case of semidilute solutions, it is important to define two critical concentrations c* and c_e.[48] A polymer chain in solution assumes a conformation confined in its hydrodynamic volume. The concentration c* is a limiting concentration, which essentially separates the dilute from the semi-dilute concentration regimes. It represents the point at which the concentration inside a single polymer chain is equal to the solution concentration and is given by the following equation

$$c^* \approx \frac{1}{[\eta]} \tag{1.3}$$

In the semidilute unentangled regime, the concentration is large enough for some chains to overlap, yet the degree of entanglement is not significant (figure 1.6b). In this case the process is dominated by electrospraying. With increasing concentration towards the semidilute entangled regime, the chain entanglement becomes more substantial due to topological constraints that are induced by the larger occupied fraction of the hydrodynamic volume in the solution.[49]

The critical entanglement concentration, c_e, is the crossover concentration between semidilute unentangled and semidilute entangled regimes. Above this concentration, an increase in the zero shear viscosity is observed because of extensive chain entanglements. An approximation for the entanglement concentration is given by

$$c_e \approx \frac{\rho M_e^0}{M_w} \tag{1.4}$$

where M_w is the molecular weight, ρ is the density of the polymer and M_e^0 is the average molecular weight between entanglements in the undiluted (pure) polymer and is given by $M_c/2$, which will be different depending on the polymer used.[50]

As a result, continuous fibers are generated during the electrospinning process. Yet, the transition from beaded to continuous fibers occurs gradually over a range of concentrations.[51-52]

Figure 1.6 Physical representations of three solution regimes (a) dilute, (b) semidilute unentangled and (c) semidilute entangled. Reproduced with permission from ref 50 © Elsevier Inc. 2005.

Overall, chain entanglement is the primary factor in determining the morphology in the fiber forming process. With increasing concentration, the progression from beads to beads with incipient fibers to beaded fibers to fibers and finally to globular fibers or macrobeads is observed.[44]

Surface tension

During electrospinning, the liquid jet is produced when electrostatic forces become greater than the surface tension of the solution. Surface tension is therefore a critical parameter. It is predominantly a function of solvent composition but it is also dependent on the solution concentration and the presence of additives.[53] In fact, if all other

variables are held constant, the surface tension defines the upper and lower boundaries of the electrospinning window. It can be generalized that if the surface tension of the solution is too high, the electrospinning process is inhibited since the process is dominated by the Rayleigh instability. As a result, sprayed droplets are generated. Therefore, reducing surface tension, in particular by adding a surfactant, allows fibers without beads to be produced.[54]

Solution conductivity and surface charge density

Solution conductivity is an important parameter for the formation of fibers. It is primarily determined by the nature of the solvent, the type of polymer and the availability of ionisable salts.[20] Essentially, polymer solutions with high conductivity will have a greater charge carrying capacity compared to those with low conductivity. Thus, when the voltage is applied, the jet from the solution of high conductivity is subjected to greater tensile force, which consequently decreases the diameter of the resulting fibers. However, an extremely high conductivity can lead to a highly unstable jet in the presence of strong electric fields causing excessive bending instability and broadening the diameter distribution. Alternatively, if the solution has very low conductivity, there is insufficient elongation of the jet by the electrical forces. In this case, it is difficult to obtain uniform fibers due to the large number of beads.[55]

Solution parameters are the key factors that will determine the morphology, dimensions and structural form of electrospun fibers and can be tuned and controlled, depending on the desired result. Concisely, concentration, viscosity and molecular weight are interdependent properties that will alter the viscoelastic forces of the solution. Additionally, the surface tension can be optimized by the concentration, molecular weight and solvent used. The effect of the solvent boiling point on the electrospinning of polymer fibers will be addressed later.

1.3 Applications of electrospun fibers

Electrospinning can be used to produce fibers from a wide range of polymeric materials: synthetic or natural, biodegradable or nondegradable, polymer blends and composites, etc.[56-60] Since electrospinning is a relatively simple and cost effective technique, it has attracted tremendous attention in different fields for a great number of applications. Moreover, this technique produces fibers with large surface area, which allows accessing and tailoring specific properties and morphologies that are not as easily achieved with other conventional fiber-forming techniques.[61] Electrospun fibers have found their use in a number of areas such as in environmental engineering and biotechnology for membrane and filter fabrication, in the energy area for solar cells, in tissue engineering and drug delivery, and in chemical and biological sensors.[16]

Electrospinning is being extensively combined with other techniques to produce composite materials. Electrospun fibers, due to their high porosity, interconnectivity, microscale interstitial space and large surface to volume ratio, are ideal materials for membrane preparation. They have been shown to be effective in size exclusion membranes for particulate removal from wastewater or air.[62] Electrospun superhydrophobic organic/inorganic membranes can be used in membrane distillation.[63] Titanium dioxide (TiO_2), synthesized by combining electrospinning with the TiO_2 sol-gel technique, is a promising photocatalyst.[64] Carbon nanofibers are also a promising class of materials for conducting supports of catalysts in (bio)-electrochemical applications.[65]

Two examples will be described in more details as representative applications. Electrical components and devices is an area where electrospun fibers are being extensively employed. The elongation force that is applied on the jet by the high electrical field induces an orientation of the polymer chains. The electron mobility achieved in single fiber transistors is analogous to the best values obtained with a thin film-based device, and the results are unaffected by the dielectric surface treatment.[66] Poly(vinylidenefluoride) (PVDF), due to its electroactive properties and high dielectric

constant, can be used as nanofiber mats in separators for Li-ion batteries. The resulting nanoporous structure provides increased ionic conductivity in a membrane immersed in electrolyte solution. Moreover, the alignment of electrospun PVDF fibers enhances the tensile strength and modulus of membranes. In comparison with existing polypropylene separators, controlled thickness and diameter distribution of PVDF fibrous membranes improves not only the mechanical strength but also results in little capacity loss due to charge and discharge capacities. Low conductivity of PVDF caused by its high crystallinity is improved by using a diblock copolymer. It has been shown that electric double-layer capacitors prepared using electrospun PVDF-PHFP (poly(vinylidene fluoride-hexafluoropropylene)) fibers displays excellent specific capacity and cycling efficiency.[67]

In tissue engineering, the generation of nanofibrous scaffolds using synthetic or natural biodegradable and biocompatible polymers permits the cellular microenvironment to be simulated. Electrospun fibers offer advantages over other materials because they can mimic the extracellular matrix to a certain extent.[68] For instance, Salehi *et al.* have focused their work on developing aligned and transparent nanofibrous electrospun scaffolds of poly(glycerol sebacate) (PGS) and poly(ε-caprolactone) (PCL) polymer blends, which are structurally similar to native cornea stroma. Basically, the alignment of polymer chains is enhanced by increasing PGS content within fibers, which forces amorphous PCL into confined and cross-linked domains near the surface leading to improvement of the surface modulus.[69] Fibers can also be used in drug delivery, where the encapsulation of the active ingredient can be incorporated in the fiber through electrospinning process. Moreover, the rate of drug release can be designed for rapid, intermediate, delayed or controlled dissolution depending on the polymer carrier used or the morphology of the fibers.[70]

1.4 Properties of electrospun fibers

As described above, electrospun fibers attract tremendous attention due to their potential applications in a variety of areas. However, their internal nanostructure that will define the physical properties still needs to be investigated. A number of studies have been performed to examine properties of fibers such as their molecular orientation, thermal and mechanical properties, and internal morphology such as a core-shell organization.

The effect of solvent on fiber morphology

The solvent must be primarily selected in terms of its ability to solubilize the polymer and its boiling point, indicative of its volatility. In general, volatile solvents with low boiling point are preferred for electrospinning due to a faster evaporation as the jet travels to the collector. However, too highly volatile solvents should be avoided since they will evaporate too fast at the capillary tip potentially resulting in obstruction of solution flow of the solution from the needle.[53] On the contrary, if the solvent has very low volatility, it does not evaporate during the trajectory of the jet. As a result, a viscous solution reaches the collector instead of continuous fibers. Yet, it is essential to consider primarily the solubility of the polymer in the solvent, or more explicitly the polymer-solvent interactions that govern the conformation of the polymer chains in solution and affect the degree of entanglement. In order for the polymer to be dissolved in the solvent, the solubility parameters must not be too different. It is essentially the principle of "like dissolves like". The polymer-solvent interaction parameter χ is characterized by the sum of two components:

$$\chi = \chi_H + \chi_S \tag{1.5}$$

where χ_H is the enthalpic component of the polymer-solvent interaction and χ_S is the entropic excess component of free-volume dissimilarity.[71] Manipulations of solvent directly impacts the electrospinnability, viscoelasticity and has a strong influence on the

resulting diameter of the fibers and their morphology, among other properties.[72] For instance, the *a* constant in the Mark–Houwink–Sakurada equation of intrinsic viscosity (equation 1.2) is a function of polymer geometry that varies from 0.5 to 2.0 with a = 0.5 for theta conditions and increases with increasing solvent quality.

As the jet travels to the collector, the solvent evaporation from the jet surface can lead to inhomogeneity in the radial direction. This process can be described by a non-linear mass diffusion-transfer model (figure 1.7a).[73] This has a direct effect on polymer matrix microstructure within the dried fibers. As a consequence, a more rapid solvent evaporation from the outer flowing layers results in the formation of a solid skin on the jet surface, while solvent still remains inside the jet. It is therefore followed by a slower evaporation of the solvent from the inner layer of the fibers, which creates voids that were previously occupied by the solvent after complete solidification and drying of the fibers. As a result, there is partial relaxation of the matrix and the relaxation time is dependent on different factors including molecular weight of the polymer, concentration of the solution and flexibility of the polymer chains. Moreover, relaxation time tends to increase with evaporation of the solvent. Since the solvent acts as a plasticizer, an increase in effective glass transition temperature (T_g) also occurs.[74] This induces the generation of fibers with heterogeneous structures. Thus, the rate of solvent evaporation is governed by the nature of the solvent used and its volatility, which will directly impact the resulting morphology of fibers.[75]

During the jet trajectory to the collector, a phase separation often takes place at the liquid-air interface, which depends on volatility. Therefore, spinodal or bimodal types of phase morphologies result within the fiber. High surface pore density is expected for volatile solvents (e.g. THF) (figure 1.7b) and nearly smooth surface morphology is observed for less volatile solvents (e.g. DMF).[61] Aside from polymer solubility in the solvent, another factor must be considered, namely the impact of solvent miscibility with water. Humidity has a direct effect on the surface morphology of fibers and generally results in porous morphology when using volatile solvents. The process can be described by two mechanisms, breath figures, characterized by water droplet condensation from

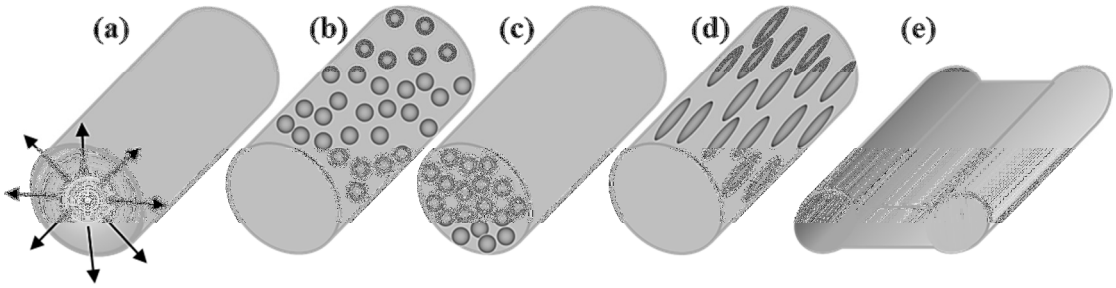

Figure 1.7 Schematic representations of (a) radial solvent evaporation of the solvent from the jet, and possible fiber morphologies: (b) surface pores, (c) internal pores, (d) elongated pores or wrinkled fibers and (e) dumbbell shaped fibers.

the atmosphere onto the surface of the fiber, or by phase separation on the surface in the presence of high humidity.[76] As was mentioned earlier, solvent evaporation leads to the formation of the solid skin. If a high boiling point solvent is used, the solvent evaporation from the core of the fiber is much slower, resulting in liquid-liquid phase separation between atmospheric moisture and the solvent leading to the formation of large solvent-rich domains. Thus, the fibers have a smooth surface with high internal porosity (figure 1.7c).[77] Moreover, slow solvent evaporation from the inside of the fiber may result in the collapse of the solidified skin, forming dumbbell or ribbon-like fibers (figure 1.7e). On the contrary, highly volatile solvents cause buckling of the fiber surface under tensile stress, producing wrinkled fibers (figure 1.7d).

Mechanical properties and molecular orientation

Mechanical properties of electrospun fibers have been extensively explored, since they govern their suitability for a number of applications. These properties largely depend on the microstructure of individual fibers and on the overall mat porosity, the density of bonding sites between fibers and the alignment of the fibers.[78] The ultimate goal of the research on mechanical properties of fibers is to simultaneously improve strength and toughness. However, the improvement of strength usually happens at the expense of toughness.[79] Recent studies have demonstrated a drastic increase in Young's modulus and strength with decreasing fiber diameter.[80-81] Highly crystalline polymers usually exhibit high strength and modulus due to the reduction of macromolecular mobility in the crystalline phase allowing for low deformation. On the other hand,

reducing the fiber diameter could lead to a decrease in crystallinity, resulting in exceptionally high ductility and toughness.[80] A generalized effect of the fiber diameter on modulus, strength and toughness is depicted in figure 1.8.

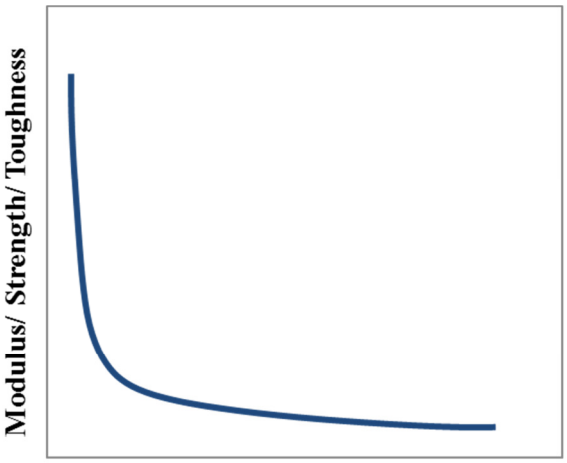

Figure 1.8 Generalized dependence of Young's modulus, strength and toughness on fiber diameter.

For amorphous and semicrystalline polymer systems, an increase in elastic modulus and strength can be attributed to improved chain orientation within the fiber with decreasing fiber size. For a deformation process, orientation is defined by two competing parameters: extensional forces and orientation relaxation. The first induces the orientation of polymer chains along the direction of deformation and the latter, because of the entropic cost associated with extending chains past their equilibrium coil dimensions, tends to return the polymer chains to their isotropic state.[78] In the straight part of the traveling jet, chain orientation is high. Yet, bending instability that forces the jet to go into the looping trajectory has a significant influence on orientation and microstructure of the resulting fibers. It is however hard to estimate since the whipping motion is very rapid and has a large amplitude.[82] A strong correlation between the modulus and the molecular orientation has been reported recently by our group for the polystyrene (PS) system at the single fiber level (figure 1.9).[83]

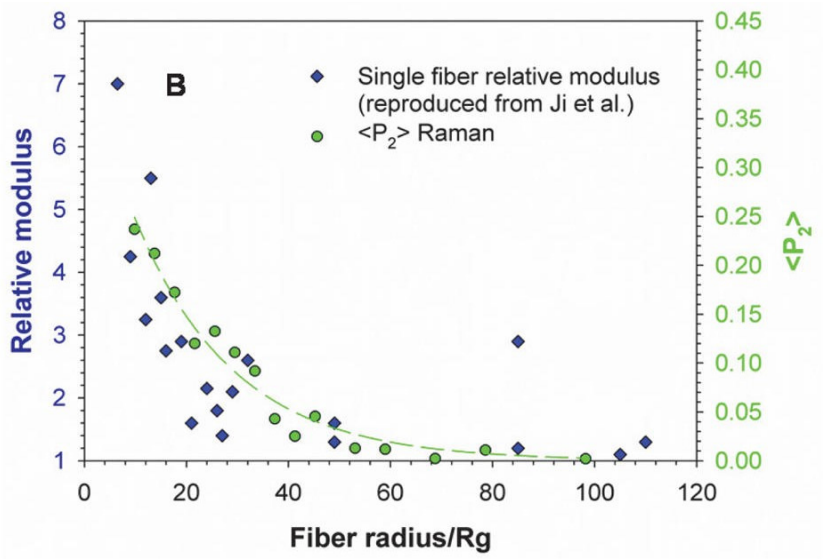

Figure 1.9 Direct correlation between the diameter dependence of relative modulus and molecular orientation. Reproduced with permission of ref. 84 Copyright © 2015 American Chemical Society.

Chain organization in oriented fibers has been described by various models, such as the formation of confined supramolecular structures. Nanoscale organization into core-shell microstructure was also proposed, where the oriented chains would be located either in the core or in the shell of the fiber.[81, 84] Camposeo *et al*.[85] correlated the mechanical properties of electrospun fibers to their internal nanostructure and the core-shell organization. The preparation of fiber involves fast axial stretching of the polymer solution accompanied by radial contraction towards the core. As a result, the fibers display core-shell morphology with enhanced axial orientation at the fiber center. The fibers therefore have a much stiffer and denser core as compared to the shell. On the other hand, the study of poly(vinyl chloride) (PVC) electrospun fibers by Stachewicz *et al*. has demonstrated improved mechanical properties of the oriented shell compared to the isotropic core with much lower elastic modulus.[86] Moreover, as the fiber diameter decreases, the volume fraction of the shell becomes more important, leading to a higher overall fiber elastic modulus.

Thermal properties

The electrospinning process has an effect on thermal properties of fibers, such as their crystallinity, crystallization temperature T_c, melting temperature T_m and glass transition temperature T_g. For instance, it has been shown that T_c increases for electrospun fibers in comparison to bulk samples for Nylon 11.[87]

The size dependence of properties of electrospun fibers has also been observed in thermal measurements, notably the change in glass transition temperature (T_g). Wang and Barber have investigated the T_g of electrospun poly(vinyl alcohol) (PVA) as a function of fiber diameter using indentation tests. They have observed a depression of T_g by 7 ºC with decreasing diameter from bulk values to the smallest diameter of about 100 nm. They have attributed this effect to polymer chain confinement within the fiber surface and amorphous regions within the fiber volume.[88] On the other hand, the study of polyamide-6,6 by Baji *et al.* revealed an increase in T_g by around 7 ºC when the diameter of fibers decreased from micron size down to 200 nm. Higher values of T_g for the fibers with small diameters is caused by shear-induced molecular chain alignment during electrospinning, with smaller fibers experiencing higher draw ratios. Higher glass transition values also indicate better molecular coupling resulting in improved strength and stiffness.[89] Yet, for PS systems, no changes in T_g were reported as a function of fiber diameter even though a large increase of shear modulus was observed.[90]

Thermal conductivity

A challenge with bulk polymeric materials is their inherent low thermal conductivity, on the order of 0.1 $Wm^{-1}K^{-1}$. As a consequence, it limits their use in many applications requiring this property.[91] Electrospun fibers, due to the partial disentanglement and aligned and ordered molecular chains that result from high strain rates exerted on the liquid jet during the process, can be potentially used as materials with enhanced thermal conductivity compared to the bulk counterparts. However, a limited number of studies were performed on thermal conductivity of electrospun fibers. Recently, it was observed

that the thermal conductivity of electrospun Nylon-11 was as high as 1.6 $Wm^{-1}K^{-1}$, which is an order of magnitude higher than its bulk value of 0.2 $Wm^{-1}K^{-1}$.[92] Ma *et al* have studied the thermal conductivity of PE electrospun fibers as a function of resulting structure and applied voltage. The highest value of thermal conductivity measured was 9.3 $Wm^{-1}K^{-1}$, showing a significant increase compared to the bulk material (0.4 $Wm^{-1}K^{-1}$). This enhancement is believed to be due to an increase in molecular orientation and an enhanced level of crystallinity in the electrospun fibers. Also, an increase in applied voltage promotes higher values of thermal conductivity.[91]

1.5 Electrospinning of polystyrene

Atactic polystyrene (PS), being colorless and transparent, is one of the most used plastic materials for insulation and packaging due to its low cost and high expansion capacity. It is an amorphous polymer with a T_g of around 100 ºC, having high electrical resistance and low dielectric loss. It is also hard, stiff and very brittle.[93] PS is extensively used in both academic and industrial areas due to its simplicity, well known structure and properties in a number of materials and applications. It is often used as a model system in the academic area because it can be synthesized with well controlled M_w and very low PDI. In the area of electrospun fibers, PS has also been employed as a polymer of choice. A great number of studies have been performed, investigating the effects of a variety of solution and processing parameters on the electrospinning of PS.[94-98] However, regardless of the system used, the internal microstructure of electrospun fibers is still not entirely understood. In fact, even with a model system like PS, there is still limited knowledge about the fundamental structural organization within the fibers.

The morphology of electrospun PS fibers, characterized by their diameter and topography, has been investigated in terms of different parameters. For instance, Jarusuwannapoom *et al.* studied the electrospinnability and morphology of PS using different solvents with varying properties, such as their volatility and χ.[97] They have

selected the most suitable solvents for electrospinning of PS, namely chloroform, 1,2-dichlorethane, DMF, ethyl acetate, methylethylketone (MEK) and THF, all of which generated continuous fibers without defects. According to them, electrospinnability is determined by high enough boiling point and not-so-high values of viscosity and surface tension of polymer-solvent solution. Moreover, depending on the solvent, different morphologies of PS fibers were obtained. For instance, round fibers were obtained from DMF solutions, whereas a ribbon-like morphology was characteristic of PS/MEK systems. The diameter of round fibers (or width in the case of ribbon-like fibers) has a tendency to increase with increasing concentration of the solution. On the other hand, buckling of the shell due to compressive radial stress that is influenced by ultra-fast solvent evaporation (with highly volatile solvents like chloroform) from the shell of the fiber leads to the formation of wrinkled fibers. Additionally, beaded fibers are only obtained for solutions of low concentration. This bead formation has been attributed to low viscosity of the solution.[96]

The final fiber morphology depends on the process variables such as initial polymer concentration, rate of solvent evaporation relative to the rate of phase separation and temperature.[98] It has been shown that the porosity of fibers formed with low boiling point solvents depends on the molecular weight of the polymer and relative humidity.[76] The formation of surface pores and their size is therefore influenced by the polymer/solvent phase separation due to rapid solvent evaporation. Basically, the solvent-rich phase leads to pore formation as the polymer-rich phase solidifies. Thus, the volatility of the solvent plays a critical role in the surface pore formation process.[99] For instance, highly volatile solvents such as carbon disulfide (CS_2), smooth fibers with low packing density of pores were obtained as a result of polymer/solvent phase separation. Relative humidity also affects the porosity of electrospun fibers. It has been shown that with increasing relative humidity, the pore formation also increased. PS/THF systems (high volatility) generated fibers with high surface pore density due to solvent miscibility with water from the atmosphere. Decreasing the solvent volatility by employing DMF resulted in smooth fibers with small pores on the surface.

In addition, Pai *et al.* [98] have studied the effect of the relative humidity on the morphology of PS/DMF systems. Essentially, in humid environments, water vapor absorbs into the jet and ultimately acts as a nonsolvent, resulting in liquid-induced phase separation. This precedes the solidification due to the slow evaporation rate of DMF. As a result, wrinkled fibers were obtained when the system was electrospun with low relative humidity, whereas an increase in humidity leads to the formation of smooth fibers with porous interiors, rather than a homogeneous consolidated solid structure.

The effect of the solvent on the resulting fiber morphology has been previously studied by our group using PS/poly(vinyl methyl ether) (PVME) blends.[100] Miscible fibers were obtained from benzene solutions, characterized by a single glass transition, similar to solvent-cast films, indicating that the structure of the miscible blends was not affected by the electrospinning process. On the contrary, clear phase separation occurred when fibers were electrospun from a chloroform solution, resulting in the core-shell morphology due to solvent evaporation kinetics in which the interior is composed of PS-rich phase and the surface is highly enriched in PVME. In contrast, PS/PVME solvent-cast films from chloroform are characterized by the formation of microdomains.

Prior to investigating the chain entanglement in polymer fibers, it is necessary to consider freeze-dried films. The freeze-drying technique allows preparing samples with lower chain entanglement density in comparison to the equilibrium bulk state.[101] It involves an extremely rapid freezing of the solvent in a dilute solution, followed by removal of the solvent through sublimation. As a result, this process prevents chain reptation and re-entanglement is prohibited. The studies of freeze-dried PS samples by IR spectroscopy have demonstrated that there are IR bands that can be indirectly related to the amplitude of the disentanglement.[102] Partial disentanglement of polymer chains has also been found in spin-coated PS films.[103]

The heterogeneity within fibers electrospun from a single polymer component has also been investigated. Under high electric field, the solution is elongated and stretched within the liquid jet, resulting in partial disentanglement. It was reported by the Zussman

group that, in the first millimeters of the jet, the chains are fully extended, hence partially disentangled. This phenomenon could be maintained on the outer shell of the fiber due to rapid solvent evaporation whereas the structure of the core is closer to bulk entanglement due to the presence of residual solvent, creating a density gradient within the fiber (figure 1.10).

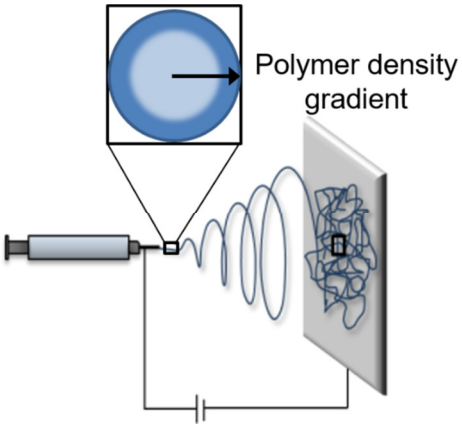

Figure 1.10 Schematic representation of the core-shell morphology and the polymer density gradient due to the solvent evaporation during the electrospinning process. Reproduced with permission of ref. 107 Copyright © 2015 American Chemical Society.

In addition, there is a competition between diffusion of the solvent into the skin and the evaporation of the solvent to the surroundings. Hence, fast solvent evaporation and high stretching forces acting on the liquid jet during electrospinning force the chains to be frozen in an out-of-equilibrium state.[104] Guenther *et al.* demonstrated, through theoretical analysis and simulations, that in electrospun fibers polymer macromolecules are inhomogeneously distributed in the cross-section of the fiber.[105]

It has recently been demonstrated by our group that partial disentanglement of polymer chains occurs in the shell of electrospun PS fibers by relating new bands in the IR spectra to a conformation allowed by chain disentanglement, whereas the core maintains bulk entanglement, which is schematically represented in figure 1.11.[106] In

order to observe partial disentanglement in the fibers, a highly volatile solvent is thought to be necessary. Therefore, PS fibers were electrospun from chloroform solution to ensure ultra-fast solvent evaporation.

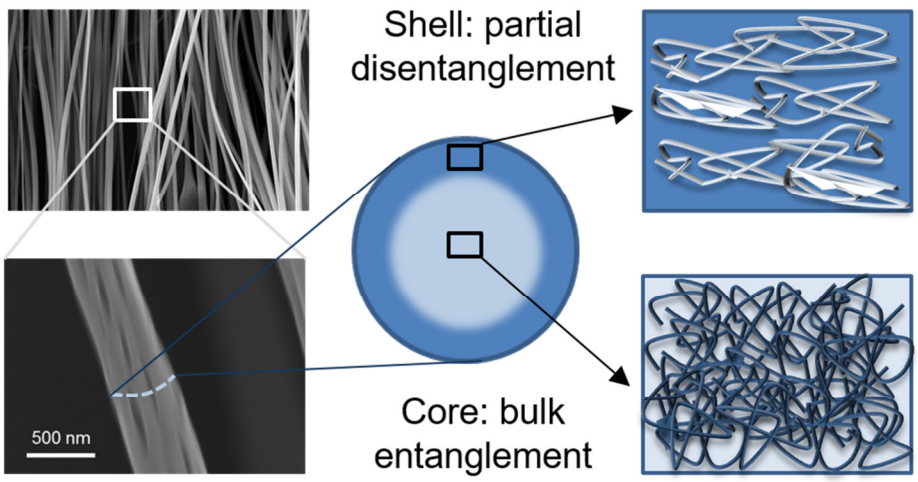

Figure 1.11 Schematic representation of partially disentangled shell and bulk entangled core within electrospun fibers. Reproduced with permission of ref. 107 Copyright © 2015 American Chemical Society.

It was shown by ATR-IR studies of PS fibers that partial disentanglement depends on solution concentration, where fibers electrospun from low solution concentrations allow detecting partial disentanglement. In fact, the band associated with partial disentanglement substantially increased when the concentration decreased from 15% w/v down to 10% w/v. The volume fraction of the shell is expected to increase with decreasing concentration and consequently with decreasing diameter of the fiber. The ability to evaluate the amplitude of disentanglement in PS fibers was made possible by earlier studies of freeze-dried PS films that not only associated specific IR bands to partial disentanglement, but also demonstrated that the band intensities decreased with increasing solution concentration.[102] Furthermore, partial disentanglement displayed a dependence on electrospinning time, which is the time during which fibers accumulate on the collector. Long electrospinning time (10 min or more) will generate more closely packed fibers. In this case, evaporation of the residual solvent is slowed due to increased

local vapour pressure and it can act as a plasticizer leading to chain re-entanglement. The evaporating solvent will then penetrate the shell of a given fiber from both its core and from neighbouring fibers. Alternatively, fibers collected for short time periods (about 1 min) are less affected by solvent evaporation since they are more isolated. As a result, partial disentanglement is observed for short collection times only.

Additionally, further studies were performed using Raman spectroscopy on single PS fibers, which allowed associating Raman bands with a conformation made possible by partial disentanglement of the chains.[83] Moreover, radial distribution of these bands was mapped, showing that partially disentangled chains are mainly located in the shell of the fiber. It was possible to conclude that they originated from incomplete re-entanglement rather than from stress-induced disentanglement. These results are in complete accordance with the conclusions made from IR spectroscopy. The excess of isotropic intensity (EID) of a Raman band associated with a conformation made possible by disentanglement was estimated as a function of fiber diameter. As observed for the orientation and modulus dependence of the fiber diameter, the average EID values followed an exponential increase with reduction of diameter. It is therefore due to the increasing volume fraction of the shell for smaller fibers.

1.6 Objectives and structure of the thesis

The present work focuses on the electrospinning of PS fibers and the investigation of the heterogeneity in the radial distribution of their density. As was shown earlier, a model for the diameter dependence of molecular orientation and radial chain organization was proposed for PS fibers prepared using a highly volatile solvent, chloroform. It is now necessary to investigate, first, the thermal properties of this system using temperature modulated differential scanning calorimetry (TMDSC) and to broaden the scope of electrospinning conditions to validate and expand our model. The thermal properties of PS electrospun fibers are studied as a function of solution parameters,

including the solution concentration, molecular weight of the polymer and the nature of the solvent, keeping the diameter of the fibers constant.

This thesis is presented in 4 chapters. The first chapter presented the background aspects of electrospinning and more details on the system of interest. Chapter 2 will present the instruments used in the study and the experimental parameters, as well as the theoretical basis of the characterization techniques. Chapter 3, in the first part, presents the results obtained for the electrospinning of PS from chloroform solutions as a function of molecular weight and concentration. In particular, it includes in-depth analysis of the thermal properties of the system with the effect of annealing on these properties and their correlation with the core-shell organization of the fibers. In the second part, the morphology of the fibers will be studied as a function of volatility of four solvents as well as concentration and molecular weight. A third part focuses on the investigation of the molecular organization at the single fiber scale for PS fibers electrospun from chloroform solution using AFM-IR. Finally, the thermal properties of PS fibers prepared in the four solvents are presented. Chapter 4 summarizes the main results and conclusions obtained from this work along with ideas for future research.

Chapter 2

EXPERIMENTAL DETAILS AND METHODOLOGY

2.1 Materials and sample preparation

The polymers used in this study are atactic polystyrene (PS) with three weight-average molecular weights: 210 000 g/mol (Scientific Polymer Products Inc), 929 000 g/mol (PDI = 1.10) and 2 000 000 g/mol (PDI = 1.30) (Pressure Chemicals). They were used as received. The solutions were prepared in four different solvents, namely chloroform ($CHCl_3$), methyl ethyl ketone (MEK), tetrahydrofuran (THF), (Fisher Scientific) and N,N-dimethylformamide (DMF) (Sigma Aldrich) that were used as received.

Polymer solutions were prepared by weighing the polymer with an analytical balance (Mettler Toledo AB265-S) and dissolving it in the desired solvent at room temperature. The solution concentrations are expressed as weight per volume of solvent (usually 3 ml) (w/v) and are reported in percentage. The stirring time of the solution is dependent on the molecular weight of the polymer. The solutions prepared with high molecular weight polymer (900 000 and 2 000 000 g/mol), which were received in the form of flakes, were stirred for at least 4 hours using a stirring plate, whereas the solutions with low molecular weight (210 000 g/mol) PS pellets were stirred for at least 12 hours in order to obtain homogeneous solutions.

All fibers subsequently obtained by electrospinning were dried at room temperature under vacuum for at least 48 hours before any measurements and analyses took place.

2.2 Electrospinning setup

As described in section 1.2, the mechanism of electrospinning is rather complex, but its setup is extremely simple, allowing for a convenient operation (figure 2.1). Since electrospinning involves fast solvent evaporation, the setup is mounted in a fume hood. It includes three major components: high voltage power supplies (1 and 2), a spinneret for which a needle is used (3) and an electrically conductive collector (5). The polymeric solution is loaded into the 5 ml glass syringe with a flat-end metallic needle having an internal diameter of 0.41 mm. It is subsequently fed at a specific rate of 0.01 mL/min set by a PHD 2000 syringe pump (Harvard Apparatus) (4). A CZE 1000R high-voltage power supply (Spellman High Voltage Electronics) is used to apply a positive voltage of 15 kV to the needle.

A rotating collector with a Teflon disk 10 cm in diameter was used to collect fibers for thermal analysis. A negative potential of 2 kV (Power Designs) was imposed on the center of rotating disk collector with a metallic ring of 1 mm, which acts as a counter electrode. The spinning of the disk is powered by a DC motor equipped with a power controller, allowing a controlled and constant speed, which was set to 300 rpm for all experiments. The collector and the needle were enclosed in a plastic chamber in order to confine the scattering of fibers during electrospinning and reduce the effects of environmental conditions. A 15 cm distance was set between the tip of the needle and the edge of the collector. The rotating movement of the collector and the applied voltage force the majority of fibers to align on the metal ring and only partially cover the overall surface of the disk. It therefore allows to recover fibers that are aligned along a principal axis and to collect large quantities of fibers. The fibers were electrospun for a long period of time and collected at regular intervals of 10 minutes.

A two-rod collector was used to prepare fibers for AFM-IR measurements. The fibers were electrospun directly onto an IR transparent window (BaF_2) attached between two rods of the collector for a few seconds in order to isolate individual fibers.

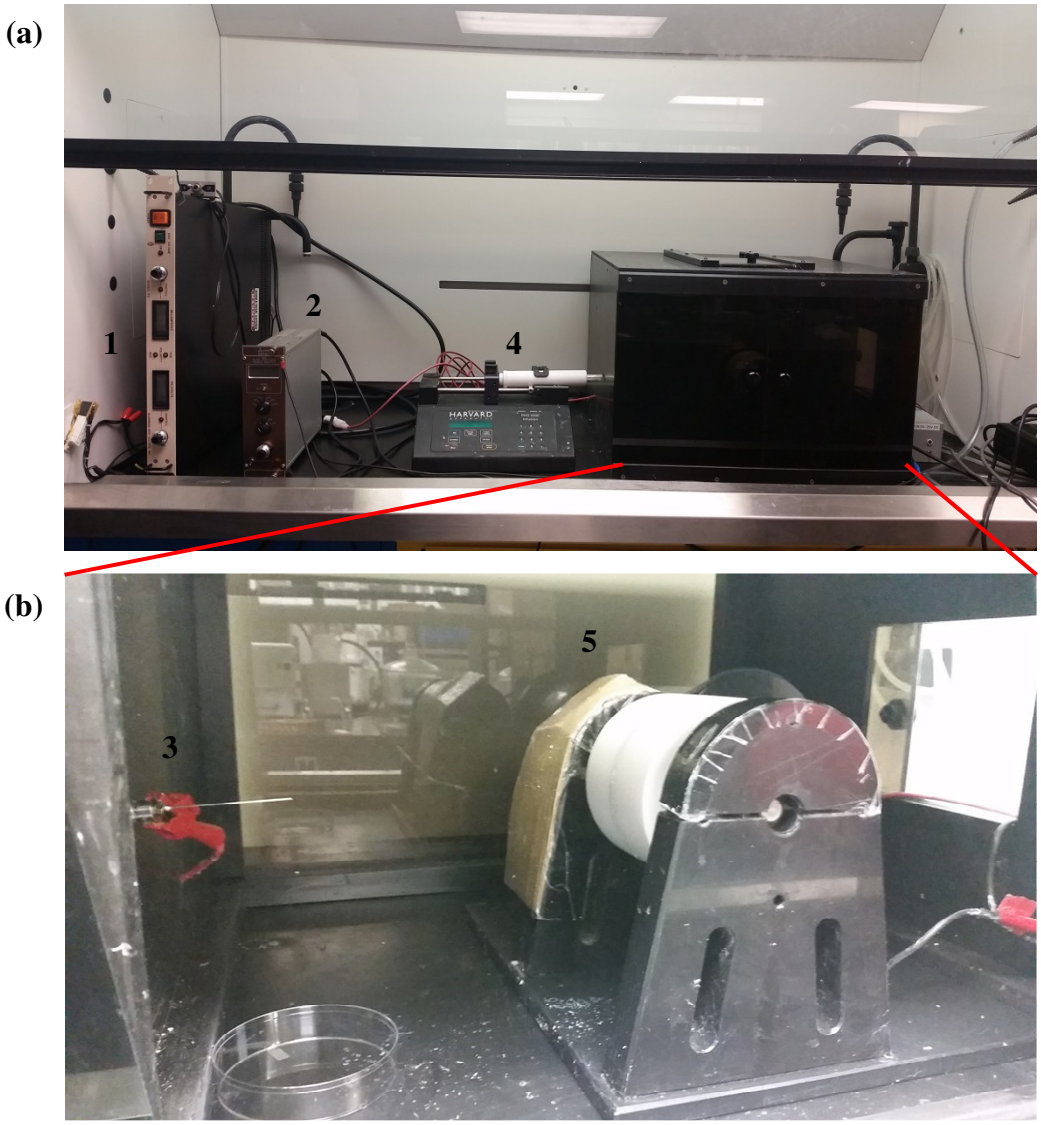

Figure 2.1 Photographs of the electrospinning setup used in our laboratory. (a) general view including high voltage power sources (1 and 2) and automated injector (4) and (b) close look at the needle (3) and rotating disk collector (5).

2.3 Thermal analyses

Atactic PS is an amorphous polymer, which means that its main characteristic is the glass transition temperature. Thermal phenomena that occur at and around T_g were measured with a DSC Q2000 (TA instruments) in standard and modulated modes. It is done by measuring the difference in heat flow (mW) between the sample and the

reference recorded as a function of temperature. The calorimeter is purged with nitrogen gas. The calibration was performed using an ultrapure indium sample with T_f = 156.6 ºC and ΔH_f = 28.5 J/g. Standard aluminum pans (Perkin-Elmer 219-0041) were used to encapsulate samples of around 8 mg. For standard DSC, a heating rate of 10 ºC/min was used and three runs were completed for each sample for a temperature range from -10 to 225 ºC. The cooling cycle was at the maximum cooling rate of the instrument. Since the T_g of PS is around 100 ºC, this range allowed to obtain stabilized baseline and correct measurement of T_g. To allow the instrument to equilibrate, an isotherm of 5 min was included before each heating and cooling ramps.

Temperature modulated DSC (TMDSC) represents an extension of the conventional DSC technique. In this method, a sinusoidal modulation of temperature is overlaid on the standard linear ramp (figure 2.2a). Hence, due to the temperature modulation, the heating rate is not constant, but rather varies periodically (figure 2.2b). The modulated heating rate is set between maximum and minimum values that are determined by the average heating rate (the rate for conventional DSC), the period and the amplitude of the superimposed temperature waves. Therefore, the sinusoidal change in temperature required the selection of two additional parameters, the modulation period and temperature amplitude.

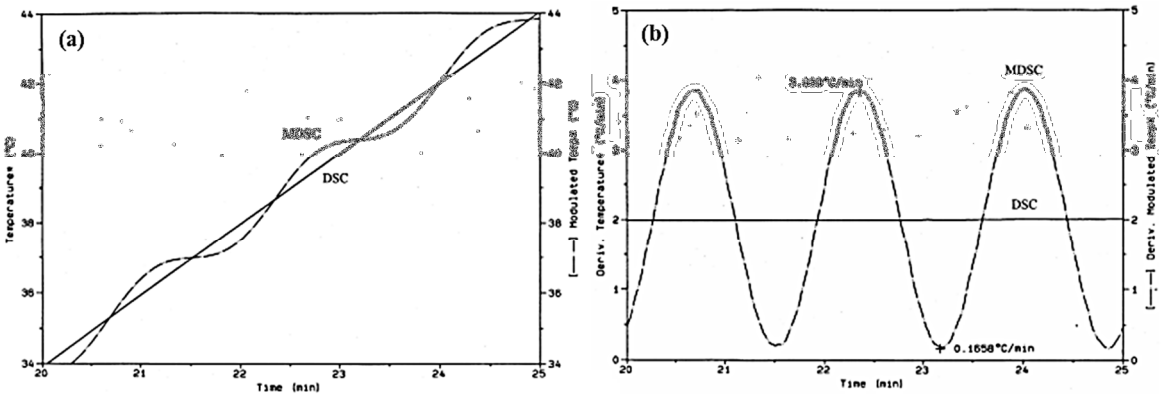

Figure 2.2 Temperature as a function of time (a) and heating rate as a function of time (b) for typical DSC and TMDSC experiment. Reproduced with permission of ref. 108 Copyright © 1999 Elsevier Science.

The modulation temperature profile is determined according to equation 2.1.

$$\frac{dT}{dt} = \beta + A_T\,\omega\cos(\omega t) \qquad (2.1)$$

where dT/dt is the instantaneous heating rate (ºC/min), β is the underlying heating rate (ºC/min), A_T is the modulation amplitude (ºC), ω is the angular frequency = 2π/modulation period (min^{-1}) and t is time (min). Large modulation amplitude results in increased sensitivity for transitions such as the glass transition. On the other hand, if the amplitude is too large, the material may not be able to follow the modulation.

As a result, due to the sinusoidal change in temperature, the signals that are measured in TMDSC are a modulated heat flow and a modulated heating rate (figure 2.3). The simultaneous application of both linear and modulated heating rates allows obtaining the total heat flow, which is calculated from the average of modulated heat flow according to equation 2.2.

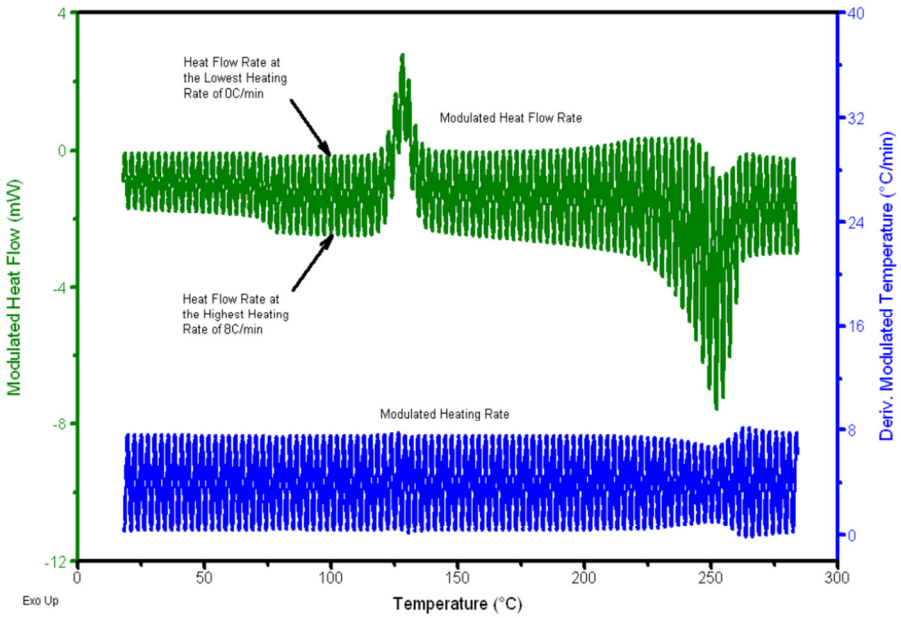

Figure 2.3 Modulated heating rate (input) and modulated heat flow (output) for the TMDSC experiment. Reproduced with permission of ref. 108 Copyright © 1999 Elsevier Science.

$$\frac{dH}{dt} = Cp\frac{dT}{dt} + f(T,t) \qquad (2.2)$$

where dH/dt is the total total heat flow rate (mW or mJ/s), C_p is the heat capacity of the sample (J/ºC), dT/dt is the heating rate (ºC/min) and *f*(T, t) is the heat flow function of temperature and time (mW).

The total heat flow, which is the sum of all heat flow occurring at any point in time and temperature, has two components: one is a function of the applied heating rate (dT/dt) and the other is a function of time at a given temperature. In other words, the reversing heat flow (C_p(dT/dt)) is a thermodynamic component, characteristic of reversible transitions such as the glass transition and most melting points. The nonreversing heat flow *f*(T, t) is a kinetic component that allows to separate thermal events such as enthalpic relaxation, crystallization, evaporation and decomposition. An example of MDSC curves, including the total, reversing and nonreversing heat flow signals, is presented in figure 2.4.[107-108]

It is important to choose the modulation period (40 s/cycle) and modulation temperature (0.531 ºC) appropriately. A slower heating rate than in the conventional DSC method is necessary in order to allow a sufficient number modulation cycles during a thermal event. For this experiment, a heating rate of 5 ºC/min was used.

Thermogravimetric analysis was performed with a TGA 2950 (TA Instruments) in order to identify the heating range for the DSC analysis, to certify the absence of solvent in the samples prior to DSC measurements and to define the maximum heating temperature during the DSC run. Samples of around 5 mg were heated with a rate of 10 ºC/min over a temperature range from 25 to 600 ºC under nitrogen atmosphere.

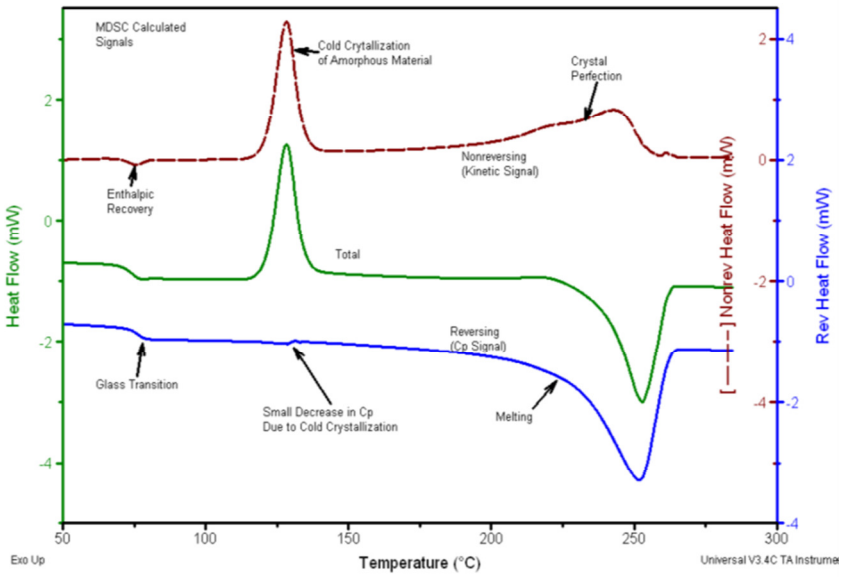

Figure 2.4 Deconvoluted heat flow signals (total, reversing and nonreversing) obtained by TMDSC. Example is presented for quenched poly(ethylene terephthalate) (PET) sample. The total heat flow signal (green), equivalent to the conventional DSC signal, shows the glass transition, the cold crystallization exotherm, and the melting of the formed crystals. In the reversing (blue) and nonreversing (red) components, in this region endothermic melting (in the reversing heat flow) and exothermic (re)crystallization (in the nonreversing heat flow) compete, resulting in a net 'zero' effect in the total heat flow. The glass transition is observed in the total and reversing heat flow signal, whereas the nonreversing heat flow signal reveals the presence of enthalpic recovery peak otherwise not seen in the total heat flow. Reproduced with permission of ref. 108 Copyright © 1999 Elsevier Science.

2.4 Microscopic analysis

Scanning electron microscopy (SEM) was used in order to obtain details about the morphology of electrospun fibers and to estimate their diameter and diameter distribution. The principle of SEM is to focus a beam of high-energy electrons over a surface to create an image. The topography and morphology of the sample is derived from the interactions between electrons and the sample. This interaction creates

secondary electrons that are emitted by atoms on the sample that are excited by the electron beam. The number of secondary electrons that are detected directly depends on the angle at which the beam encounters the surface, or sample topography. SEM images were recorded using a JEOL LSM-7400F (JEOL Ltd.) field emission scanning electron microscope under high vacuum mode and with an acceleration voltage of 20 kV. In order to enhance the resolution of the image, a thin layer of gold of around 5 nm was deposited on fibers prior to imaging.

2.5 AFM-IR

AFM-IR is a technique that combines atomic force microscopy (AFM) and infrared spectroscopy (IR) for nanoscale characterization. It allows to obtain IR spectra at a precise position of the AFM tip and IR maps of spatial variation of the absorbance of a specific IR band of interest. The absorption of a specific wavelength by the sample results in the thermal expansion of the sample on the nanosecond time scale. It causes a modulation of the oscillating AFM cantilever, which creates a "ringdown" at a particular frequency that decays with dissipating heat. As a result, the positive amplitude of the oscillation represents the intensity of the IR band. The IR spectrum is obtained at a spatial resolution of 50-100 nm as the frequency of a pulsed laser is tuned through the IR region.[109]

The high-resolution AFM images and IR spectra of single electrospun PS fibers were acquired with a NanoIR2 AFM-IR (Anasys Instruments). The AFM imaging was performed in the contact mode. The fibers were electrospun directly onto IR transparent BaF_2 windows in order to have a good contact between the sample and the substrate and avoid movement during imaging. Each spectrum was recorded in the spectral region from 1000 to 1800 cm^{-1} at a resolution of 4 cm^{-1}/point by coaveraging 256 cantilever ringdowns for each data point. The power of laser was 49.08%. The IR spectra were

normalized with respect to the band at 1492 cm^{-1} associated with the ν_{19a} C=C aromatic stretching vibration. The size of the IR maps was 1 x 5 μm^2.

Chapter 3

RESULTS AND DISCUSSION

3.1 Thermal behavior of PS fibers electrospun from chloroform solutions

The electrospinning of PS in a volatile solvent, such as chloroform, has been previously studied and provided evidence for a core shell organization of chains within fibers. Moreover, measurements by Raman and IR spectroscopy allowed observing conformation sensitive bands that were associated with partial disentanglement of chains and its localization. It allowed to conclude that these electrospun fibers are structurally heterogeneous both radially and longitudinally.[83, 106] In this work, the heterogeneity of PS fibers is studied by DSC taking into consideration the effect of concentration and molecular weight, as well as the effects of different solvents on the thermal behaviour of PS fibers (which will be discussed in section 3.4).

Figure 3.1a shows an SEM image of PS fibers with a molecular weight of 900 000 g/mol electrospun from a 12.5% chloroform solution. These conditions generate unbeaded fibers with a wrinkled morphology and an average diameter of 1.7 μm. The morphology and the mechanism of formation of wrinkled fibers are discussed in section 3.3. The corresponding DSC thermogram of the first heating run for the PS electrospun fibers is presented in figure 3.1b and features a T_g at around 105 ºC. The glass transition temperature represents the transition from a glassy to a rubbery state of the material and it depends on the structural characteristics of the sample and other parameters such as the heating rate.

Another thermal transition is observed that appears as an overshoot at T_g, characterized by an endothermic peak at around 109 ºC, and represents an enthalpic relaxation event.[110] The fibers are stretched under high electric field during electrospinning, which translates into mechanically induced stress. The enthalpic relaxation peak at the glass transition may be due to relaxation of this stress. Moreover,

enthalpy relaxation can also occur when the material is annealed below T_g. Since the DSC experiment was performed at a relatively moderate heating rate (5 ºC/min), some degree of annealing is imposed on the sample during the heating ramp, contributing to the enthalpic relaxation peak. The system studied in this work is fairly simple, consisting of only one polymer, and it was expected to have only one characteristic thermal transition, namely T_g. Yet, unexpected thermal events were observed below the glass transition. These sub-T_g events have to be investigated since it is unclear whether they represent an endothermic peak, an exothermic peak or even both (figure 3.1c).

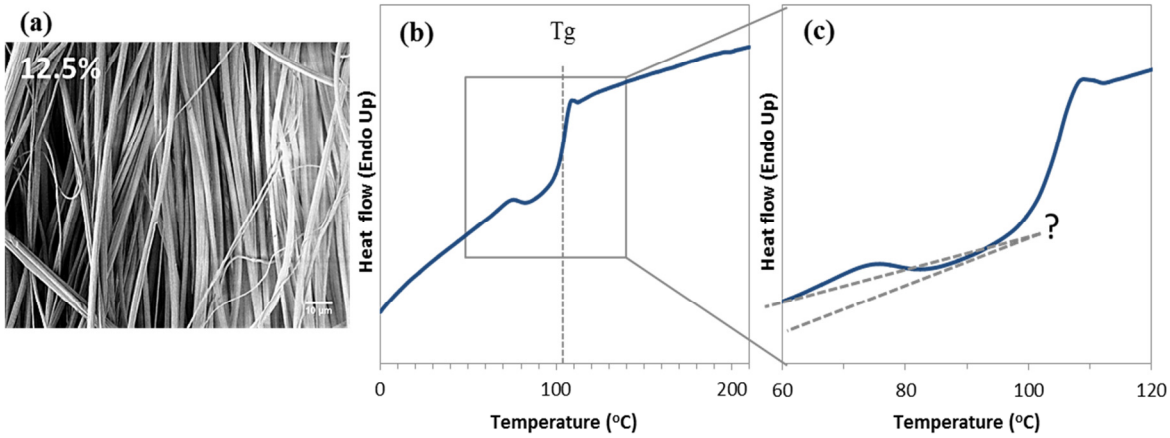

Figure 3.1 (a) SEM image of PS fibers electrospun from a 12.5% w/v chloroform solution (Mw = 900 000 g/mol) (the scale bar is 10 μm) with the corresponding DSC thermogram for the first heating run (b) and the zoomed region around T_g (c).

An additional endotherm below T_g can be generally classified as a secondary relaxation in the vicinity of the glass transition. Unlike the structural relaxation that occurs at T_g, which is characterized by molecular motions involving relatively large segments of the polymer backbone chain, secondary relaxations occurring below T_g are due to localized molecular motions since the mobility is considerably limited in the glassy state of the material. Since these motions are very localized, there is no clear increase in the heat capacity. Yet, this sort of mobility was associated with an endotherm below T_g.[111] Moreover, these secondary motions can in turn have an influence on macroscopic properties of the polymer, for instance stepwise changes in the physical and mechanical properties such as the modulus, thermal expansion coefficient and the

dielectric constant. They can be classified into three types of motion. The first represents a rather localized crankshaft motion, characterized by a rotation about certain backbone bonds. Another type of motion involves rotation of the side group about the bond linking it to the main chain. Lastly, it can present itself in the form of internal motion of a unit within the side group. All these motions contribute to the secondary loss.[112]

In fact, such behaviour has been previously observed for glasses with a sub-T_g exotherm preceded by an endotherm that progress with aging of glasses.[113] For PS systems, the endotherm was found at T_g – 30 ºC immediately after preparation of the material, which then became more pronounced and moved by 3 ºC closer to T_g after 20 days. It was not associated to changes in conformational population but rather to process-induced increase in the strain energy of the glass stored in the distorted bonds or angles. Hence, the exothermic peak below T_g was associated to the release of the strain energy. Furthermore, Petrie[114] investigated the effect of annealing of organic glasses on their thermal behavior and has demonstrated that the magnitude of the sub-T_g endothermic peak is strongly dependent on the pre-treatment of the sample before annealing, which involved liquid nitrogen quenching or application of high pressure. On the other hand, the position of the peak was independent of pre-treatment but determined by annealing conditions. The development of endothermic maxima below T_g was considered as a general feature of physical aging of polymeric glasses characterized by an approach towards equilibrium with a broad distribution of relaxation times.[115] Moreover, it was established that a great portion of the normal recovery in aged glasses is due to the volumetric recovery of the glass. The sub-T_g endotherm was then associated to the dilation process, where the effective increase in the free volume of the aged glass would provide sufficient space to permit this internal stress to relax.[116-117] Aging or annealing of polymer glasses amplify the sub-T_g thermal events that arise from the interplay between the time-dependent changes in the volume and the relaxation of the frozen strain energy.

In order to investigate the sub-T_g events observed in PS fibers, temperature modulated DSC was performed to separate thermal events from the total heat flow signal. Figure 3.2 presents TMDSC thermograms showing total, reversing and nonreversing heat flow signals for PS fibers electrospun from a 12.5% w/v chloroform solution with a T_g at 105 °C. Reversing heat flow, characterized by reversible thermodynamic events in the system, shows only the T_g. From the nonreversing heat flow, it is possible to observe the enthalpic relaxation at T_g along with the sub-T_g events. Moreover, the comparison between the first and second heating scans in the total and nonreversing heat flows suggests that there is indeed an exotherm that is preceded by an endothermic peak, since the sub-T_g transitions are no longer present in the second heating run, showing only the expected enthalpic relaxation peak at T_g.

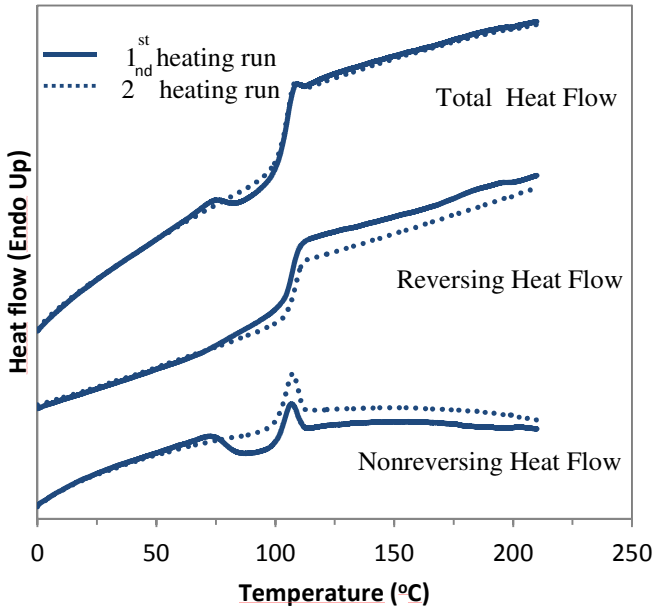

Figure 3.2 TMDSC thermograms of PS fibers electrospun from a 12.5% from chloroform solution (M_w = 900 000 g/mol) showing the total, reversing and nonreversing heat flow for the first heating run (solid line) and the second heating run (dotted line).

TMDSC is a thermoanalytical technique that not only allows the separation of the measured heat flow into its kinetic and thermodynamic components, but also allows a

more accurate determination of the change in specific heat capacity (ΔC_p) as well as T_g. In the complex situation where an endotherm preceded by a exotherm below T_g is observed and to fully investigate the origin of these events, it is important to define the actual baseline. To do so, two low temperature baselines, one at the endotherm and one at the exotherm below T_g, were traced in order to calculate ΔC_p and T_g from the total heat flow signal in the first heating run. Measurements were also made using the reversing heat flow, due to the absence of sub-T_g events, along with the second heating runs (figure 3.3). First, it can be seen from the graphs that the measured values of ΔC_p are different depending on the chosen baseline for the first heating run in the total heat flow, whereas the values obtained from the second heating run can be considered as their average. This observation supports the claim that there is in fact both an endotherm and an exotherm below T_g. As for the measurement of T_g, the values obtained from the reversing heat flow are displaced to higher temperatures in comparison to the total heat flow. This is due to the fact that the total heat flow comprises the enthalpic relaxation, hence shifting the T_g to lower apparent temperatures.

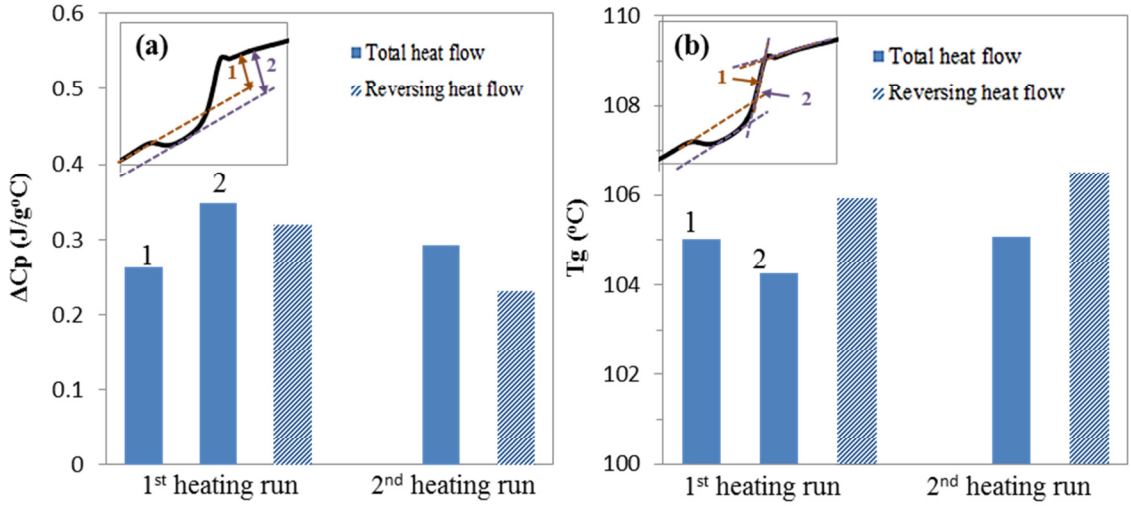

Figure 3.3 (a) Estimate of ΔC_p using two possible baselines for the total heat flow signal (first and second heating runs) and for the reversing heat flow. (b) Corresponding measurements of T_g.

It was previously proposed that PS fibers have a core-shell organization consisting of two phases: a partially disentangled shell and the bulk entangled core.[106] The results

obtained by TMDSC can be correlated with this model, where the two enthalpic relaxation peaks associated with the normal and the secondary phases could be associated with the core, since it constitutes the majority of the fiber, and a less dense shell, respectively.

As mentioned earlier, the sub-T_g annealing of organic glasses would influence the position of the endothermic peak below T_g. Generally, annealing of amorphous polymers below T_g results in changes in physical properties, such as density, enthalpy and modulus. There is a decrease in enthalpy upon annealing, which is recovered during reheating to above the glass transition. The recovery is manifested as an endothermic peak or inflection in the heat capacity at T_g.[118] Therefore, if the sub-T_g endotherm observed for PS fibers is associated with the presence of a secondary phase, whereas the ordinary phase is characterized by the main glass transition, annealing of fibers would allow to study this phenomenon and to evaluate the presence of two phases with different thermal properties. The goal is then to understand whether annealing converts the secondary phase into the normal phase or amplifies it.

Four annealing temperatures were selected, which are depicted on the DSC curve in figure 3.4. Annealings were performed directly at the maximum of the secondary enthalpic relaxation peak (75 °C) and at the onset and the offset of the peak (65 and 85 °C), respectively in order to see the evolution of the thermal behavior of both the secondary and the normal phases with annealing. Moreover, annealing was done at a temperature well below T_g and the secondary endotherm (45 °C). This condition was not expected to have an effect on the enthalpic relaxation of the normal phase, yet still could affect the thermal behavior of the secondary phase. The annealing times were also varied depending on the temperature used.

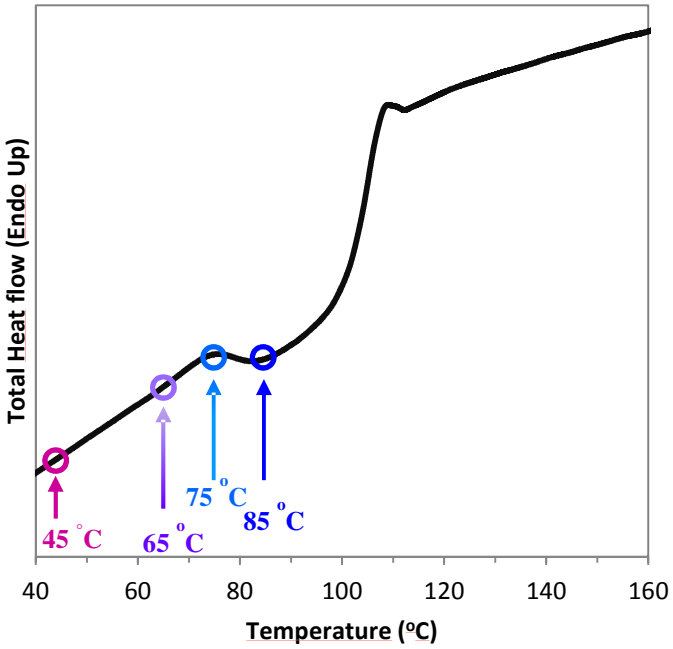

Figure 3.4 Representation of sub-T_g annealing temperatures for PS fibers electrospun from 12.5% w/v chloroform solution (M_w = 900 000 g/mol).

The resulting TMDSC curves are depicted in figure 3.5. The top two curves represent the second and first heating runs, respectively, for the sample that was not annealed. The following curves are ordered by the increase of annealing temperature and time. Primarily, it is important to note that annealing does not influence the position of the T_g as can be observed from the reversing heat flow signal (figure 3.5b). Moreover, the effect of annealing on the enthalpic relaxation peaks of the normal phase (peak 1) and the secondary phase (peak 2) are much better defined in the nonreversing rather than in the total heat flow due to the absence of contribution of the glass transition.

First, annealing at 45 °C was performed for 48 h since it is well below the glass transition and should not affect the normal enthalpic relaxation. Yet, it resulted in the displacement of the secondary endotherm to higher temperatures by 6 °C and resulted in more pronounced exotherm. Annealing at 65 °C for 3 h or 24 h further displaces the secondary endotherm, which becomes more defined and closer to the T_g. On the other hand, there is no clear effect on the enthalpic relaxation peak corresponding to the

normal phase. Annealing at 75 °C for 3 h, corresponding to the temperature of the maximum of the endothermic peak of the original curve, results in two enthalpic relaxation peaks without exotherm in between. Annealing under this condition affects not only the secondary phase (peak 2) but also the normal phase of PS, since the intensity of the normal endotherm appears (peak 1) to decrease in intensity. Increasing the annealing time to 24 h at 75 °C or increasing the temperature to 85 °C results in one enthalpic relaxation peak, suggesting that only one phase remains. Yet, the position of

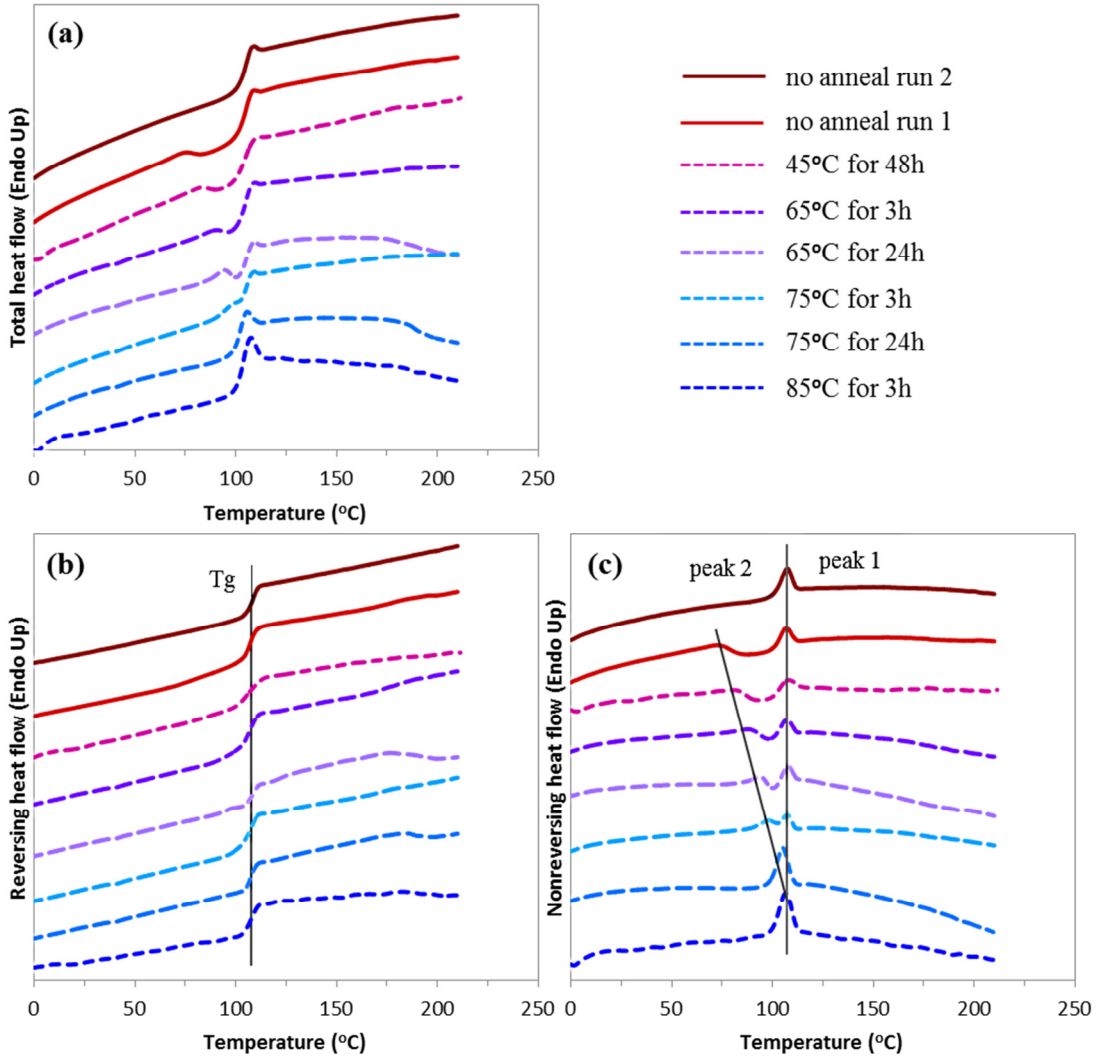

Figure 3.5 TMDSC thermograms of PS electrospun from 12.5% from chloroform solution (M_w = 900 000 g/mol) showing the total, reversing and nonreversing heat flows following different sub-T_g annealing temperatures and times.

the endotherm for the curve after annealing at 75 °C for 24 h is slightly shifted to lower temperature by 2 °C. This means that there is still a contribution of the secondary enthalpic relaxation to the overall peak and that residual secondary phase remains in the system. The evolution of the position of the two endotherms in the nonreversing curves is shown in figure 3.6.

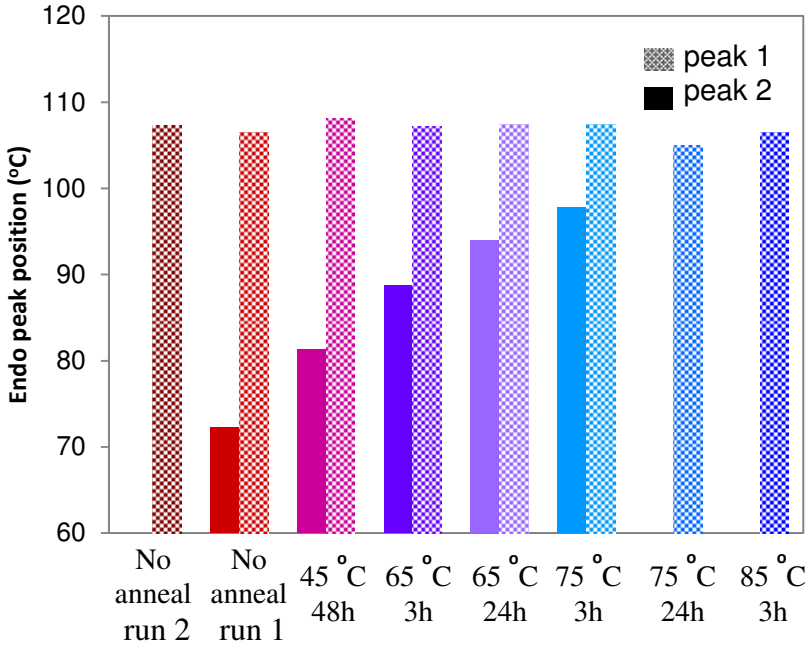

Figure 3.6 The position of the normal (peak 1) and secondary (peak 2) enthalpic relaxation peaks as a function of annealing conditions.

In order to further investigate the phenomenon of two phases constituting PS fibers, solutions were electrospun using PS with three different molecular weights, 210 000, 900 000 and 2 000 000 g/mol at two concentrations each (table 3.1). All previous studies in this work and those that led to the model of core-shell organization were performed on PS with a molecular weight of 900 000 g/mol, since it was hypothesized that a high molecular weight is necessary in order to prevent incomplete re-entanglement in the outer shell of the fiber, which could be associated with the presence of the secondary phase observed by TMDSC. Therefore, a much higher molecular weight (2 000 000 g/mol) was used in order to validate this hypothesis as well as a much lower molecular weight (210 000 g/mol), where chains are expected to be fully (or at least much more)

re-entangled due to lower viscosity of solution. Additionally, different concentrations were used since the solution concentration has an effect on the diameter of the resulting fibers and the goal was to investigate the thermal behavior of the fibers while keeping the diameter constant. Moreover, it was previously demonstrated that the presence partially disentangled chains in the outer shell of the fibers was more pronounced at low solution concentrations, hence the interest of studying fibers prepared at two concentrations for each molecular weight.[106]

Table 3.1 Concentrations used to electrospin PS fibers of different molecular weights from chloroform solutions.

MW (g/mol)	**210 000**	**900 000**	**2 000 000**
Concentration (% w/v)	25% 22.5%	12.5% 10%	10% 8%

Figure 3.7 presents the TMDSC thermograms of the PS fibers electrospun using two molecular weights, 900 000 and 2 000 000 g/mol at two different concentrations each. Primarily, the secondary endotherm followed by a broad exotherm is observed in the first heating run for a higher molecular weight PS as well as for all concentrations used. It is clearly seen that the increase in molecular weight results in displacement of the secondary endotherm by about 15 ºC to lower temperatures and further from T_g. On the other hand, the position of the glass transition does not change for both molecular weights and remains at 105 ºC. This displacement of the secondary relaxation can be due to the faster solidification of the solution jet for higher molecular weight since the solution is more entangled and viscous. The resulting fibers are therefore farther from equilibrium. Moreover, this trend is not only present at the common concentration of 10% w/v but also in the 8% samples and occurs in spite of a lower solution concentration.

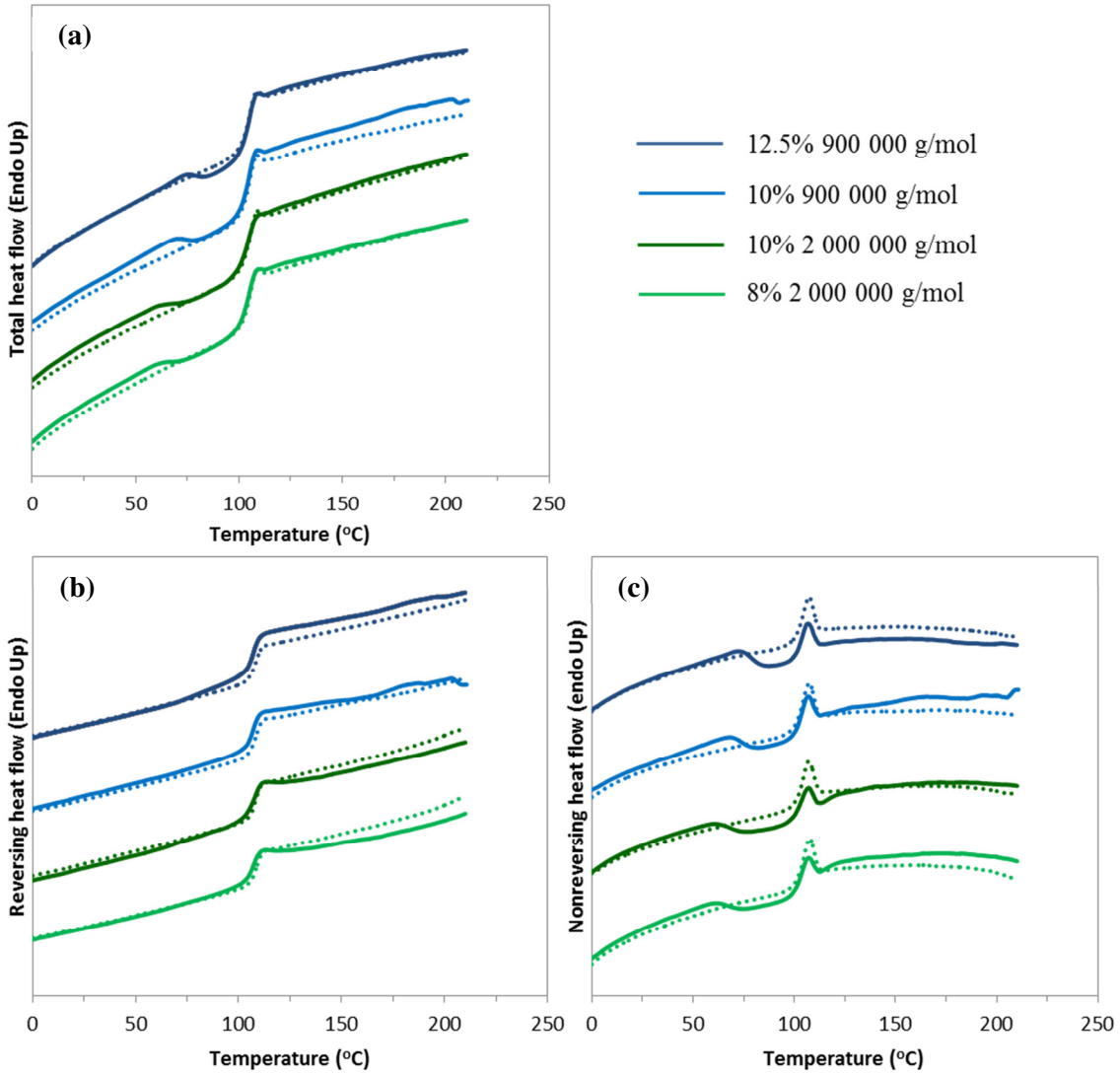

Figure 3.7 TMDSC thermograms of PS electrospun from 12.5 and 10% from chloroform solution (M_w = 900 000 g/mol) and 10 and 8% (M_w = 2 000 000 g/mol) showing the total, reversing and nonreversing heat flows. Solid lines represent the first heating run and dotted lines the second heating run.

As was shown earlier, different annealing conditions were used in order to see the evolution of the sub-T_g events with temperature and time. One condition, namely annealing at 75 °C for 3 h, was selected and applied to all samples in the study since it allows to obtain two clear endotherms in the nonreversing heat flow, normal and secondary, without the contribution of the exotherm, hence providing the possibility to investigate the enthalpic relaxations occurring in the system.

The results of annealing PS fibers electrospun from two high molecular weights and concentrations are depicted in figure 3.8. No clear information can be extracted from the total heat flow due to the overlap of two distinct thermal events, the glass transition and

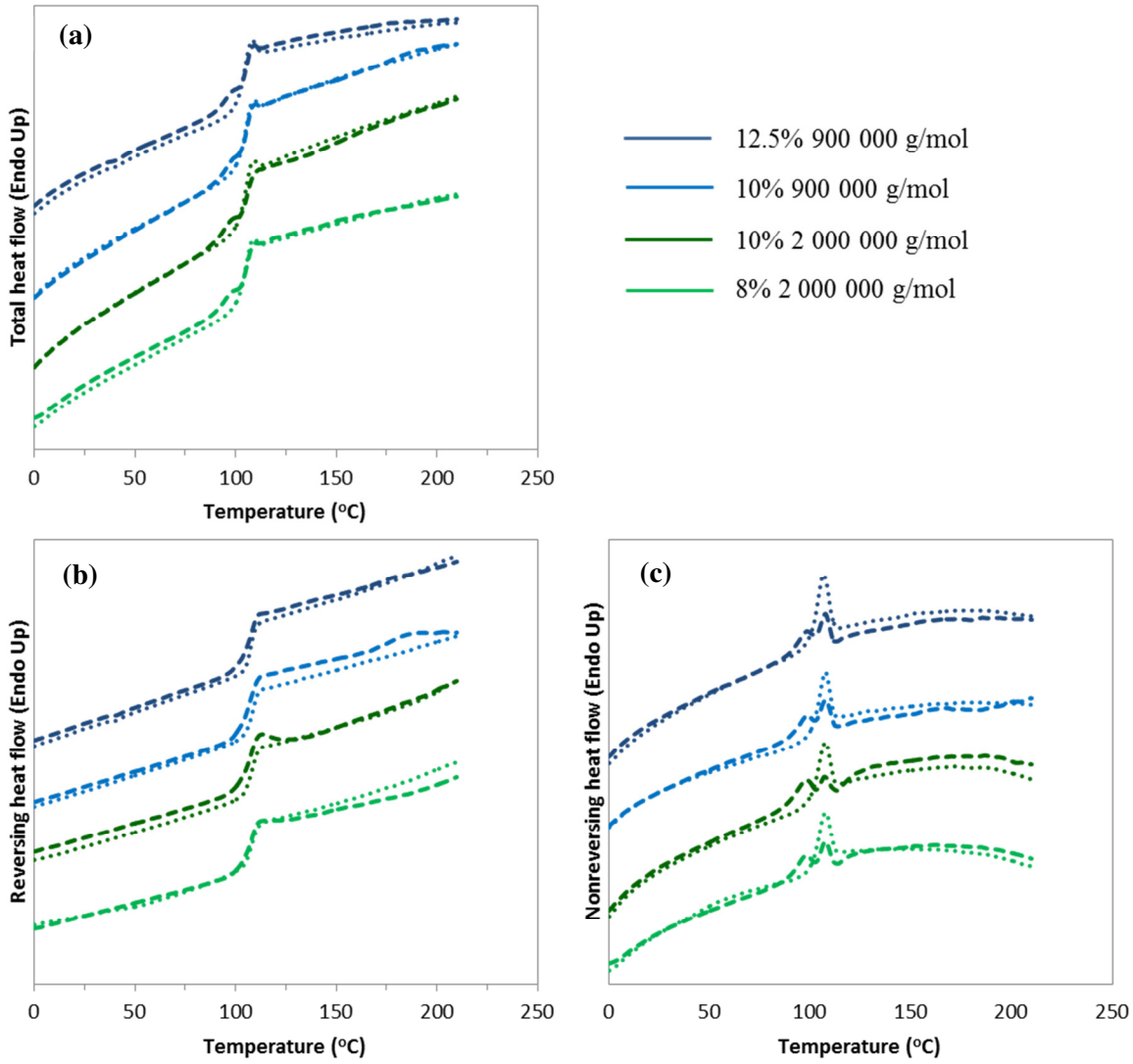

Figure 3.8 TMDSC thermograms of PS electrospun from 12.5 and 10% from chloroform solution (M_w = 900 000 g/mol) and 10 and 8% (M_w = 2 000 000 g/mol) annealed at 75 ˚C for 3h showing the total, reversing and nonreversing heat flows. Dashed lines represent the first heating run and dotted lines the second heating run without annealing.

the enthalpic relaxation. Yet, from the nonreversing heat flow, two endotherms can be clearly seen. The relative intensity of the secondary enthalpic relaxation appears to be higher for 2 000 000 g/mol PS than its lower M_w counterpart, especially for the common

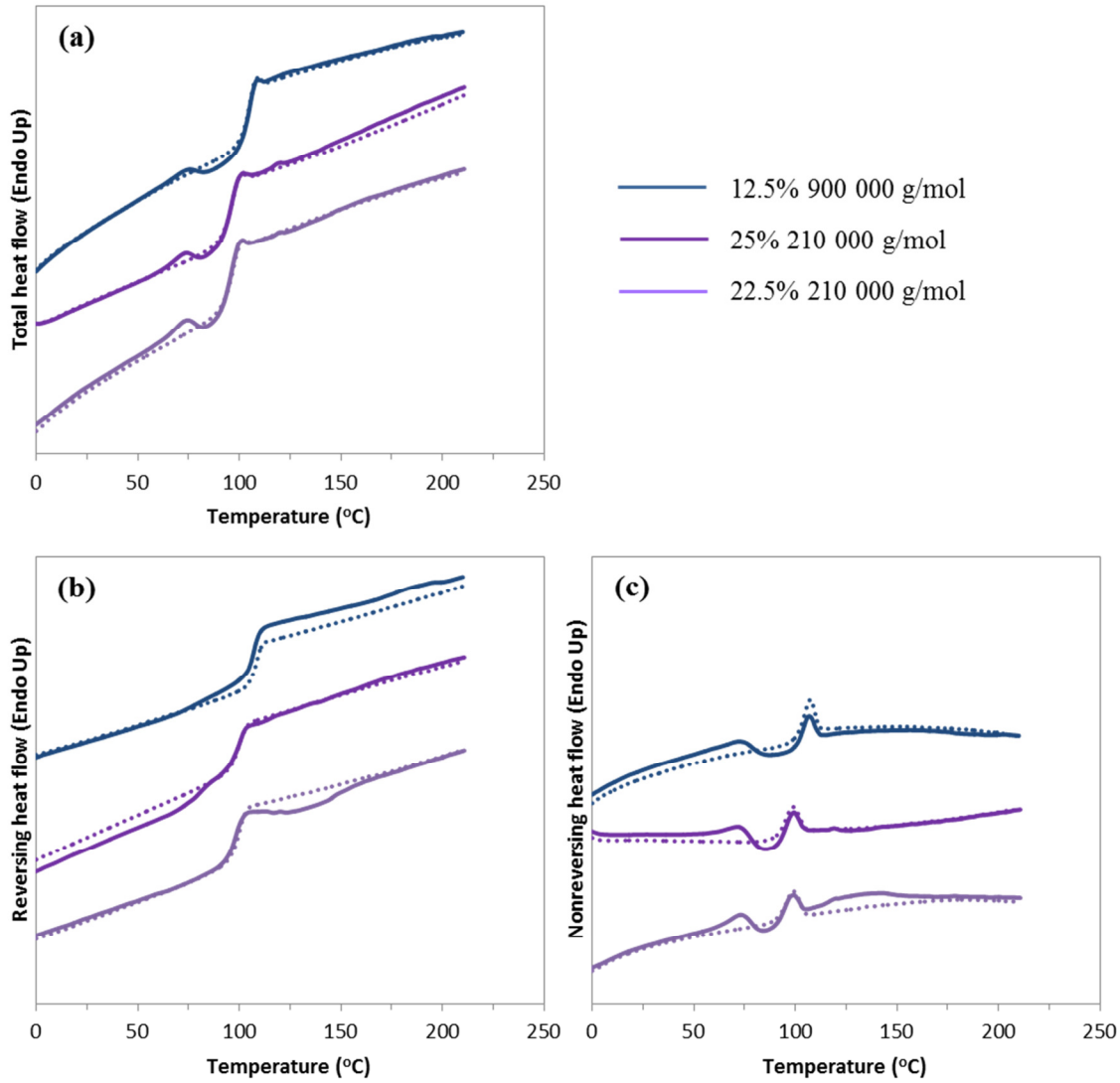

Figure 3.9 TMDSC thermograms of PS electrospun from 12.5% (M_w = 900 000 g/mol) and 25 and 22.5% (M_w = 210 000 g/mol) chloroform solution showing the total, reversing and nonreversing heat flows. Solid lines represent the first heating run and dotted lines the second heating run.

10% solution. What would appear as an endotherm at the glass transition at this condition in the reversing heat flow results from a poor separation of the total heat flow.

The thermal behavior of the system was also measured using PS with a much lower molecular weight, 210 000 g/mol, again using the fibers electrospun from 900 000 g/mol PS at 12.5% w/v as a reference (figure 3.9). The unusual thermal events observed in the reversing and nonreversing heat flow curves of 22.5 % PS (210 000 g/mol) are the artefacts due to the poor separation of the total heat flow. It can be observed that decreasing the molecular weight does not influence the position of the secondary endotherm as seen from both the total and nonreversing heat flow signals. However, even though the secondary endotherm remains at approximately 75 °C, it is the position of the T_g that shifts to lower temperature for the lowest molecular weight polystyrene. Thus, the trend of ΔT between T_{peak2} and T_g as a function of molecular weight is the following:

$$\Delta T_{2\ 000\ 000\ g/mol} > \Delta T_{900\ 000\ g/mol} > \Delta T_{210\ 000\ g/mol}$$

The values of the glass transition temperature were measured from the TMDSC curves for all three molecular weights used in this study (figure 3.10). The T_g values are very similar for the higher molecular weights (900 000 and 2 000 000 g/mol) and decrease by about 9 °C for the 210 000 g/mol polymer. It is essential to note that the glass transition does not occur at a precise point. In comparison to boiling or melting temperature of small molecules, for example, T_g is much more difficult to determine precisely due to the fact that the transition occurs over a comparatively large range of

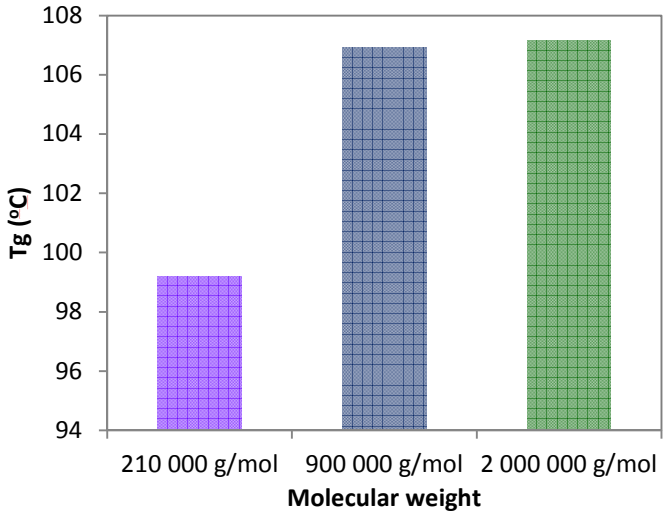

Figure 3.10 Effect of the molecular weight on the glass transition temperature of PS electrospun fibers (measured by TMDSC).

temperatures. Moreover, it strongly depends on the experimental conditions such as the method, heating rate and the duration of the experiment.[119]

The dependence of the T_g on the molecular weight is observed due to its dependence on the length of the polymer chain and relative fraction of chain ends. For polymer systems, this dependence can be expressed by the Flory-Fox equation below, showing inversely proportional relationship between T_g and M_n:

$$T_g = T_{g,\infty} - \frac{K}{M_n} \tag{3.1}$$

where $T_{g,\infty}$ is the maximum T_g that can be achieved at a theoretically infinite molecular weight, K is an empirical parameter related to the free volume in the polymer and M_n is the number average molecular weight. Generally, free volume is the volume not occupied by the polymer chains in the material, where a high free volume provides polymer chains a greater degree of movement to achieve different physical conformations.[120] There must be cooperative motion of several segments in the rubbery state and if the free volume is too low, the cooperative motion becomes frozen. In the free volume theory, the glass transition temperature is the temperature at which the free space accessible for the molecular motions reaches this minimum value.[121] Free volume depends on the number of polymer chain ends, hence on the molecular weight, because the ends of the chain exhibit more molecular motions since they possess more free volume than the segments within the polymer chain. A lower molecular weight polymer has a higher density of chain ends and thus a T_g shifted to lower temperature.[119, 122] Hence, taking into consideration the position of T_g, the secondary relaxation peak is closer to T_g for the lower molecular weight PS due to enhanced mobility of the chain and longer solidification rate. It was observed by increased T_g - T_{peak2} as a function of increasing molecular weight.

The evolution of the secondary enthalpic relaxation was investigated for the low molecular weight PS by annealing the fibers. In order to perform a comparable study, the annealing temperature was lowered from 75 °C to 66 °C due to the shift of the glass transition temperature. Therefore, the annealing condition that generates two

endothermic peaks can be regarded as T_g - 30 °C for all three molecular weights used in this study. Figure 3.11 depicts TMDSC thermograms of the low molecular weight PS electrospun from two concentrations, along with 12.5% w/v, 900 000 g/mol used as a reference. As a result of annealing, two endotherms are present in the nonreversing heat flow signal, but displaced to lower temperatures as compared to the higher molecular

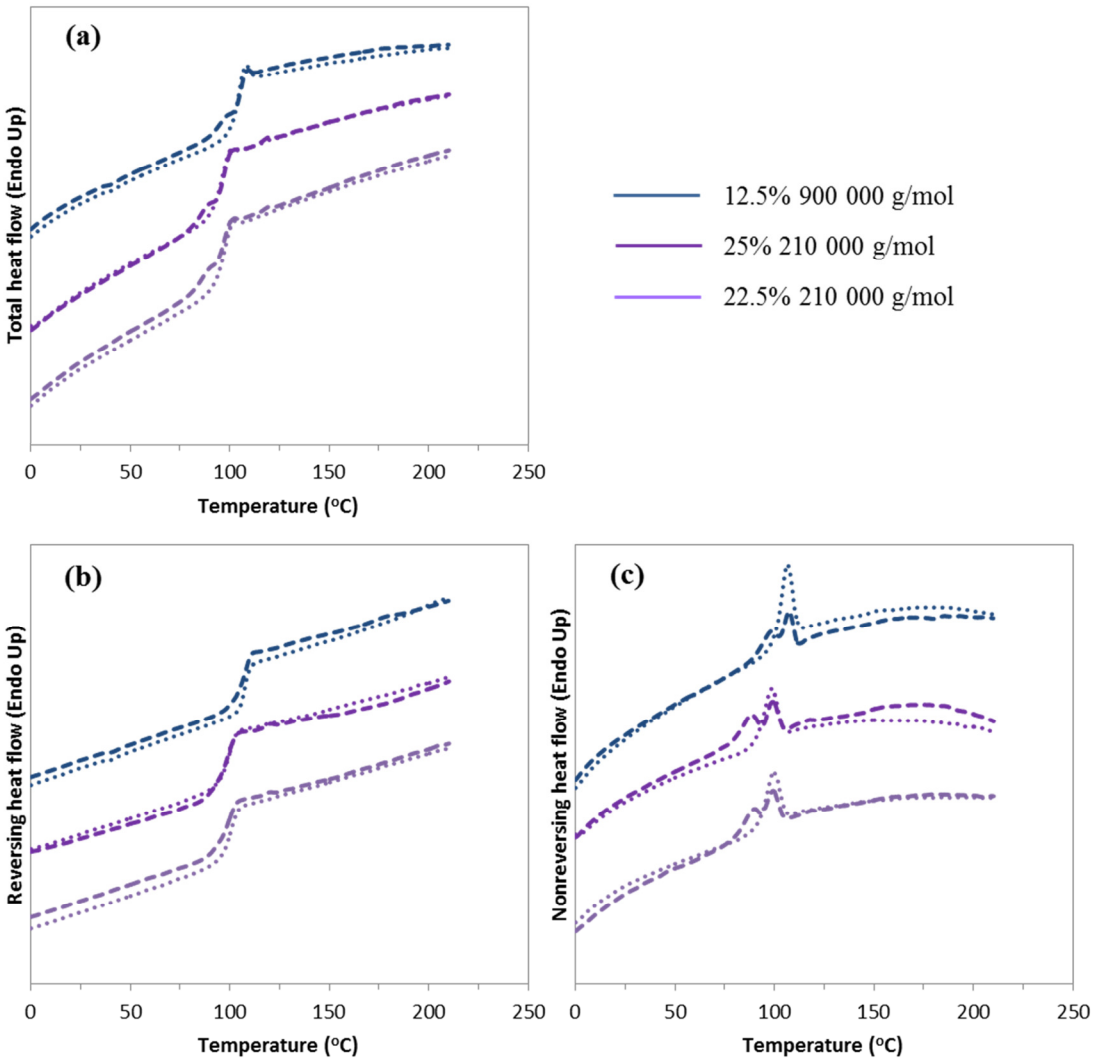

Figure 3.11 TMDSC thermograms of PS fibers electrospun from 12.5% from chloroform solution (M_w = 900 000 g/mol) and 25 and 22.5% (M_w = 210 000 g/mol) annealed at T_g – 30 ˚C for 3 h showing the total, reversing and nonreversing heat flows. Dashed lines represent the first heating run and dotted lines the second heating run.

weight PS.

As a side note, when the fibers of 210 000 g/mol PS were annealed at 75 °C, only one enthalpic relaxation peak was observed, emphasizing the importance of selecting the annealing conditions as a function of the position of T_g. In fact, it is analogous to annealing of the 900 000 g/mol PS fibers at 85 °C, where one endotherm was also obtained. These two results essentially represent the similar effect of annealing PS fibers at T_g – 20 °C.

The glass transition is a second order-like transition, since it involves a change in heat capacity at T_g without latent heat release. Thus, if the sub-T_g endotherm represents a secondary enthalpic relaxation, characterized by the presence of the secondary phase in the system, there should be a secondary glass transition, T_{gs}. Yet, there is no clear evidence of the presence of the T_{gs}, which could be due to its absence or its difficult observation because of the small volume of the secondary phase and the potential overlap with the endothermic peak.

The relaxation behavior of two-phase systems was extensively studied for miscible polymer blends, such as polystyrene/poly(vinyl methyl ether) (PS/PVME) fibers.[123] The main characteristic of miscible polymer blends is that the resulting material has properties, such as the glass transition and enthalpic relaxation, somewhere between those of the two unblended polymers. In theory, two enthalpic relaxation peaks could appear, close to the onset or the offset of the glass transition region. This can be observed in phase-separated blends if both polymers had a discrete effective T_g in the blend. On the contrary, physical aging experiments close to T_g have demonstrated that a single enthalpic relaxation peak appeared in the middle of the glass transition for a miscible blend but that the portion of this peak varied strongly with the annealing temperature. This phenomenon was ascribed to the presence of a continuous range of local T_{gs} due to the presence of nanoheterogeneities. Therefore, annealing in the vicinity of the T_g could yield an enthalpic relaxation peak that can be used as indicator of the underlying presence of a T_g, even this transition is not directly observed.[124] In the case of PS/PVME, the heterogeneities were of chemical composition. This concept can be related to the pure PS system, in which the nanoscale heterogeneity of the molecular

environment would be a consequence of local density and degree of entanglement. Hence, the endotherm below T_g could be interpreted as a characteristic of the enthalpic relaxation associated with the secondary phase, where the glass transition temperature T_{gs} would be overlapped by the relaxation peak.

The thermodynamic properties such as entropy, specific volume or enthalpy, undergo a change in slope at T_g when plotted against temperature. It then becomes possible to further investigate the effect of annealing at different conditions presented earlier in figure 3.5 by considering enthalpy vs. temperature graphs for the proposed two phase model for the PS system (figure 3.12). For original unannealed PS fibers, the secondary phase is found at T_g - 30 °C, characterized by a small enthalpic relaxation peak. During the DSC experiment, as the T_g of the secondary phase is reached, it becomes mobile enough to allow motion. Then the exotherm following the endothermic peak occurs as the secondary phase attempts to convert into the normal phase (figure 3.12a and red curve in figure 3.5).

Annealing below the glass transition densifies the material and minimizes the free volume and enthalpy due to the absence of large-scale motions of chains below T_g.[125] Annealing of fibers at 45 °C for 48 h does not have an effect on the normal phase, since it occurs well below T_g. Enthalpy loss during annealing at very low temperature (T_g – 60 °C) is limited due to the high polymer viscosity below T_g. This concept is based on the free volume model, where the chain segments can relax solely when the available free volume is larger than the critical volume defined by the cooperative length of the polymer segment.[126] It does, however, affect the secondary phase by slightly densifying it and displacing the secondary enthalpic relaxation and (presumably the T_{gs}) to higher temperatures by almost 10 °C. The annealing process itself is exothermal. Heating the sample after annealing first leads to shifted peak 2 endotherm followed by partial return to the normal phase through an exothermal peak (figure 3.12b and pink curve in figure

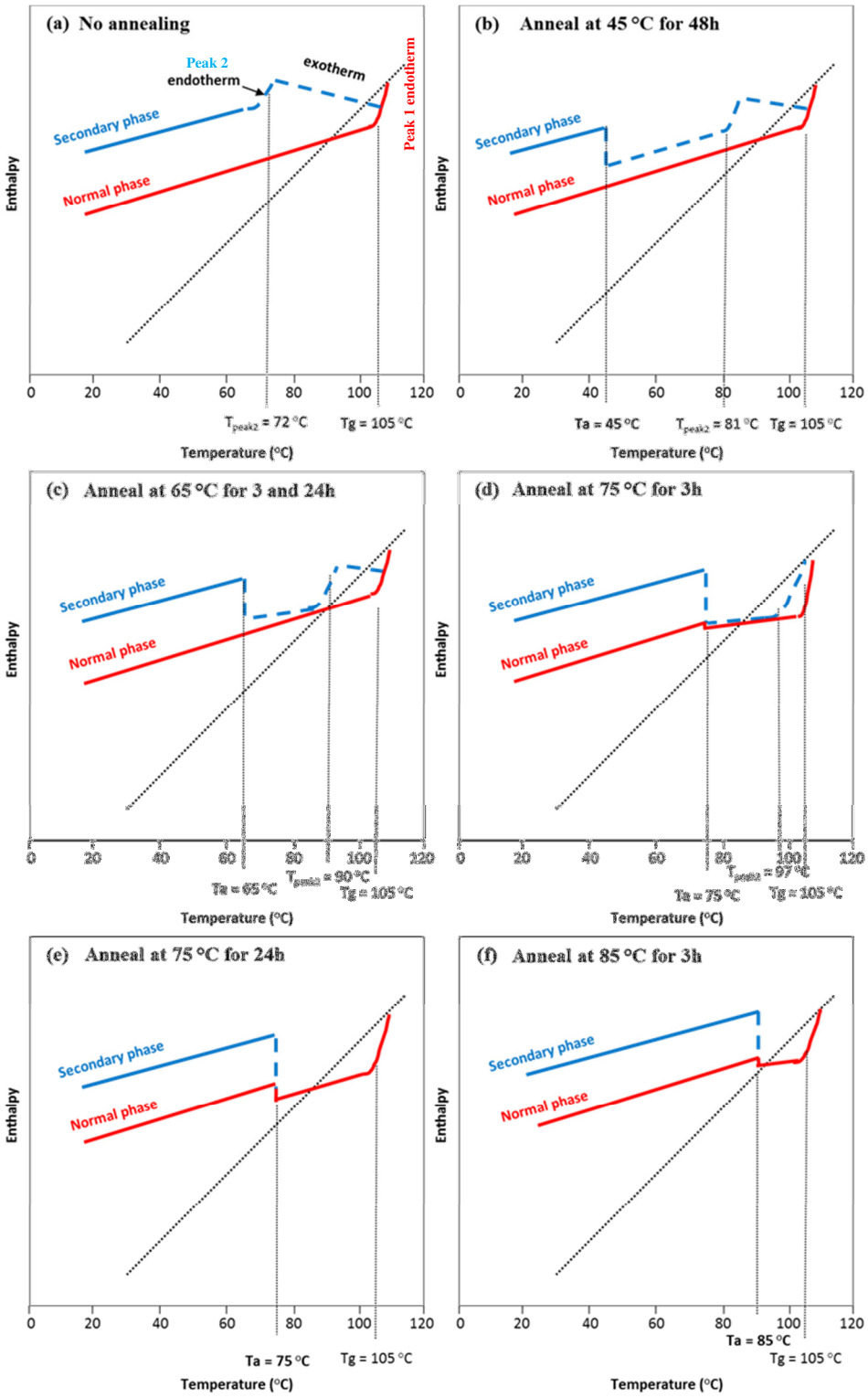

Figure 3.12 Schematic representation of the effect of annealing on the enthalpy-temperature curve showing the normal phase (red) and the secondary phase (blue) without annealing (a) and for the annealing conditions at 45 °C for 48h (b), at 65 °C for 3h and 24h, at 75 °C for 3h (d), at 75 °C for 24h (e) and at 85 °C for 3h (f).

3.5). Annealing below T_g results in a decrease in volume and therefore an increase in density of the secondary phase.[114, 127]

Increasing the annealing temperature to 65 °C is still exothermic and provokes a partial return of the secondary phase density and enthalpy towards the normal curve more efficiently than previous condition. The normal phase is not affected by annealing. The secondary phase remains less dense than the normal phase after the annealing process, yet it became denser due to increased temperature of annealing; the secondary endotherm is also displaced to higher temperatures followed by a small exothermic peak (figure 3.12c and purple curves in figure 3.5). The annealing of fibers at 75 °C for 3 h completely eliminated the exotherm between the two endotherms, due to the displacement of the secondary endotherm to higher temperatures (97 °C). Moreover, the normal phase is now also affected by annealing since 75 °C is sufficiently close to T_g. Thus, the annealing is exothermic for both normal and secondary phases (figure 3.12d and light blue curve in figure 3.5) and leads to overlapped endothermic peaks upon heating and reaching T_g. The final annealing condition at 85 °C for 3 h and 75 °C for 24 h affects both phases in the system. The process is exothermal and provokes an almost complete return of the secondary phase to the normal phase, resulting in a single enthalpic relaxation peak at T_g upon post-annealing heating. However, the position of the peaks is not identical, where the peak obtained from annealing at 75 °C for 24 h is displaced to lower temperatures by 2 °C. It is possible that some residual secondary phase remains in the system at this condition, resulting in the overlap of two peaks (figure 3.12 e and blue curve in figure 3.5, and 3.12f and navy curve in figure 3.5).

Annealing of amorphous polymers their below glass transition temperature provokes changes in many physical properties such as a decrease in volume and enthalpy. The rate of this relaxation depends on the temperature and the thermal history of the material.[127] Enthalpic relaxation is a particularly convenient property to investigate due to its accessibility from the nonreversing heat flow signal in TMDSC. Moreover, enthalpic relaxations allow to further investigate the influence of the molecular weight of the polymer and the concentration of the solution and to correlate these thermal phenomena

to the core-shell model proposed in previous work, where the core would be characterized by the main normal phase and the shell by the presence of the secondary phase. Figure 3.13a presents the nonreversing heat flow signal from TMDSC measurements for PS fibers with the three molecular weights studied. ΔH represents the enthalpic relaxation of samples whose thermal history was first erased by heating well above T_g and were then annealed at 75 °C for 3 h. Since the amount of enthalpic relaxation is related to the free volume present in the system, high molecular weight polymers, having less free volume and lower mobility due to the longer chains, generally have lower values of ΔH.[128-129] Indeed, a small decrease in enthalpic relaxation with increasing molecular weight was observed experimentally (figure 3.13b).

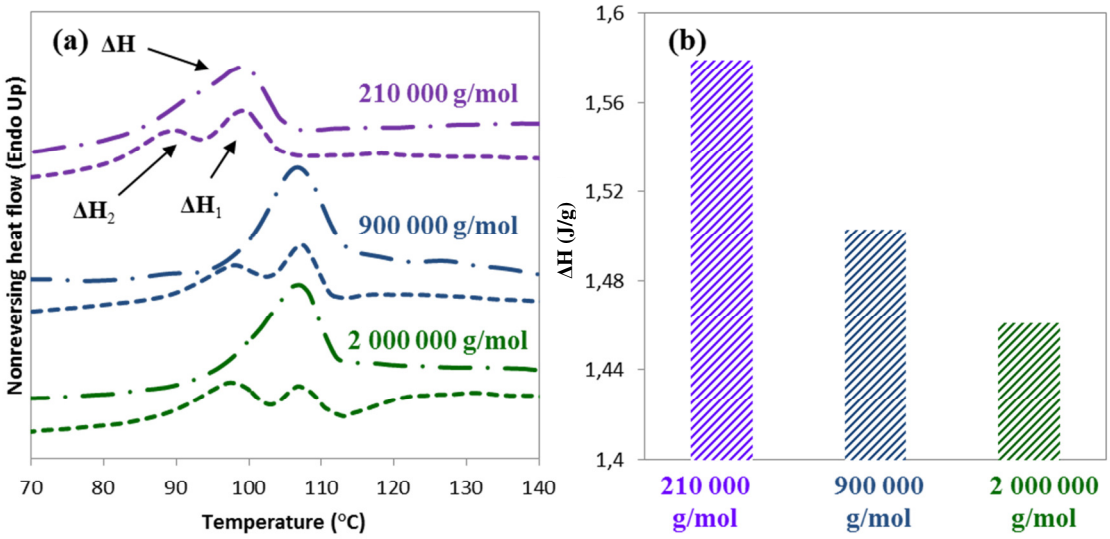

Figure 3.13 (a) TMDSC curves of PS fibers electrospun from chloroform solution showing the nonreversing heat flow signal for three molecular weights. (- - - - -) is the first heating run for fibers annealed at 75 °C for 3h and the (- · - · -) are the results of identical annealing conditions on samples whose thermal history was previously erased by heating well above T_g. (b) Enthalpic relaxation of the samples with erased thermal history annealed at 75 °C for 3h.

Furthermore, the enthalpic relaxations for the normal phase (ΔH_1) and the secondary phase (ΔH_2) were also estimated as a function of both the molecular weight and concentration for the samples annealed at T_g - 30 °C for 3h. This annealing condition generates enthalpic relaxations for two phases without an apparent contribution of the

exotherm between the two endotherms. Considering first the ΔH_1 of the normal phase, its values increase with decreasing concentration for a given molecular weight. The decrease in concentration results in more free volume present in the system, contributing to the increase in enthalpic relaxation. The effect of concentration on the enthalpic relaxation becomes more pronounced with increasing molecular weight, since the length of the chains affects the amount of relaxation (figure 3.14a). On the other hand, the ΔH_2 of the secondary phase is unaffected or decreases with decreasing concentration for a given molecular weight (figure 3.14b). Although the effect is small, it is consistent with previous results from an ATR-IR study where the band associated with this partial disentanglement was more pronounced for fibers produced from a lower solution

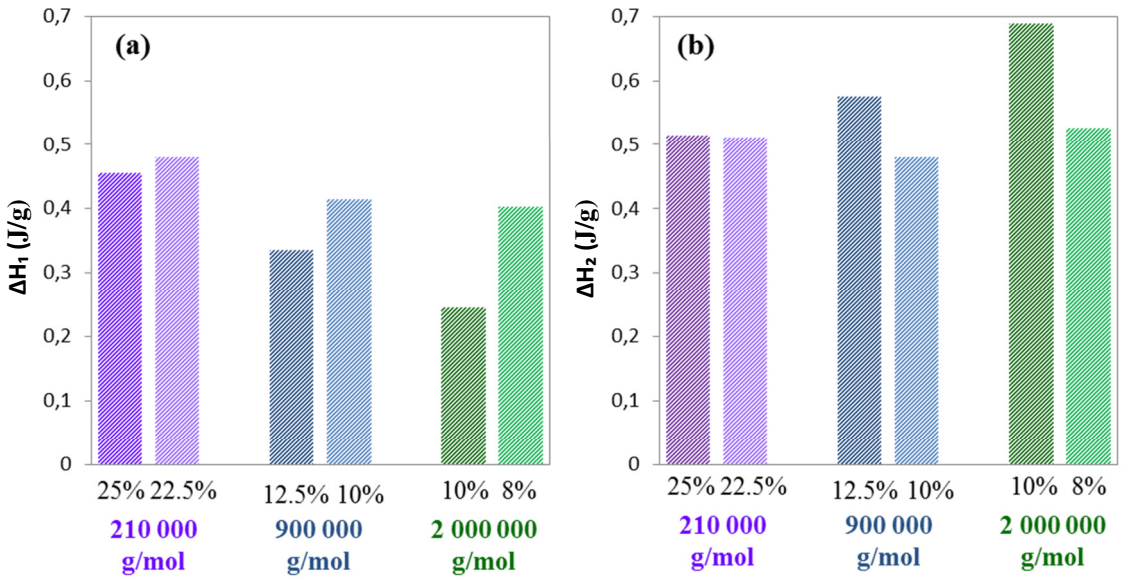

Figure 3.14 Enthalpic relaxation of the fibers annealed at 75 °C for 3h as a function of molecular weight and concentration for (a) the normal phase (ΔH_1) and (b) the secondary phase (ΔH_2).

concentration.[106]

It is essential to note that the lower concentration used in this study for each molecular weight generated beaded fibers, which are much bigger in diameter than the fibers. SEM images of PS fibers electrospun from chloroform solutions for three molecular weights and at two concentrations are shown in the appendix (figure A1).

Even though the outer shell solidifies faster than the core due to ultrafast solvent evaporation during electrospinning, beads, due to their size, are predominantly composed of entangled chains. Therefore, beads are expected to be determined by bulk entangled polymer. Consequently, the contribution of the beads must be taken into consideration since the measurements were performed on the bundles of fibers, which complicates the study of the effect of the concentration and molecular weight on the formation of the secondary phase and estimation of ΔH_2.

For unbeaded fibers obtained using the highest concentration for each molecular weight, enthalpic relaxation of the secondary phase increases with increasing molecular weight. Since the fibers electrospun from chloroform solutions at different concentrations and molecular weights all have approximately the same diameter (figure A1), it is possible to conclude that the volume fraction of the secondary phase would increase with increasing molecular weight (figure 3.15). This could explain the concomitant decrease in ΔH_1 of the normal phase with increasing molecular weight. Thus, solution concentration and molecular weight of the polymer strongly influence the structural organization of PS fibers.

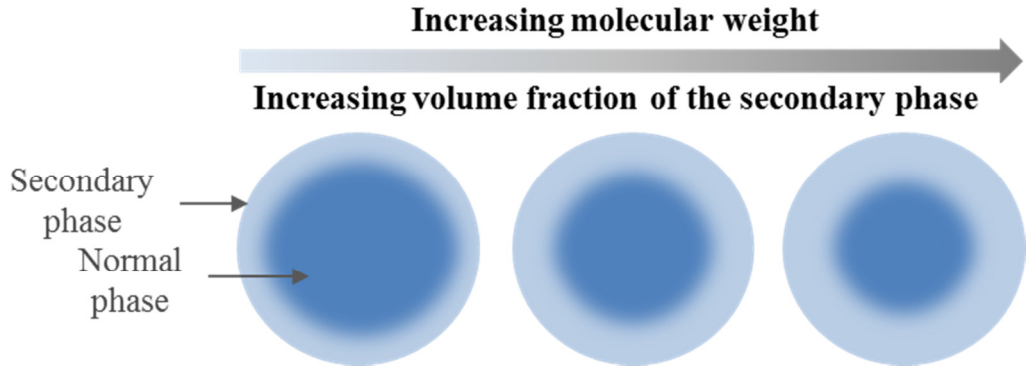

Figure 3.15 Schematic representation of the volume fraction of the secondary and the normal phases in PS fibers as a function of molecular weight

An alternative quantification of the amount of the normal and secondary phases was performed for the system by normalizing the ΔH_1 and ΔH_2 values with respect to the ΔH value determined for PS sample with erased thermal history that was annealed at the same conditions. It resulted in a small fraction of the normal phase, ranging from 15 to

30%. The results seem implausible since it is believed that the normal phase is dominant within the fibers with the secondary phase present in a thin shell. Yet, the greater relative amount of the secondary phase could possibly be explained by the effect of self-plastification of the mobile phase during annealing of the secondary phase in the DSC experiment. Essentially, the secondary phase could act as a plasticizer for the normal phase, resulting in lower ΔH_1 values.

3.2 AFM-IR characterization of single PS electrospun fibers

As indicated in the introduction, ATR-IR spectroscopy was previously used in order to detect and quantify conformation sensitive bands associated with partial disentanglement in PS electrospun fibers. [106] It was reported that highly volatile solvent such as chloroform and a short collection time of around 1 min are necessary to observe these bands. The IR bands characteristic of partial disentanglement are located at 1262, 1098 and 803 cm^{-1}, and their intensity increases with decreasing solution concentration from 15 down to 10% w/v. The bands associated with partial disentanglement were first reported in PS samples freeze-dried from highly diluted solutions, where the density of chain entanglements is lower than in the equilibrium bulk state.[102] On the other hand, these bands were completely absent in solvent-cast films and PS solutions, which indicates that a specific local conformation is required in order to observe them.

The above measurements were performed on fiber bundles and are therefore characteristic of bulk behaviour. In order to further investigate the specific molecular conformation within PS fibers and the two phases observed in the previous section by thermal analysis, a novel technique, AFM-IR, which allows a direct investigation of the molecular organization at the single fiber scale, is employed. Essentially, this technique is a combination of atomic force microscopy (AFM) and IR spectroscopy for nano-scale characterization that provides AFM images and IR spectra simultaneously.[109] Due to the novelty of this technique, little research has been done on electrospun fibers using AFM-

IR. The Rabolt group used AFM-IR in order to investigate the morphological details of individual electrospun fibers.[130] As a result, the topographical information obtained by this powerful technique allowed to correlate the structure, processing conditions and chain orientation/crystallinity. In fact, they were able to investigate the formation of the stable, and most particularly of the metastable, crystalline phases in biodegradable and biocompatible poly[(R)-3-hydroxybutyrate-co-(R)-3-hydroxyhexanoate] (PHBHx) electrospun nanofibers. To the best of our knowledge, this technique has never been applied to study the microstructural organization of PS electrospun fibers.

It must be mentioned that the AFM-IR measurements were performed by Elise Siurdyban, a postdoctoral fellow in our research group, and the results are included in this thesis on the basis of collaborative work. The author spent a substantial amount of time optimizing and establishing instrumental parameters for the analyzed system due to the novelty of the technique and early problems with the instrument.

The AFM-IR measurements were performed on PS fibers electrospun from 10% w/v chloroform solutions using a molecular weight of 900 000 g/mol. These conditions were selected based on the results obtained by ATR-IR described earlier that showed the substantial increase of the 1262 cm^{-1} band for low solution concentrations in comparison to higher concentrations. Moreover, the instrument is highly sensitive to the thickness of the sample that should not exceed 1 µm. The thickness of PS fibers prepared with a concentration of 10% is on average 0.8 µm. The measurement of fibers electrospun from higher concentrations becomes challenging since their average size is close to 2 µm.

Since the AFM-IR technique allows taking an IR spectrum at a precise position of the AFM tip, two different tip positions were used to take spectra on a single PS fiber, specifically at the edge and at the center of the fiber as shown on the AFM image in figure 3.16a. A difference in the absorption of the 1262 cm^{-1} band between the edge and the center of the fiber was expected. According to the core-shell model, only the shell is partially disentangled, so that the presence of the 1262 cm^{-1} band should be seen at the

edge of the fiber. The signal at the center of the fiber should be more characteristic of the bulk core.

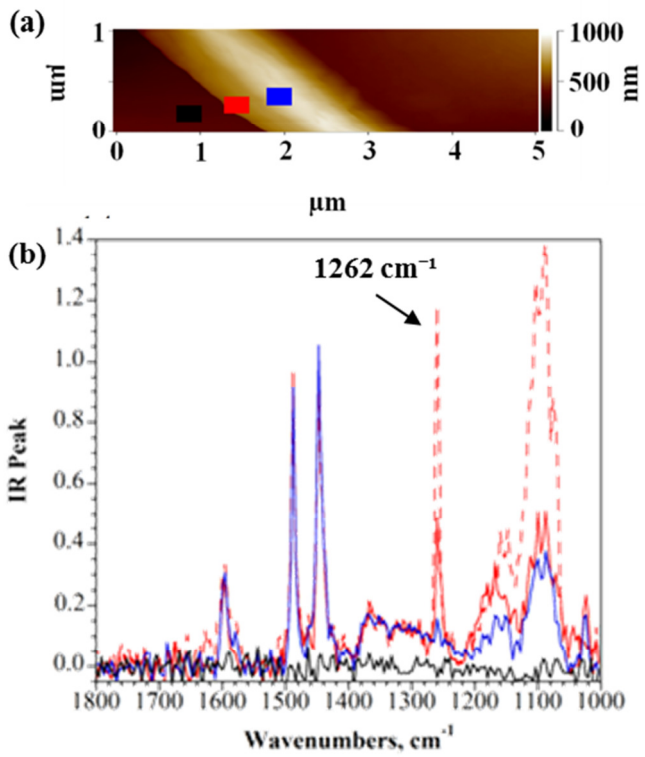

Figure 3.16 (a) AFM image of a single PS fiber electrospun from a 10% w/v chloroform solution and transferred onto a BaF_2 substrate. (b) IR spectra of the single PS fiber shown in the AFM image. The color markers on the AFM image indicate the approximate position of the AFM tip for each IR spectrum. The two red spectra are taken at the edge of the fiber.

In fact, the IR spectra at three different tip positions on the PS fiber in figure 3.16b clearly show a strong absorption of the 1262 cm^{-1} band at the edge, since it is mostly composed of the outer layer of the fiber. The band intensity substantially decreases when the spectrum is taken at the center of the fiber due to a strong contribution of the core to the absorption signal. The IR spectrum on the bare BaF_2 substrate is taken as a reference to demonstrate the lack of absorption in the region of interest. It is noteworthy that previous ATR-IR measurements that were performed on bundles of fibers resulted in very weak intensity of the 1262 cm^{-1} band in contrast to a very strong absorbance

observed here by AFM-IR. Even though the relative intensities are very different for these two techniques and cannot be directly compared, the results from ATR-IR suffer from an underestimation of the absorption of the 1262 cm^{-1} band due to the contribution of the beads to the measurements since they have a very thin shell and a strong contribution of the core to the signal. Hence, results from AFM-IR, performed on a single fiber, represent a more realistic indication of the heterogeneity within PS fibers.

Additionally, chemical maps of the single PS fiber were acquired. Essentially, maps obtained with AFM-IR show the spatial variation in the absorption of a specific band and therefore the spatial variation in concentration of the chemical structure at the origin of this band. The mapping was performed to obtain the spatial distribution of the 1262 cm^{-1} band on the PS fiber. In order to have a qualitative representation of the band distribution, chemical mapping of the 1449 cm^{-1} band, which is due to a highly intense aromatic C=C stretching vibration of PS, was also performed. Figure 3.17a shows an AFM image of the PS fiber and figures 3.17b and 3.17c are the chemical maps of the 1449 and 1262 cm^{-1} bands, respectively. It can be seen that the C=C vibration group of polystyrene is present on the whole surface of the fiber, characterized by a strong absorption signal, although the intensity is not uniform on the fiber (figure 3.17b). Since the scan is performed in contact mode, the cantilever is highly sensitive to the topography of the fiber and the wrinkled morphology of the PS fibers electrospun from chloroform solutions results in an inhomogeneous surface. The absorption intensity is also proportional to the sample thickness. Therefore, due to the wrinkled morphology, the thickness is not uniform along the fiber and the absorption is weaker at the wrinkles.

On the other hand, the 1262 cm^{-1} band is clearly present solely along the edge of the fiber and is much weaker at its center (figure 3.17c). Even though the strong absorption is only observed at the left edge of the fiber, it is expected to occur at the right edge as well. The absence of symmetrical absorption for the 1262 cm^{-1} band on both edges of the fiber is an artefact of the AFM measurement. Since the scan is performed in contact mode from left to right, and is highly sensitive to the roughness and topography of the sample, there is a decrease in sensitivity of the AFM tip as it goes from the fiber to the

substrate. This can be clearly seen in the AFM image (figure 3.17a), where the left edge of the fiber is well defined, whereas the right edge is blurred, the same phenomenon can also be seen in figure 3.16a.

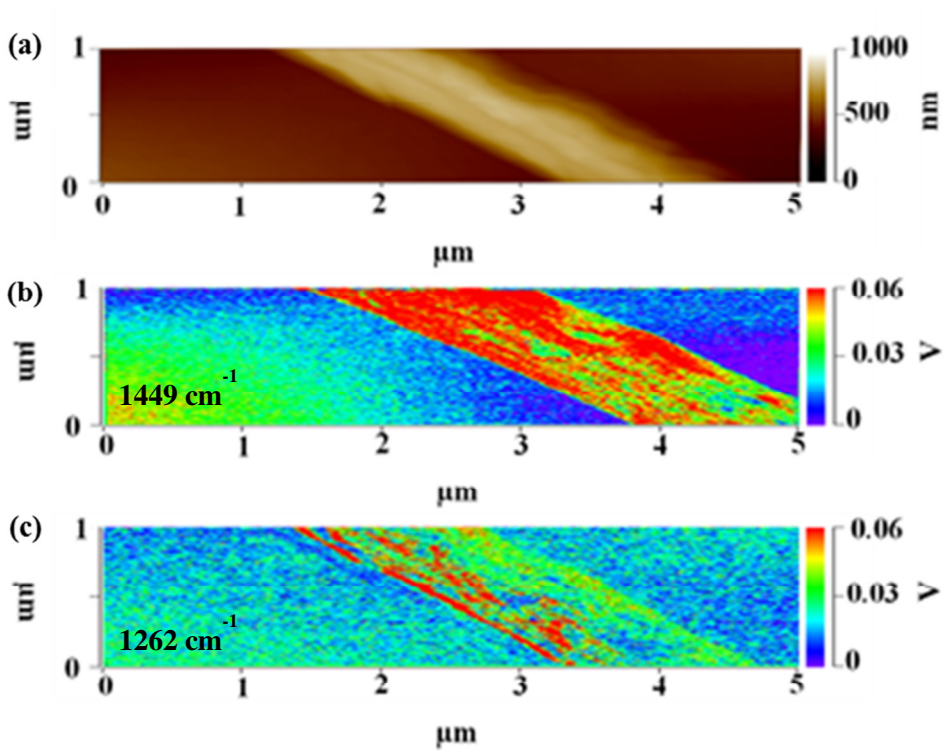

Figure 3.17 (a) AFM topographic image of a single PS fiber electrospun from a 10% w/v chloroform solution transferred onto a BaF_2 substrate; corresponding chemical maps of the 1449 cm^{-1} band (b) and the 1262 cm^{-1} band (c).

Overall, the AFM-IR measurements on the PS fibers clearly demonstrate the discrepancies in chemical composition between the edge of the fiber and its center, which can be interpreted as a support for the presence of two phases within the fibers. The results are therefore consistent with the TMDSC data, where a small secondary enthalpic relaxation peak was observed well below the glass transition of bulk PS. Thus, the band associated with partial disentanglement appears to be characteristic of the secondary phase in the outer shell of the fiber.

Furthermore, annealing of the PS fibers at different conditions was performed to investigate their thermal behavior, as was done for the secondary phase using TMDSC in the previous section. Thus, if the secondary phase can be characterized by the presence of the 1262 cm^{-1} band, the next step is to assess what happens to the secondary phase with annealing in terms of the presence and spatial variation of the 1262 cm^{-1} band. PS fibers were subjected to three different annealing conditions: 75 ºC for 3 h, 75 ºC for 24 h and 150 ºC for 3 h. The corresponding chemical maps are depicted in figure 3.18a, b and c, respectively. As earlier, the spatial variation in the intensity of the 1262 cm^{-1} band is complemented with the absorption of the 1449 cm^{-1} band as a reference signal from bulk PS. Incidentally, the effect of different annealing conditions on the thermal behavior described in the previous section was studied on PS fibers electrospun from 12.5% w/v solutions, whereas the AFM-IR measurements were performed on a lower concentration of 10% w/v. Yet, the results can be compared since it has been demonstrated that the fibers exhibit the same thermal behavior with annealing for all concentrations (figure 3.8).

First, there is a clear difference between the absorption of the 1262 cm^{-1} band without annealing (figure 3.17c) and after 3 h at 75 ºC (figure 3.18a). The band is still present but displaced from the edge of the fiber towards the center, accompanied by a decrease in absorption intensity. It is clear that the fiber is nevertheless still composed of two phases. Similarly, two enthalpic relaxations were observed in the TMDSC curves representative of a two-phase system (figure 3.8). It should be recalled that 75 ºC is the temperature at which the secondary endotherm was observed in the unannealed fibers in TMDSC curves (figure 3.7). Therefore, annealing at this temperature should make the secondary phase denser. Since the 1262 cm^{-1} band is associated with partial disentanglement, the densification of the secondary phase translates to a decrease in the band intensity.

Increasing the annealing time from 3 to 24 h at 75 ºC results in further decrease in the intensity of the 1262 cm^{-1} band (figure 3.18b). The result is identical when the fibers were annealed well above the normal glass transition at 150 ºC (figure 3.18c). The only

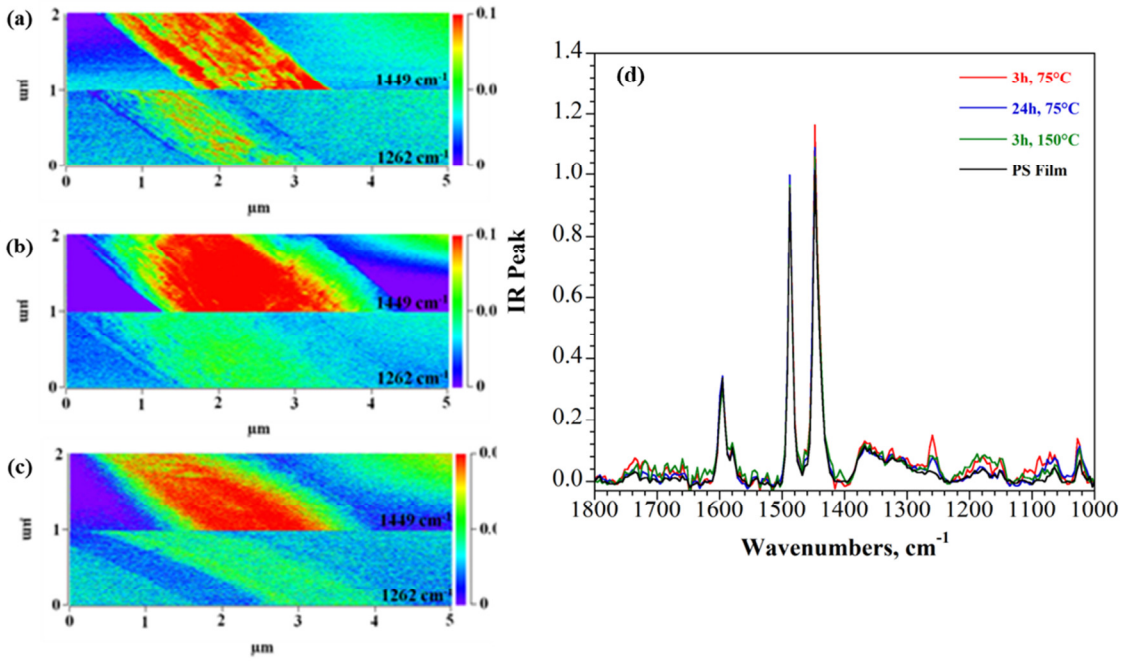

Figure 3.18 Chemical mapping of the 1449 cm^{-1} (top) and 1262 cm^{-1} band (bottom) of PS single fibers electrospun from 10% w/v chloroform solutions transferred onto a BaF_2 substrate for different annealing conditions (a) 75 °C for 3 h, (b) 75 °C for 24 h and (c) 150 °C for 3 h, and (d) corresponding IR spectra.

difference is that the fiber becomes much softer and flatter, since the polymer transitioned from the glassy to the rubbery state. In fact, at 150 ºC, the fibers are still not fully in the viscous state and retain their structural characteristics. It is due to the fact that the polymer is in the rubbery plateau region. It is generally determined by dynamic mechanical studies, where at the glass transition there is a sharp drop in the elastic modulus, which becomes almost constant in the rubbery plateau region. There, a polymer exhibits long range rubber elasticity; it can be substantially stretched and snap back to its original length upon release for short deformation times.[131] Moreover, the length of the rubbery plateau is a function of the number of entanglements per molecule and therefore increases with increasing molecular weight of the polymer. For a high molecular weight such as 900 000 g/mol, the rubbery plateau of PS spans over a wide range of temperatures.[132-133] Hence, the intensity of the band remains similar for these two annealing conditions, which is clearly seen in the IR spectra in figure 3.18d. Yet,

only one phase was observed during thermal analysis after annealing under these conditions. This means that the secondary phase does not fully transform into the normal/main phase and that there is still a small amount of the residual secondary phase even above T_g. Moreover, the IR spectrum of a spin-coated PS film was acquired as a reference, where the band at 1262 cm^{-1} was expected to be absent (black spectrum in figure 3.18d), which is indeed the case.

A model of the effect of annealing on the microstructural organization in the PS fibers can be summarized as depicted in figure 3.19. At ambient conditions without annealing, two distinct phases are present, where the normal phase is characteristic of normal bulk PS and the secondary phase where the chains are partially disentangled in the outer shell and are characterized by an intense IR band at 1262 cm^{-1}. The annealing at 75 ºC for 3 h makes the secondary phase denser, which translates to a decrease in the

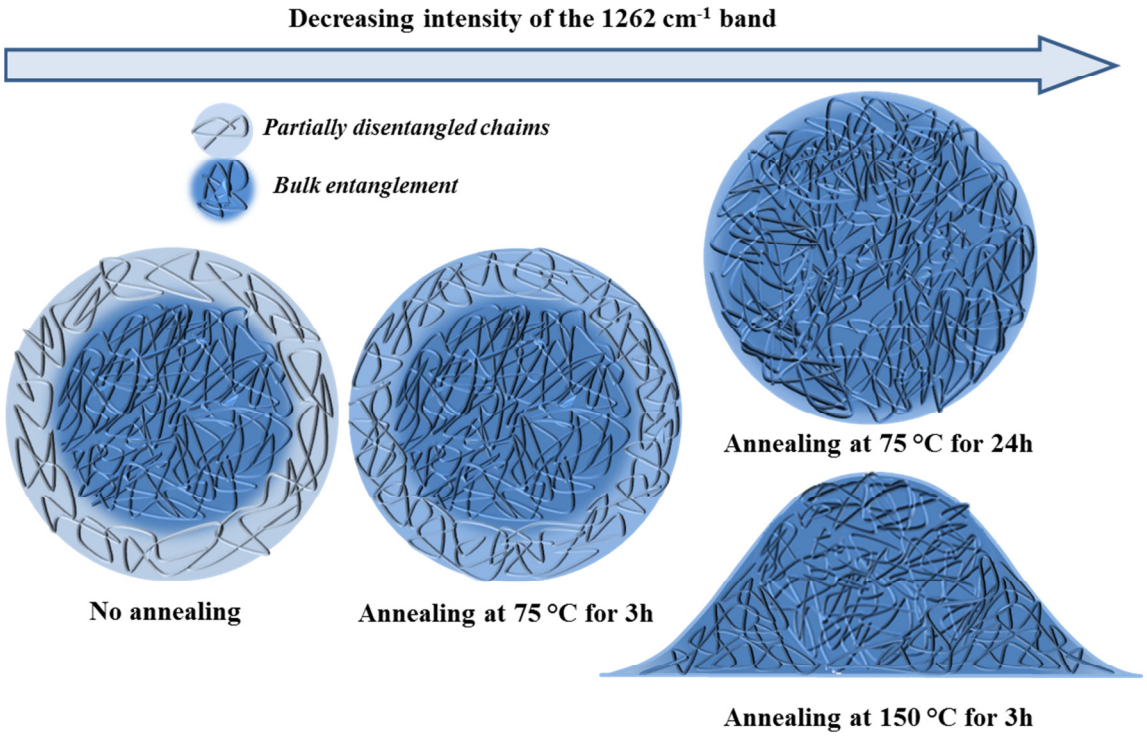

Figure 3.19 Schematic representation of the two phase system in the cross-section of PS fibers with partially disentangled chains in the outer shell and bulk entanglement in the core. The effect of different annealing conditions on the internal microstructure is presented where darker color represents a denser phase and lighter color a less dense phase.

1262 cm^{-1} band intensity. Increase in annealing time or temperature above the glass transition results in a further decrease in the 1262 cm^{-1} band intensity, although the residual secondary phase remains. Overall, these results are complementary to the observations by thermal analysis and allow for a more complete understanding of the internal organization of chains in PS fibers.

3.3 Effect of solvent and concentration on morphology of PS fibers

In the previous work, only PS fibers electrospun from chloroform solutions were studied since it was hypothesized that a low boiling point solvent is necessary in order to observe additional IR conformational bands associated with partially disentangled chains in the outer shell of the fiber. Hence, the two previous sections were focused on the detailed analysis of the thermal properties and AFM-IR characterization of PS/$CHCl_3$ system. Next, our goal is to use TMDSC to test this hypothesis by using solvents of different boiling points. Since another hypothesis was that a wrinkled morphology is also necessary for the observation of these IR bands, the effect of the solvent on the morphology of the PS fibers is also investigated.

During the electrospinning process, many processing and solution parameters can be tailored in order to optimize properties of the resulting fibers or their morphology. In this work, all processing parameters, namely the applied potential, flow rate and working distance, were kept constant for all systems prepared. The parameters that were varied are the solvent, solution concentration and molecular weight in order to study their effect on fiber morphology. Table 3.2 outlines the properties of the four solvents used this work. Chloroform, tetrahydrofuran (THF) and methyl ethyl ketone (MEK) have relatively similar boiling point values and are considered to be highly volatile solvents. However, they are expected to produce different morphologies, since the fiber formation mechanism depends on the solvent and will be closely examined. N,N-dimethylformamide (DMF) on the other hand, was chosen to see the effect of high boiling point on the electrospinnability of PS fibers.

Table 3.2 Properties of the four solvents used in this work.[97]

Solvent	Boiling point (ºC)	Density (g/cm^3)	Dipole moment (Debye)
$CHCl_3$	61.2	1.470	1.01
THF	66.0	0.875	1.63
MEK	79.6	0.794	2.76
DMF	153.0	0.940	3.82

Figure 3.20 summarizes the effect of the solvent and concentration on the morphology of PS fibers. Generally, a reduction in solution concentration leads to a decrease in fiber diameter. In the present study, concentrations were selected such that the fiber diameter is in the same range in order to keep this parameter constant and avoid its possible influence on other properties of the system. Yet, solution concentration has a pronouced effect on the morphology of fibers. It can be clearly seen that at low concentration, beaded fibers are obtained for all solvent systems (except for MEK since

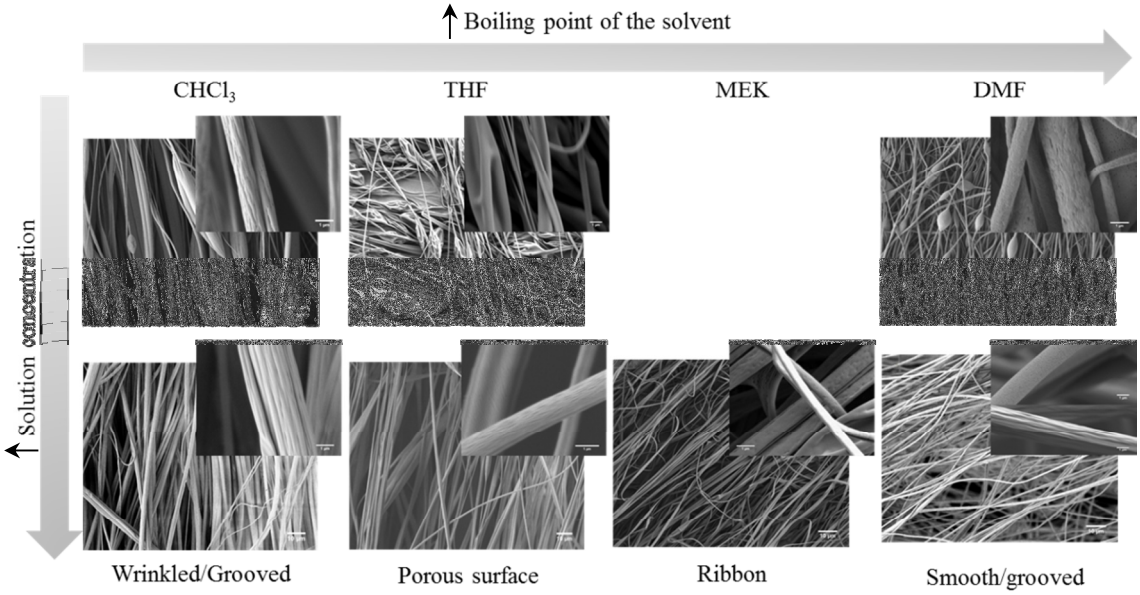

Figure 3.20 SEM micrographs of PS fibers showing different morphologies obtained by changing the solvent and solution concentration. The scale bars are 10 and 1 μm for the global and the zoomed images, respectively.

only one concentration was used that generates unbeaded fibers). In the case of low viscosity of the solution, surface tension contribution is high enough during fiber formation to lead to beaded fibers. Increase in the solution concentration generates continuous fibers. However, different morphologies are obtained depending on the solvent used.

Grooved fibers were obtained when fibers were electrospun from chloroform and DMF solutions. However, the mechanism of formation of such texture is different for those two solvents. The fist stage is the formation of a glassy skin on the jet surface, which would be the same regardless of the solvent used. In chloroform solutions, the grooved fibers are formed based on wrinkles formation and an elongation process as shown in figure 3.21b. Essentially, wrinkles originate from buckling of the cylindrical polymer shell due to the influence of compressive radial stress arising from fast removal of the solvent from the core of the fiber, due to high volatility of chloroform. The grooved texture is then formed due to the stretching of the wrinkles and rapid solidification of the jet (figure 3.21b).[98, 134-135]

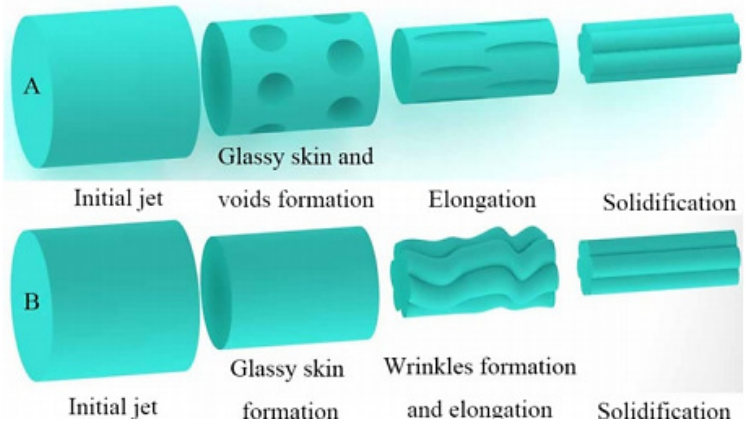

Figure 3.21 Two mechanisms of the formation of grooved fibers: void-based formation (a) and wrinkles formation (b). Reproduced with permission from ref 95 Copyright © 2015 Springer.

DMF, on the other hand, is a high boiling point solvent. The fiber formation mechanism is void-based elongation (figure 3.21a). The jet remains "wet" and stretchable due to the low volatility of the solvent. This allows the subsequent elongation

of the glassy skin and voids into grooves.[135-136] It is important to mention that water has a much greater affinity for DMF than chloroform. Hence, the voids that are formed on the surface of the fibers are due to the water condensation resulting in phase separation. Humidity will therefore have a great influence on morphology when fibers are electrospun from DMF solutions.[77, 137]

PS fibers electrospun from THF solution have a characteristic porous surface morphology. This type of texture is generated through a mechanism that was classified as breath figures, characteristerized by evaporative cooling arising from rapid solvent evaporation. It was first observed on thin films, where the pores were hexagonally ordered on the surface.[138] As the jet travels to the collector, cooling of the surface occurs and moisture present in the air, which acts as a nonsolvent for PS, condenses on the surface of the fiber in the form of droplets that act as hard spheres. As the jet solidifies, the resulting fibers have pores on the surface resulting from the imprint of the water droplets. However, the pores on the surface of the fibers are never ordered as in the breath figures pores, since the mechanism of fiber formation during electrospinning is much more complex. As the jet travels through the moist air, its motion and elongation must be taken into account, as well as the charges it carries. These factors can then influence the ordering of the pores and their density on the fiber surface.

Ultimately, another mechanism of porous surface morphology of the fibers, in comparison to breath figures, is characterized by liquid/liquid plase separation, followed

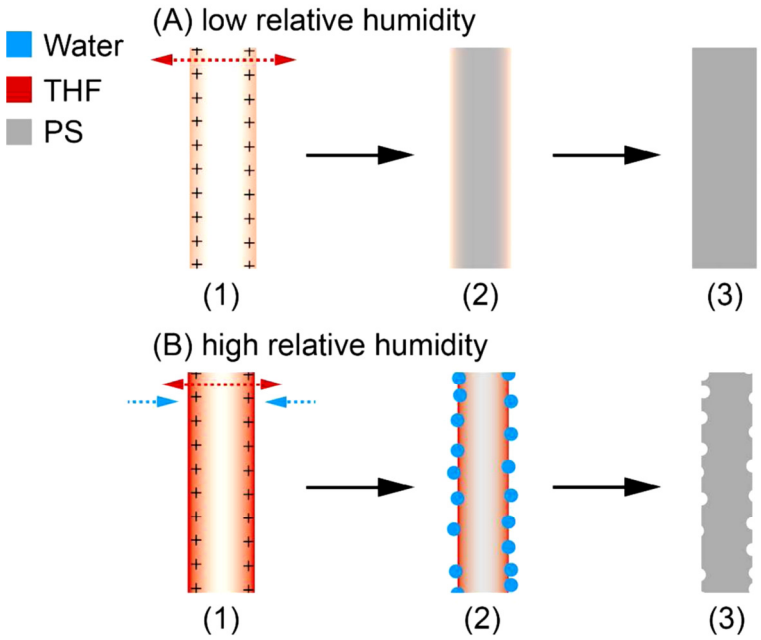

Figure 3.22 Schematic representation of the structural characteristics of the jet (1) immediately after ejection from the needle, (2) during the whipping and stretching and (3) upon drying on the collector showing the effect of low (A) and high (B) relative humidity. Reproduced with permission of ref. 139 Copyright © 2013 American Chemical Society.

by gelation of the polymer.[99] This process is probably more suitable for describing the porous morphology due to the fact that phase separation is driven by thermodynamic instability, which is in turn a driving force in the electrospinning process. The solution becomes thermodynamically unstable due to a decrease in temperature, loss of solvent or increase in nonsolvent.[76] Furthermore, since pores formed on the surface of electrospun fibers are due to the moisture condensation, relative humidity will have a direct influence on their size. It has been shown that in PS/THF systems, increase in relative humidity results in increased porosity on the surface, whereas fibers electrospun in conditions of low humidity have a smooth surface (figure 3.22).[76, 139]

Another parameter that affects the size and shape of the pores on the surface of fibers is the molecular weight. It has been demonstrated that increasing the molecular weight of the polymer causes the formation of larger pores that are less uniform in shape and size.[76] In fact, this trend is observed for the PS/THF systems prepared in this study where the pore size and distribution increases when the molecular weight increased from 900 000 g/mol to 2 000 000 g/mol, as shown by the SEM micrographs presented in the appendix (Figure A2).

The final type of morphology obtained in this work is the ribbon-like structure generated from PS/MEK solutions. In the early stages of electrospinning, a solidifying skin is formed. In this case, however, as the solvent in the core of the fiber evaporates, the atmospheric pressure forces the tube formed by the shell to come into contact at separate points.[30] The contact area then increases by the growth of connection points between the opposite sides of the tube driven by the cohesive forces. Overall, the circular cross section becomes elliptical and then flat, resulting in a ribbon-like shape, as shown in figure 3.23. The resulting width of the ribbon is nearly the same as the diameter of the tube before the collapse.

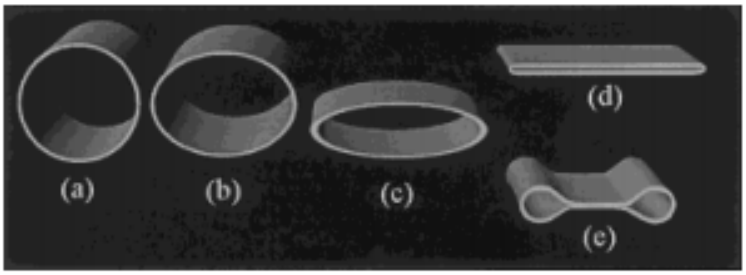

Figure 3.23 Schematic representation of the progression of the collapse of the skin of the jet to form a ribbon-shaped fiber. Reproduced with permission of ref. 30 Copyright © 2001 John Wiley & Sons, Inc.

It has been shown that ribbon-like fibers are formed from solutions of volatile solvents, which is needed for the formation of the solid shell with a solvent-rich core.[140] However, solutions with chloroform, which is more volatile than MEK, result in round fibers as was shown earlier. It can be hypothesized that intermediate volatility will

promote the formation of flat ribbon fibers. Therefore, solvent volatility is not the only factor that governs the formation of ribbon-like fibers. It would also depend on the concentration of the solution, where higher viscosity may favour a more rapid solidification of the jet and result in such morphology.[87]

Since the fiber diameter should influence the volume fraction of the secondary phase in the outer shell, the goal was to prepare fibers with similar diameters in all solvent systems in order to perform a comparative study of the thermal behavior. Moreover, the presence of beads would have an effect on the overall interpretation of the TMDSC thermograms, as was shown in section 3.1 in PS/$CHCl_3$ systems. Figure 3.24 illustrates the fiber diameters measured for all four solvent systems at different molecular weights and concentrations used in this work. Evidently, the solution concentration has a direct influence on the diameter of the fibers as well as the presence/absence of beads. In fact, the diameter increases with solution concentration and beads disappear with increasing concentration. Yet, the diameters are relatively similar for all conditions, ranging from 1 to 2 µm, with the exception of two conditions in PS/DMF system (20% w/v and 900 000 g/mol, and 15% w/v and 210 000 g/mol), whose diameters are on average 20 and 7 µm, respectively (figure 3.24d). These concentrations were chosen in order to examine the effect of molecular weight for a given solution concentration.

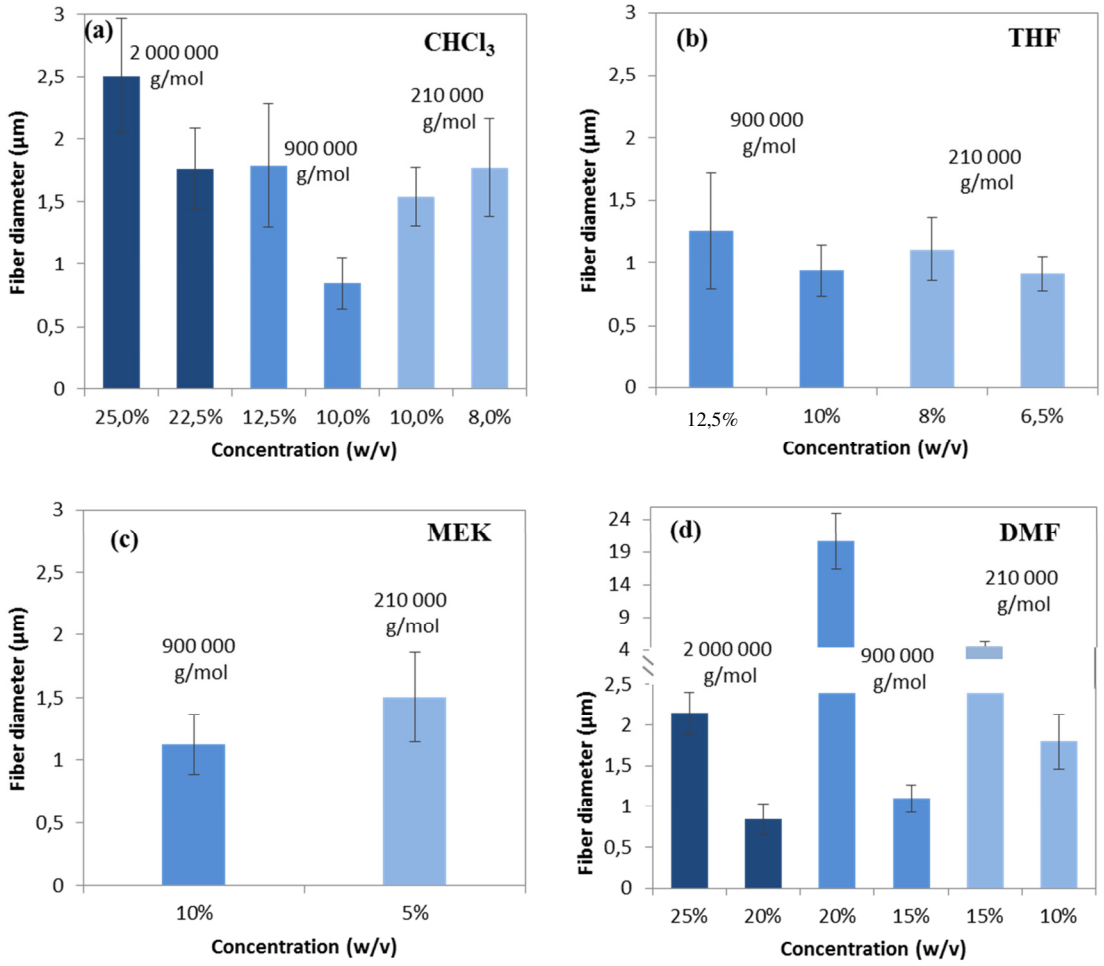

Figure 3.24 Diameter of the fibers as a function of concentration and molecular weight for fibers electrospun in four different solvents: chloroform (a), THF (b), MEK (c), and DMF (d). The error bars represent the average of 30 measurements.

3.4 The effect of solvents on the thermal behavior of PS fibers

A model for core-shell organization within PS electrospun fibers has been recently proposed by our research group.[106] The main assumption was that an ultra-fast solvent evaporation is necessary. The fast evaporation of the solvent during the jet's trajectory towards the collector would result in the formation of a solid shell, where the chains are partially disentangled. On the other hand, the solvent evaporation from the core of the fiber is more gradual, allowing for the reorganization of the chains in the most stable bulk entangled conformation. As a result, a core-shell morphology is formed. In fact, the

lack of the 1262 cm^{-1} IR band in fibers collected for long time was attributed to conformational change in the shell of the fiber due to the vapor pressure of the solvent that originated from the evaporation of the solvent from neighbouring fibers. Yet, all fibers electrospun in this work were collected after a long period of time (10 min). Moreover, a formation of the core-shell morphology has been associated in the literature with the wrinkled fiber morphology.[98] Therefore, the model for the core-shell organization within fibers was established on the PS system electrospun from highly volatile chloroform solution, which are known to have a wrinkled morphology, which was also confirmed by the morphology study in section 3.3.

For the PS fibers electrospun from chloroform solutions described in section 3.1, the presence of two phases, normal and secondary, identified by TMDSC, could be related to the core-shell organization. In this case, the secondary phase could be an indication of the shell, whereas the normal phase would correspond to the core of the fiber. The next step in this work was to generalize and refine this model using thermal analysis. In order to achieve this goal, the impact of different solvents on the thermal behavior in relation to the chain organization was studied.

Three solvents were selected that are known to produce continuous electrospun PS fibers, namely THF, MEK and DMF.[97] As discussed in the previous section, fibers electrospun from these solvents have different morphologies. The effect of solvent system used on the thermal behavior of the fibers is examined in details for the PS with a molecular weight of 900 000 g/mol for concentrations that generate unbeaded fibers with an average diameter of 1.3 µm for all solvent systems.

The main factor that differentiates these solvents is their boiling point. THF has a low boiling point of 66 ºC, which is very close to the value for chloroform (T_b = 61 ºC). Therefore, when only the effect of solvent volatility is taken into consideration in view of the proposed model, fibers electrospun from THF should be constituted of two phases. In fact, when the TMDSC thermograms of PS fibers electrospun from chloroform and THF are compared (black and red curves in figure 3.25, respectively),

both have a sub-T_g endotherm at 75 ºC followed by an exotherm. PS fibers electrospun from MEK solutions with higher boiling point (T_b = 79.6 ºC) also have an endotherm associated with the presence of secondary phase below T_g (figure 3.25, blue curves). However, it occurs at 65 ºC, which is 10 ºC lower than for chloroform and THF systems. The unusual thermal events that occur right after the glass transition should be regarded as artefacts of the measurement. These transitions, especially noticeable in the reversing

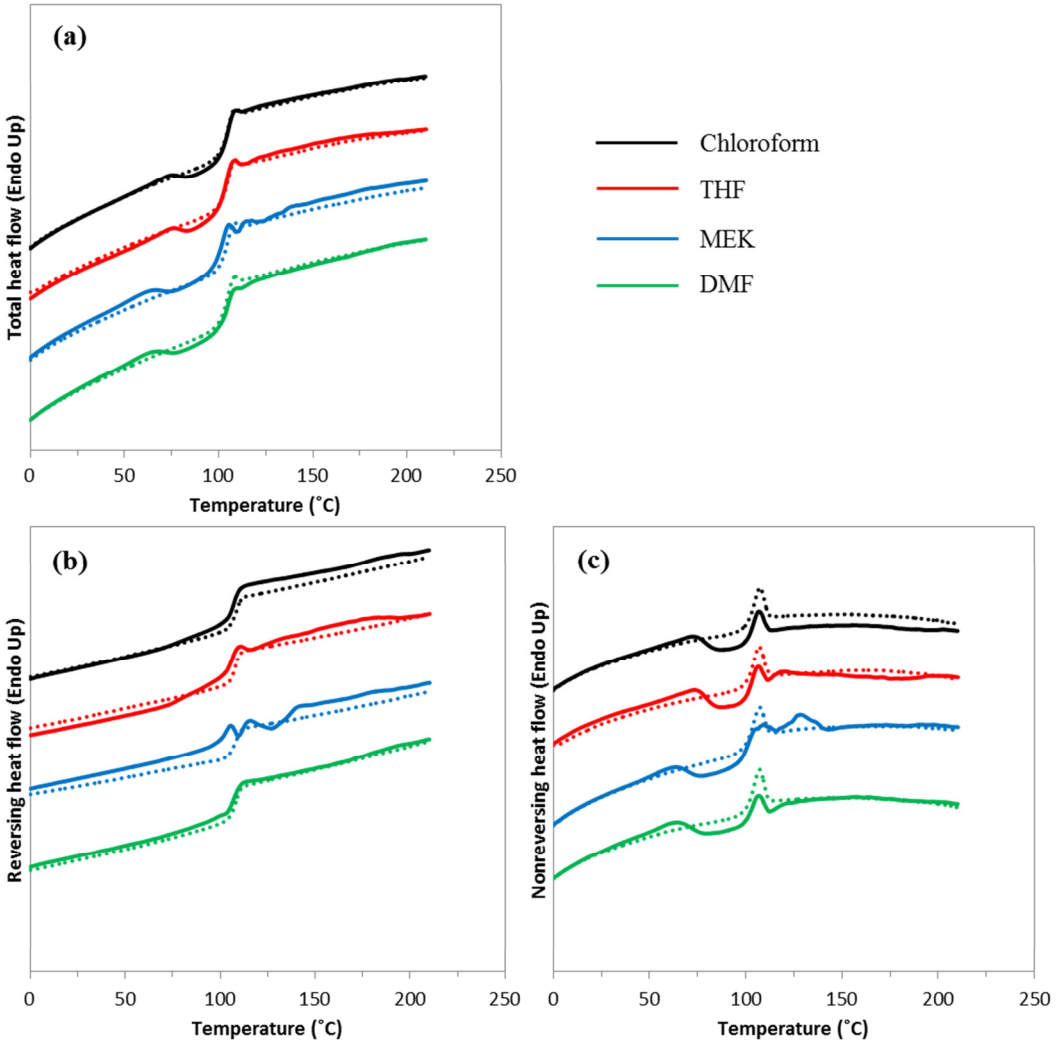

Figure 3.25 TMDSC thermograms of PS (M_w = 900 000 g/mol) electrospun from 12.5 % w/v chloroform (black), 12.5 % w/v THF (red), 10 % w/v MEK (blue) and 15 % w/v DMF (green) solutions showing the total (a), reversing (b) and nonreversing (c) heat flows. Solid lines represent the first heating run and dotted lines the second heating run.

and nonreversing heat flow, are due to a poor separation of the total heat flow and therefore cannot be used for the interpretation of the results. Yet, the total heat flow is representative of the thermal behavior of the sample.

Finally, the PS/DMF system was chosen as an extreme condition owing to a very high boiling point of the solvent (T_b = 153 ºC) (figure 3.25, green curves). Since it was originally assumed that an extremely fast solvent evaporation is necessary to observe two phases within PS fibers, using a solvent with a very low volatility such as DMF was expected to produce fibers with only one phase. Yet, it can be observed that there are indeed two phases in fibers electrospun from DMF based on the presence of the endotherm below T_g. The fibers electrospun from DMF solutions have a wrinkled morphology as in PS/$CHCl_3$ system. As in the case of PS/MEK, the secondary endotherm is located at a lower temperature (65 ºC) than for fibers prepared from chloroform or THF solutions. The solvent evaporation is much slower for these two solvents and therefore the chains are expected to be more entangled since they have more time to rearrange. Yet, the outer shell still solidifies faster than the solvent evaporation is completed, resulting in the formation of the outer shell.

Overall, it is possible to conclude that the secondary phase forms in the PS fibers regardless of the volatility of the solvent and the morphology of the fibers. All four solvents used in this work produce fibers with different morphologies, but a secondary phase is always present. Moreover, the ultra-fast solvent evaporation is not necessary as the secondary phase was observed using a solvent with high boiling point solvent such as DMF. Additionally, the solvent used to electrospun PS fibers does not affect the position of the T_g as seen in the reversing heat flow signal (figure 3.24b) and, for all solvent systems, the second heating run has solely the normal T_g representative of the bulk PS consisting of one phase.

The effect of concentration and molecular weight on the thermal properties of PS fibers electrospun from different solvents was finally studied. For PS/THF and PS/MEK systems, two molecular weights were used, namely 900 000 g/mol and 2 000 000 g/mol,

since the results were expected to be similar to those observed for PS/chloroform system. On the other hand, PS/DMF system was investigated more closely using three molecular weights in order to establish the effect of high boiling point solvent on the thermal behavior. For all three solvents, THF, MEK and DMF, the trend was identical as for PS/chloroform system described in section 3.1. The increase in molecular weight results in a displacement of the secondary endotherm further from T_g to lower temperatures, owing to higher degree of entanglements in solution. Similarly, for a given molecular weight, the enthalpic relaxation peak associated with the secondary phase shifts to lower temperatures with decreasing solution concentration. The TMDSC thermograms for all three solvent systems at different molecular weights and concentrations are presented in appendix (figures A5-A9).

Furthermore, fibers electrospun from all solvent systems were annealed at T_g -30 ºC in order to observe two isolated endotherms corresponding to the normal and the secondary phases without the contribution of the exotherm observed in unannealed samples. Two endotherms are clearly seen in the nonreversing heat flow signal for all solvent systems used and for all molecular weights and concentrations, and the results are consistent with PS/chloroform system, validating the general nature of the phenomena described in more detail in section 3.1. All TMDSC curves for annealed samples for all three solvent systems at different molecular weights and concentrations are presented in appendix (figures A5-A9).

CONCLUSIONS AND FUTURE WORK

This work has focused on the investigation of heterogeneity in microstructural organization of PS fibers prepared by electrospinning by thermal analyses. In previous studies, a model of core-shell morphology was proposed for PS fibers based on ATR-IR measurements, where the shell would be composed of partially disentangled chains whereas the core would represent the bulk entanglement.[106] Several hypotheses were made about the requirements for the formation of the core-shell morphology, namely a highly volatile solvent that ensures ultra-fast evaporation, a high molecular weight for the polymer, a wrinkled morphology of the resulting fibers, and a relatively low solution concentration.

The first part of this work presented a detailed analysis of the thermal properties of PS fibers electrospun from the highly volatile solvent used in the previous studies, chloroform, using three molecular weights of the polymer (210 000, 900 000 and 2 000 000 g/mol) at different solution concentrations. TMDSC thermograms revealed the presence of a sub-T_g endotherm followed by an exotherm that was associated with the presence of a secondary phase within PS fibers. This phase is less dense and therefore occurs below the glass transition of bulk PS. This phenomenon was observed for all molecular weights and concentrations. If the presence of two phases detected by TMDSC can be correlated with the core-shell model, the secondary phase would be characteristic of the shell of the fiber and the normal phase characteristic of the core. Since the secondary phase was observed for all conditions, it is possible to reject two of the previously made hypotheses regarding the need for a low solution concentration and a very high molecular weight. Yet, molecular weight was shown to have an impact on the ΔT between the T_g and the secondary endotherm, which increased with increasing molecular weight of the polymer.

Annealing of PS fibers below the glass transition was performed in order to further evaluate the presence of two phases with different thermal properties and to understand

whether annealing would convert the secondary phase into the normal phase or amplify the thermal events associated to it. It was found that an increase in the annealing temperature from T_g – 60 °C to T_g – 20 °C results in the displacement of the secondary enthalpic relaxation peak towards the normal T_g until only one enthalpic relaxation peak remains.

Furthermore, AFM-IR characterization of single PS electrospun fibers was performed to validate the presence of the conformation-sensitive bands associated with partial disentanglement based on the previous work.[106] It was shown that the partially disentangled band at 1262 cm^{-1} is located mainly at the edge of the fiber. Moreover, after annealing of PS fibers at T_g – 30 °C for 3h (two enthalpic relaxations peaks in TMDSC) and for 24h (one enthalpic relaxation peak in TMDSC) and even after annealing above T_g at 150 °C, there was still residual absorption at 1262 cm^{-1}, which means that the secondary phase does not fully transform into the normal/main phase and there is still a small amount of residual secondary phase even above T_g. Finally, a model of the effect of annealing on the microstructural organization in the PS fibers was proposed. The results are complementary to the observations by thermal analysis and allow for a more complete understanding of the internal organization of chains in PS fibers.

The second part of this work focused on the study of the thermal behavior and morphology of PS fibers as a function of solvent volatility. Three additional solvents were selected to electrospin PS fibers: THF having a similar boiling point to chloroform, MEK with a slightly higher T_b and DMF with a very high T_b. For all solvent systems, the secondary endotherm below the glass transition was present in the TMDSC thermograms. Therefore, the two phase molecular organization within PS fibers occurred regardless of the solvent used. Moreover, electrospinning of PS from these solvents results in different fiber morphologies: wrinkled fibers from chloroform systems, circular fibers with porous surface from THF, ribbon-like fibers from MEK and smooth and/or wrinkled fibers from DMF. Even though the mechanism that generates these various morphologies is different as a function of the solvent used, thermal analysis revealed the presence of the secondary phase, in addition to the normal phase,

in all cases. Hence, the fiber morphology and the nature of the solvent do not have a critical effect on the two phase's chain organization in PS fibers. Overall, the relative ΔT between T_g and the secondary endotherm seems to depend on the solvent volatility, hinting at an effect on chain organization.

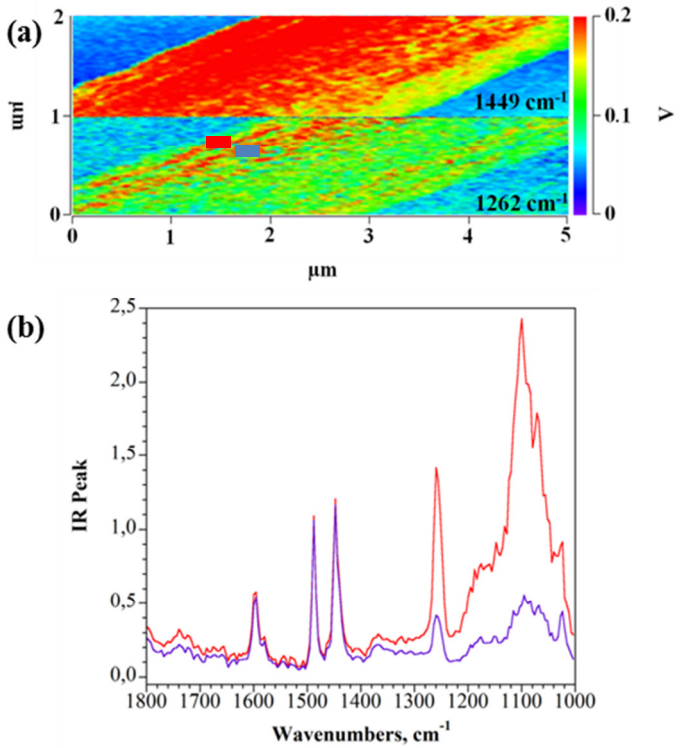

Figure 4.1 (a) Chemical mapping of the 1449 cm^{-1} (top) and 1262 cm^{-1} band (bottom) of PS single fiber electrospun from 20% w/v DMF solution (M_w = 210 000 g/mol) transferred onto a BaF_2 substrate and (b) corresponding IR spectra taken at two tip positions at the edge of the fiber.

To follow up this work, it is desirable to further investigate the two-phase organization within PS fibers using AFM-IR spectroscopy for the systems electrospun from high boiling point solvents such as DMF. The spatial variation in concentration of the chemical structure at the origin of 1262 cm^{-1} band was analysed for the PS/DMF system using a low molecular weight of 210 000 g/mol and a low solution concentration of 20% w/v, where the secondary phase was not expected to be present. However, even

in these conditions, the band associated with partial disentanglement was detected as shown in figure 4.1.

It is especially of interest to acquire the AFM-IR spectra and maps for the PS/DMF systems electrospun from high molecular weight of 900 000 g/mol at a low concentration such as 10% w/v in order to perform a direct correlation with the results obtained in this work for PS/$CHCl_3$ with 900 000 g/mol polymer and a concentration of 10% w/v. It would allow to make a direct comparison with the thermal properties obtained by TMDSC. Moreover, since the annealing at T_g – 30 ºC of both systems generate two endothermic relaxation peaks, the amount of both phases could be compared for the two solvent systems and correlated with the relative absorption of the 1262 cm^{-1} band, which provides insight into the chain organization of the outer shell and the normal core phase. It would also allow establishing a connection between the formation of the secondary phase and the morphology of the fibers electrospun from different solvent systems.

In continuation of this work, it is also of interest to study the observed phenomena in other systems, in particular in miscible blends of PS with poly(2,6-dimethyl-1,4-phenylene oxide) (PPO) electrospun from chloroform solutions. As was described in the introduction, electrospun PS fibers have diameter-dependent properties such as their molecular orientation.[83] In films of PS/PPO miscible blends, it was shown that the addition of the second component, PPO, increases the molecular orientation of the PS matrix.[141] In fact, IR measurements of the dichroic ratio of the absorption bands revealed that PPO orientation is independent of the PPO concentration in the range from 0 to 35%, whereas PS orientation increased with up to 25% of PPO and then remained constant beyond that point. Overall, the orientation of PPO was always larger than that of PS.

In spite of the compatible nature of the miscible blend, the PPO and PS chains are thus expected to orient in different ways when subjected to a uniaxial strain during electrospinning. In this context, the structural organization of chains could be studied by

AFM-IR spectroscopy, where the spatial variation of band absorption from PS and PPO at a single fiber scale could be obtained as a function of PPO fraction. In addition, thermal properties of miscible blends could be studied as a function of PPO fraction. Miscible blends are characterized by a single glass transition, whose position is dependent of the fraction of both polymers in the matrix. Preliminary measurements using DSC were performed on the PS/PPO system at a range of PPO weight fractions from 0 to 50% (figure 4.2). It can be seen that there is only one glass transition temperature characteristic of the miscible polymer blends that shifts to higher temperature towards the T_g of pure PPO (Tg = 215 ºC) with increasing PPO fraction. However, the secondary endotherm below the glass transition is observed as in the case of PS fibers studied in this work. The secondary endotherm also shifts towards higher temperatures with increasing PPO weight fraction that could be related to the decreased amount of chain entanglements with decreasing PS fraction. As a result, the secondary

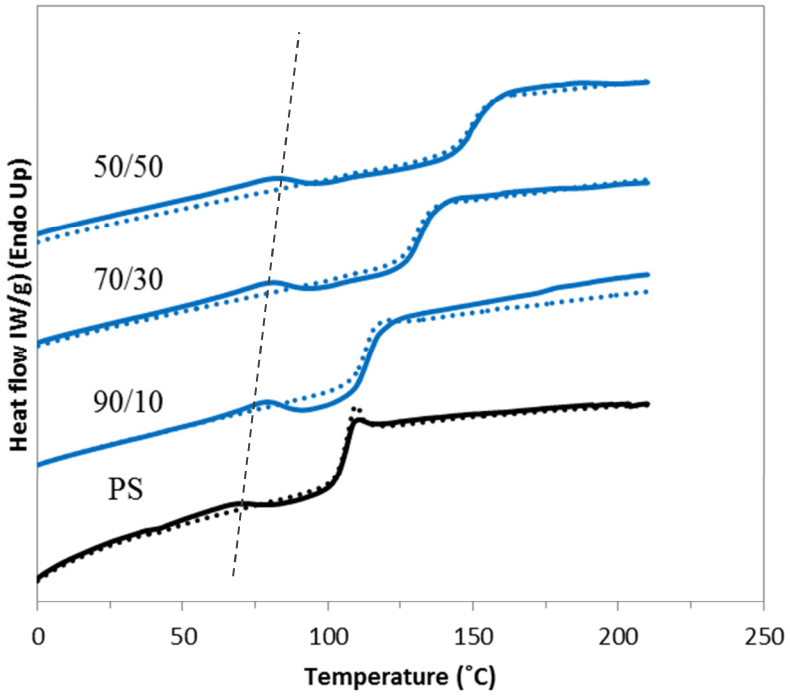

Figure 4.2 DSC thermograms of PS (black) and PS/PPO at different weight fractions (blue). Solid line represents the first heating run and the dotted line the second heating run.

endotherm becomes more pronounced. This effect, however, is less pronounced than the shift in T_g. In fact, the ΔT between T_g and the secondary endotherm increases with increasing PPO fraction. It could be associated not only with the displacement towards the glass transition of pure PPO but also with observation in this work, where ΔT increased as a function of increasing M_w of PS due to faster solidification od the solution resulting in more chain entanglement.

Thus, this system is clearly of interest to investigate in greater detail by TMDSC, in order to closely investigate the thermal events below the glass transition temperature, and to correlate the results to AFM-IR measurements, which would provide deeper knowledge of the structural organization of chains in polymer blends.

APPENDIX

1. SEM images of PS fibers electrospun from different solvents using various molecular weights and concentrations.

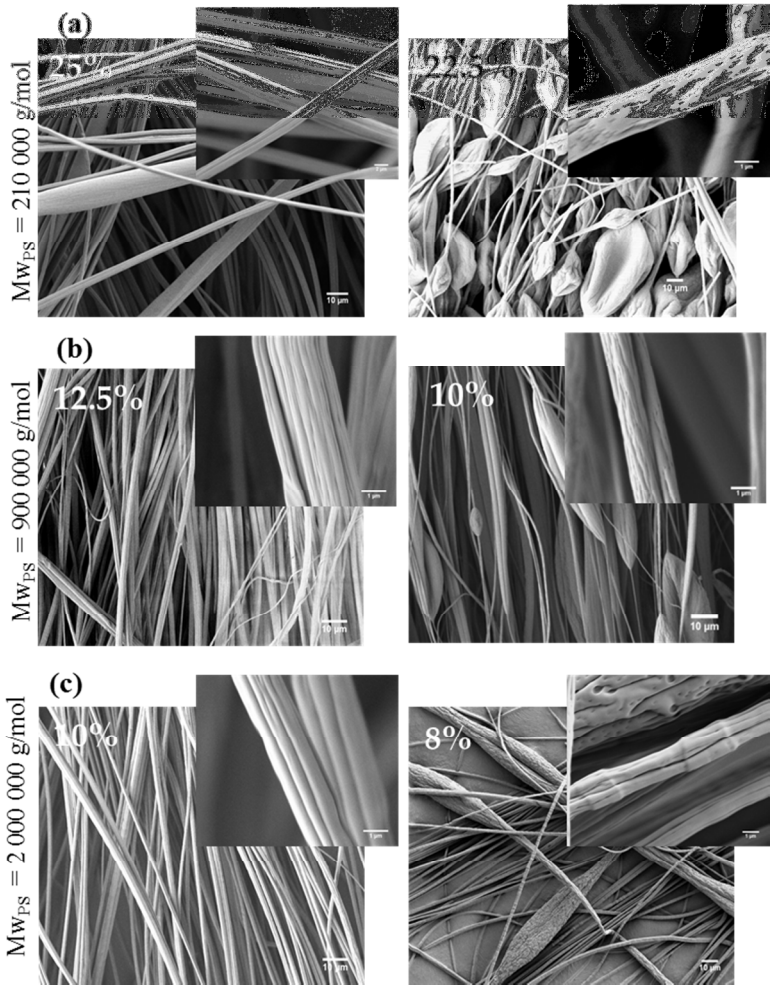

Figure A1 SEM micrographs of PS fibers electrospun from chloroform solutions at three molecular weights, 210 000 g/mol (a), 900 000 g/mol (b) and 2 000 000 g/mol (c) with two concentrations for each molecular weight.

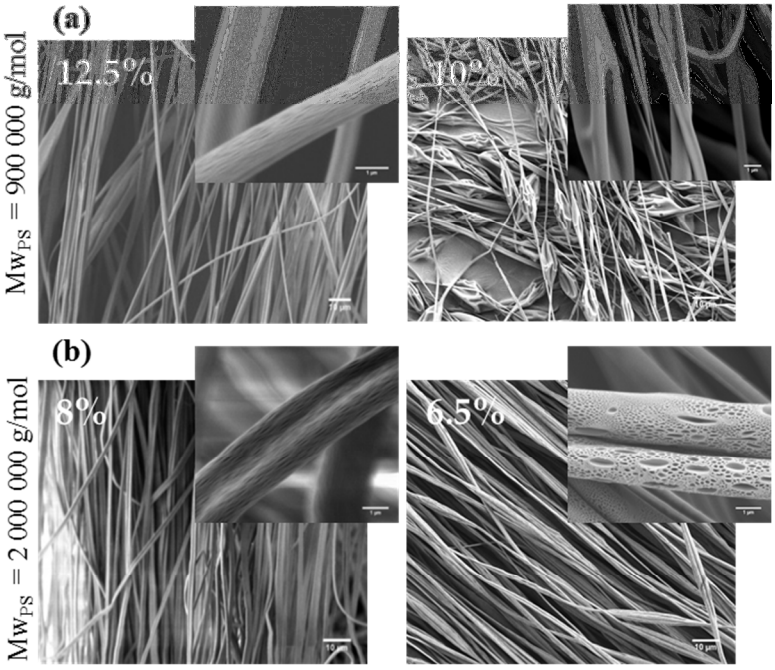

Figure A2 SEM micrographs of PS fibers electrospun from THF solutions at two molecular weights, 900 000 g/mol (a) and 2 000 000 g/mol (b) with two concentrations for each molecular weight.

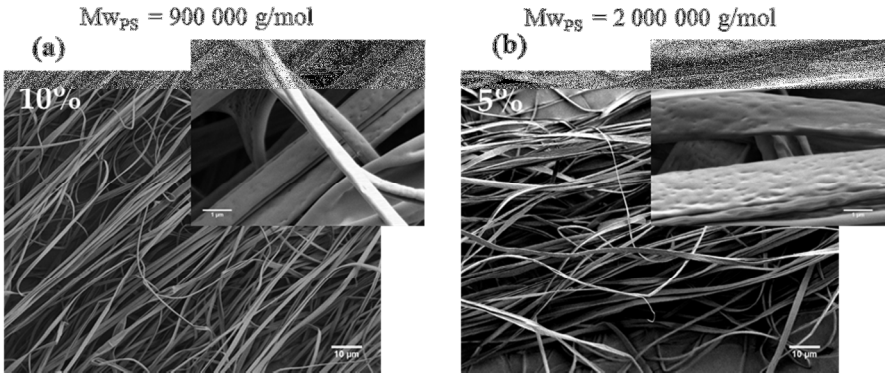

Figure A3 SEM micrographs of PS fibers electrospun from MEK solutions at two molecular weights, 900 000 g/mol (a) and 2 000 000 g/mol (b).

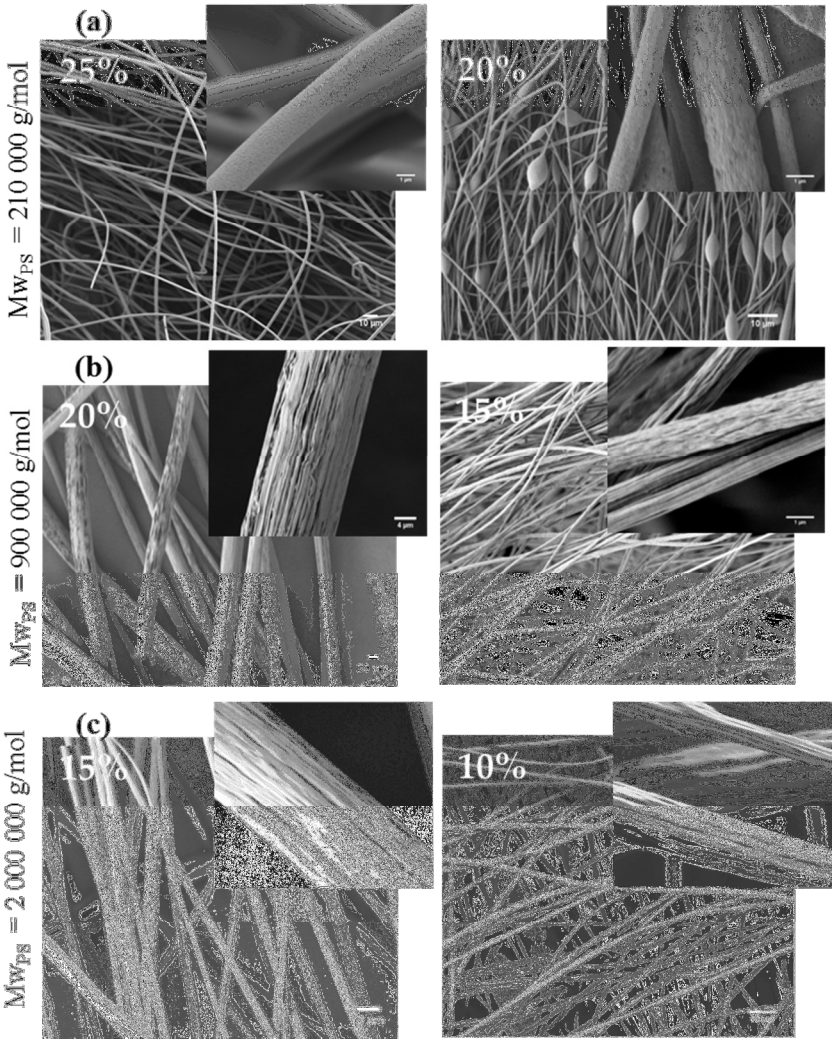

Figure A4 SEM micrographs of PS fibers electrospun from DMF solutions at three molecular weights, 210 000 g/mol (a), 900 000 g/mol (b) and 2 000 000 g/mol (c) with two concentrations for each molecular weight.

2. TMDSC thermograms of PS fibers electrospun from different solvents using various molecular weights and concentrations.

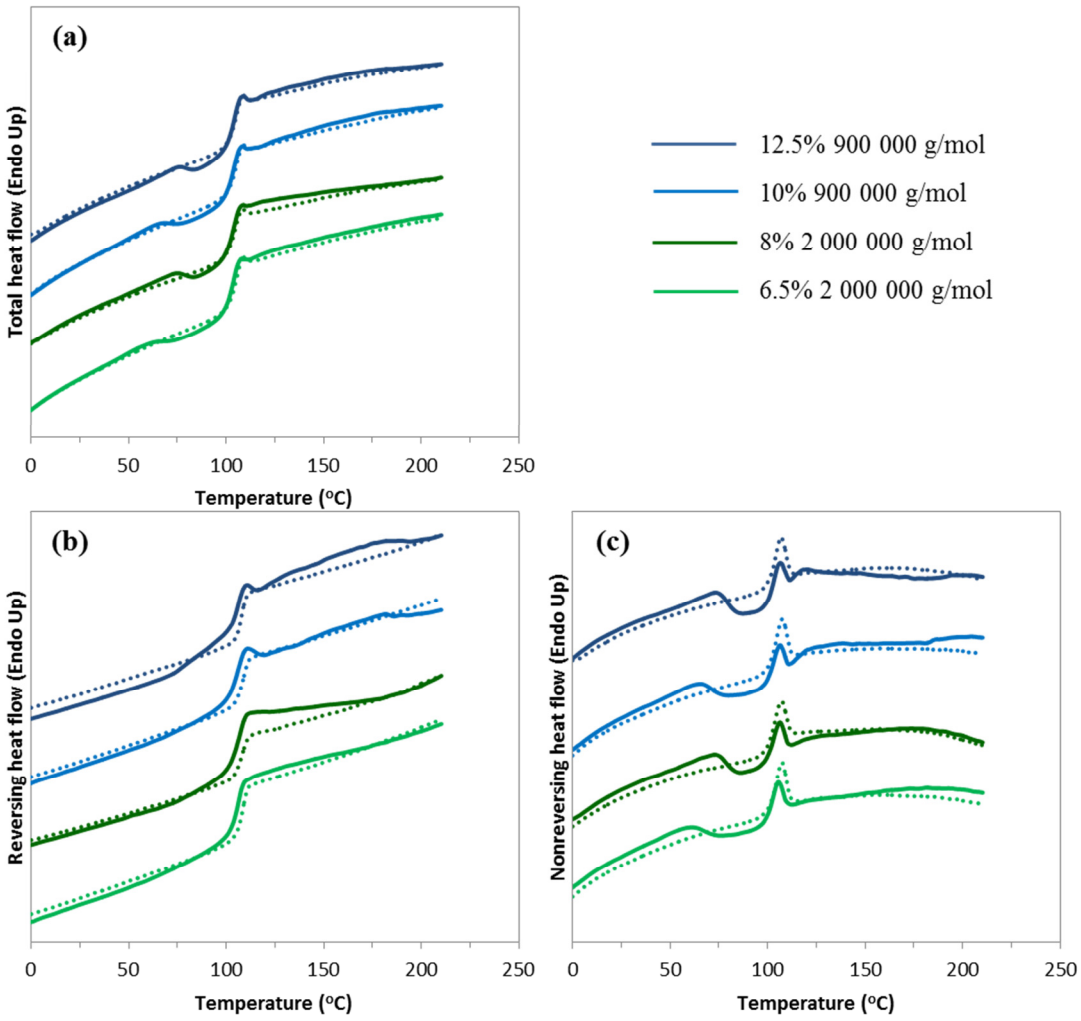

Figure A5 TMDSC thermograms of PS electrospun from 12.5 and 10% from THF solution (M_w = 900 000 g/mol) and 8 and 6.5% (M_w = 2 000 000 g/mol) showing the total (a), reversing (b) and nonreversing (c) heat flows. Solid lines represent the first heating run and dotted lines the second heating run.

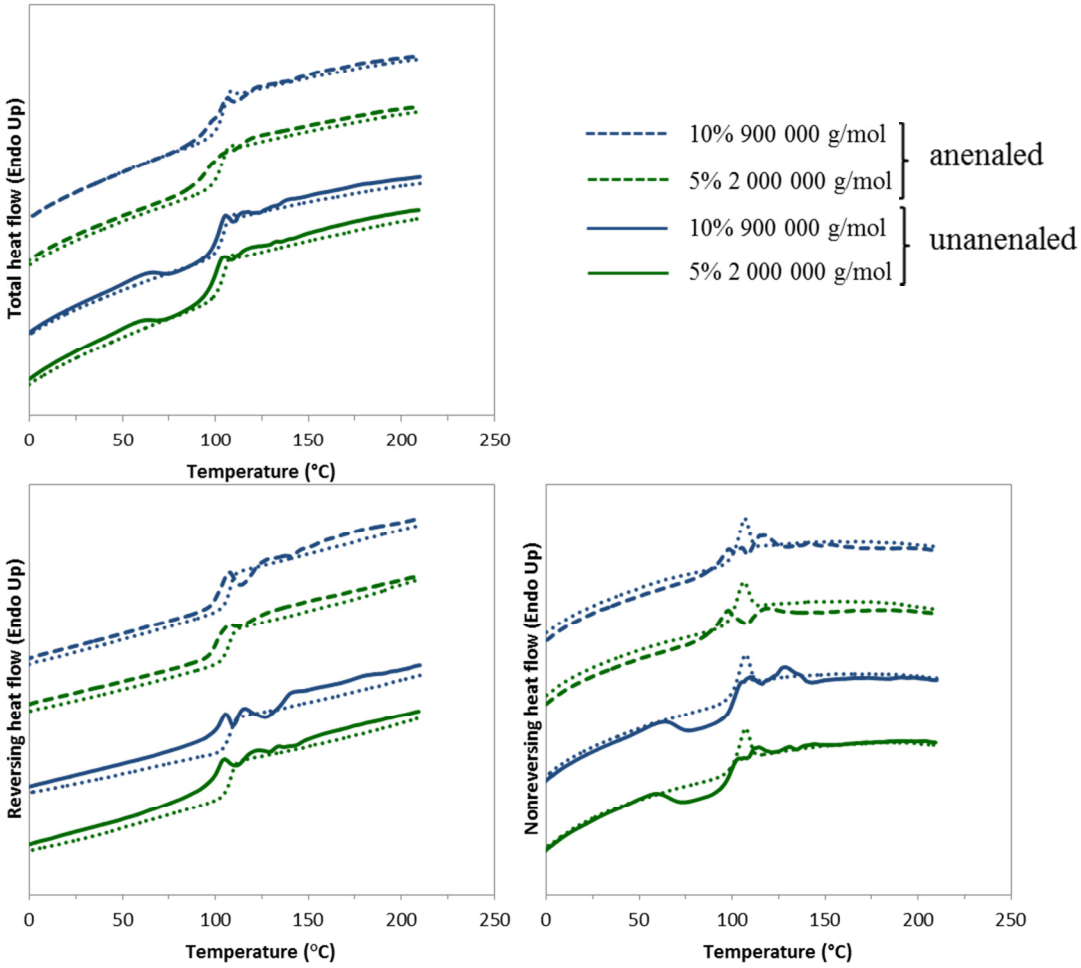

Figure A6 TMDSC thermograms of PS electrospun from 10% from MEK solution (M_w = 900 000 g/mol) and 5% (M_w = 2 000 000 g/mol) showing the total (a), reversing (b) and nonreversing (c) heat flows and the annealed fibers at 75 °C for 3h. Solid lines represent the first heating run, dashed lines represent the annealed fibers and dotted lines the second heating run.

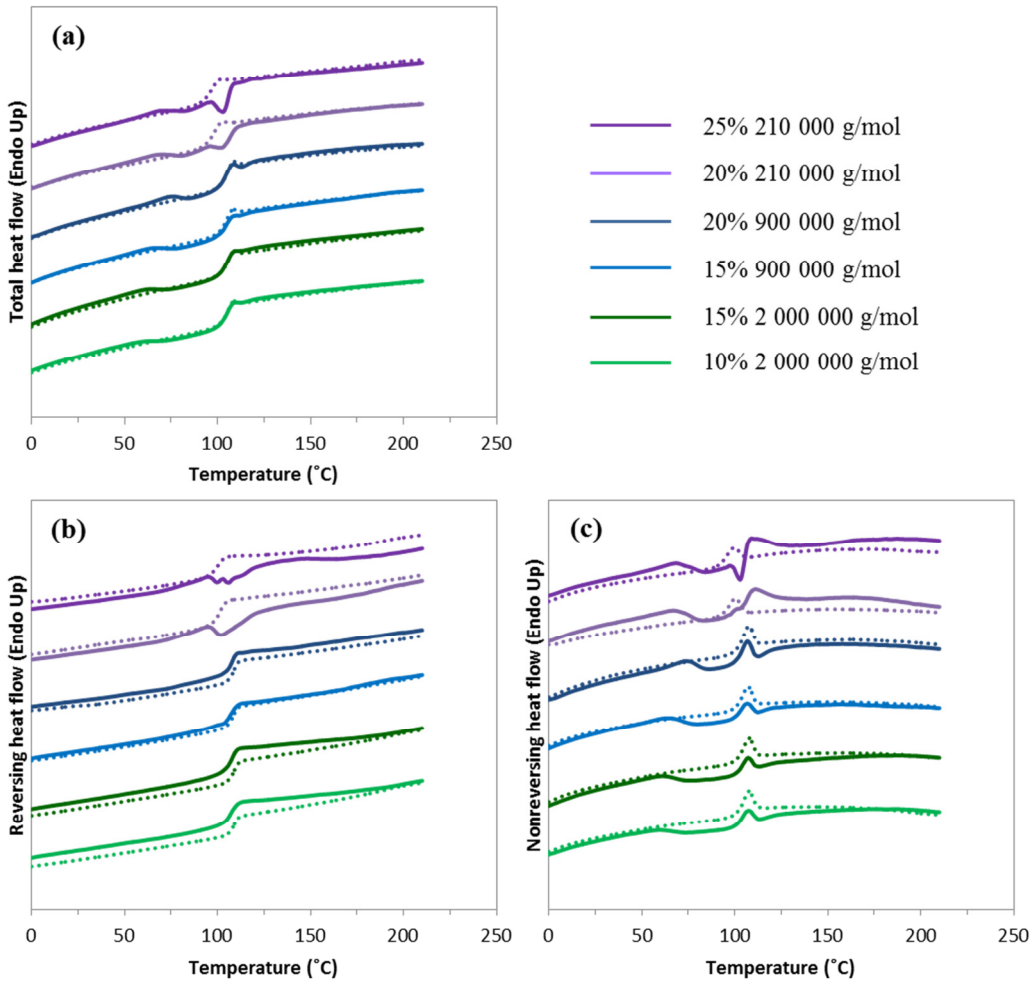

Figure A7 TMDSC thermograms of PS electrospun from 25 and 20% from DMF solution (M_w = 210 000 g/mol), 20 and 15% (Mw = 900 000 g/mol) and 15 and 10% (M_w = 2 000 000 g/mol) showing the total (a), reversing (b) and nonreversing (c) heat flows. Solid lines represent the first heating run and dotted lines the second heating run.

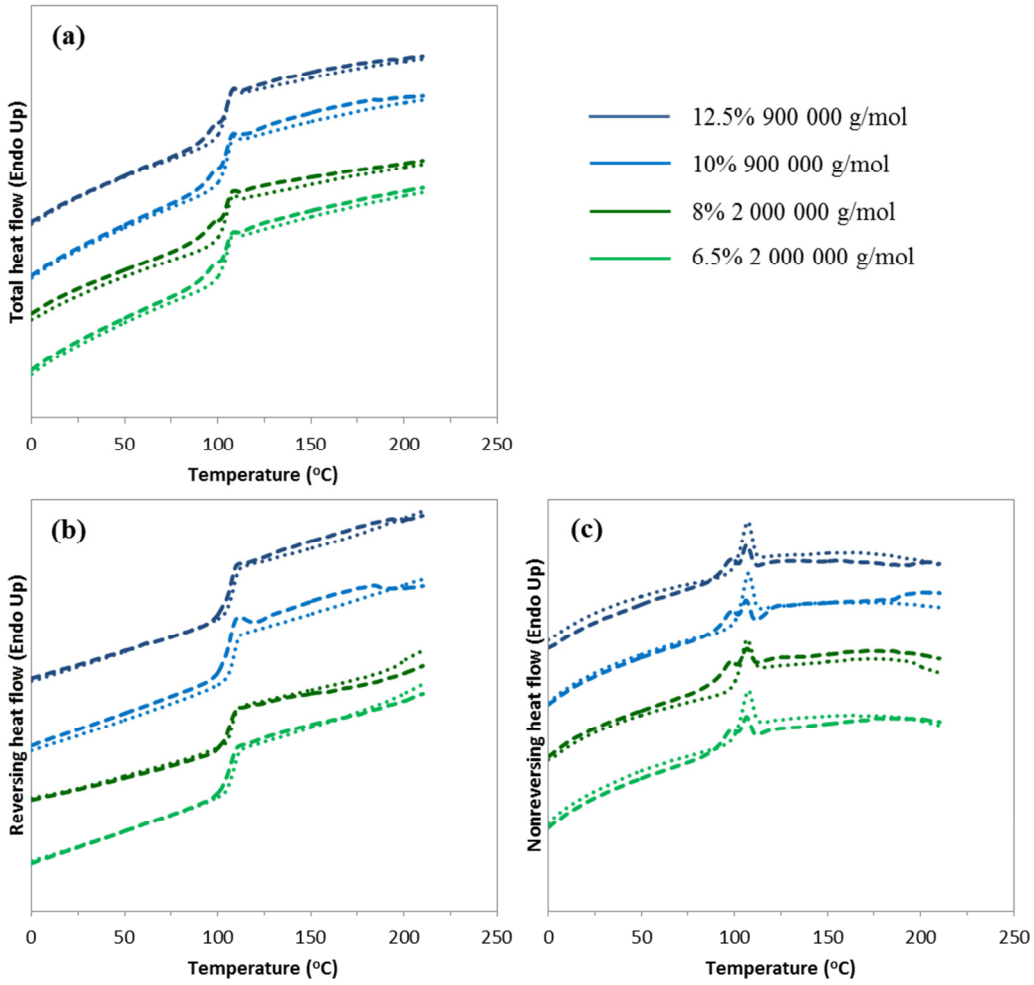

Figure A8 TMDSC thermograms of PS electrospun from 12.5 and 10% from THF solution (Mw = 900 000 g/mol) and 8 and 6.5% (Mw = 2 000 000 g/mol) annealed at 75°C for 3h showing the total (a), reversing (b) and nonreversing (c) heat flows. Dashed lines represent the first heating run and dotted lines the second heating run.

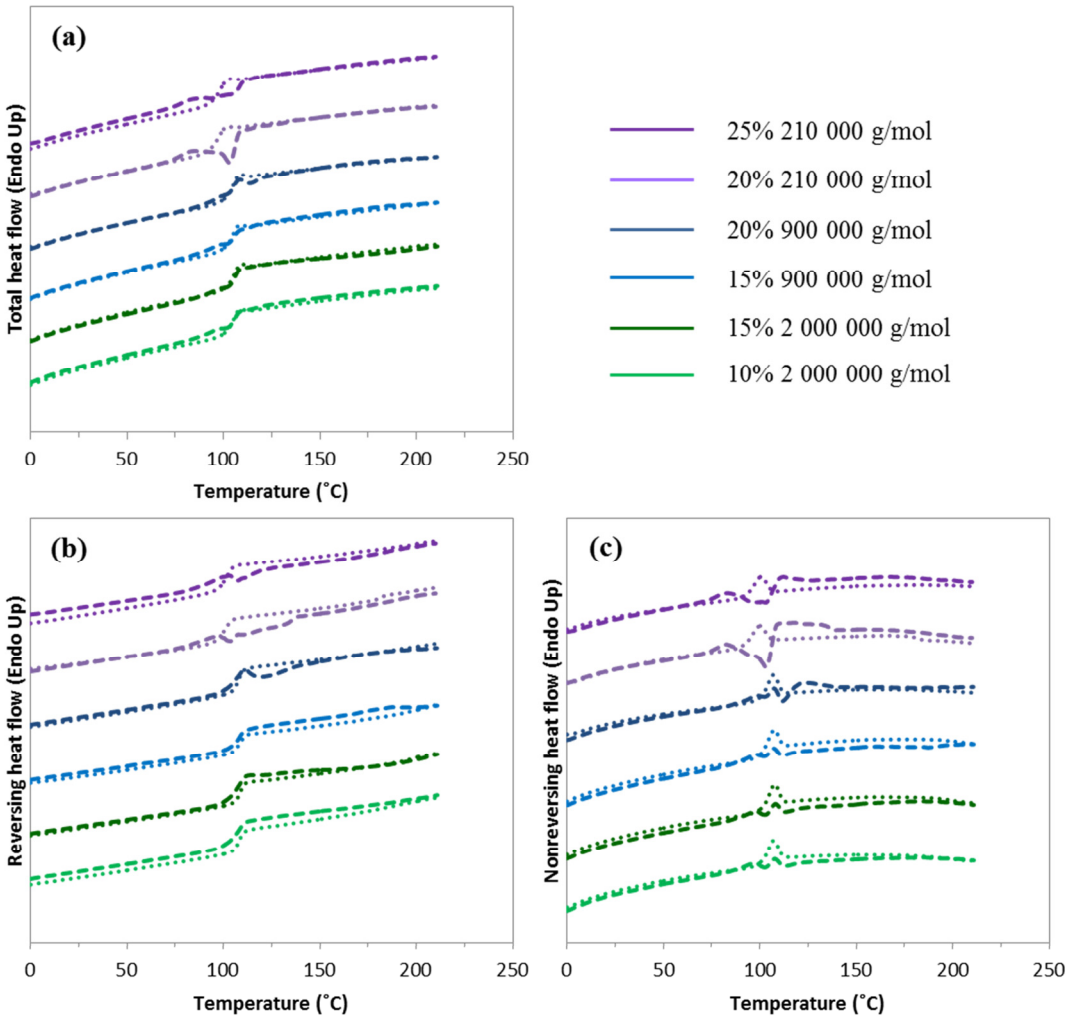

Figure A9 TMDSC thermograms of PS electrospun from 25 and 20% from DMF solution (Mw = 210 000 g/mol), 20 and 15% (Mw = 900 000 g/mol) and 15 and 10% (Mw = 2 000 000 g/mol) annealed at Tg – 30 ˚C for 3h showing the total (a), reversing (b) and nonreversing (c) heat flows. Dashed lines represent the first heating run and dotted lines the second heating run.

REFERENCES

1. Zhang, X., *Fundamentals of Fiber Science*. DEStech Publications, Inc. Lancaster: 2014.

2. Doshi, J.; Reneker, D. H., Electrospinning process and applications of electrospun fibers. *Journal of Electrostatics* **1993**, 1698-1703.

3. Chronakis, I. S., Novel nanocomposites and nanoceramics based on polymer nanofibers using electrospinning process—A review. *J. Mater. Process. Technol.* **2005,** *167* (2-3), 283-293.

4. Bose, G. M., Recherches sur la cause et sur la véritable théorie de l'électricité. *Wittenberg* **1745**, 28-46.

5. Rayleigh, L., XX. On the equilibrium of liquid conducting masses charged with electricity. *Philos. Mag. Series 5* **1882,** *14* (87), 184-186.

6. Cooley, J. F., Apparatus for electrically dispersing fluids. **1902,** *US692631*.

7. Morton, W. J., Method of dispersing fluids. **1902,** *US705691*.

8. Formhals, A., Process and apparatus for preparing artificial threads. **1934,** *US1975504*.

9. Taylor, G., Disintegration of Water Drops in an Electric Field. *Proc. Roy. Soc. Lond. A* **1964,** *280* (1382), 383-397.

10. Taylor, G., Electrically Driven Jets. *Proc. Roy. Soc. Lond. A* **1969,** *313* (1515), 453-475.

11. Zachariades, A. E., et al., High modulus polymers. A novel electrospinning process. *Polym. News* **1995,** *20* (7), 206-207.

12. Darrell, H. R.; Iksoo, C., Nanometre diameter fibres of polymer, produced by electrospinning. *Nanotechnol.* **1996,** *7* (3), 216-223.

13. Frenot, A.; Chronakis, I. S., Polymer nanofibers assembled by electrospinning. *Curr. Opin. Colloid. Interface. Sci.* **2003,** *8* (1), 64-75.

14. Bock, N., et al., Electrospraying, a Reproducible Method for Production of Polymeric Microspheres for Biomedical Applications. *Polymers* **2011,** *3* (4), 131-149.

15. Kenawy, E.-R., et al., Electrospinning of poly(ethylene-co-vinyl alcohol) fibers. *Biomaterials* **2003,** *24* (6), 907-913.

16. Ramakrishna, S., et al., Electrospun nanofibers: solving global issues. *Mater. Today* **2006,** *9* (3), 40-50.

17. Wang, X., et al., Enhancing the Electrospinnability of Low Molecular Weight Polymers Using Small Effective Cross-Linkers. *Macromolecules* **2016,** *49* (3), 891-899.

18. Bognitzki, M., et al., Preparation of fibers with nanoscaled morphologies: Electrospinning of polymer blends. *Polym. Eng. Sci.* **2001,** *41* (6), 982-989.

19. Baptista, A., et al., Electrospun fibers in composite materials for medical applications. . *J. Compos. Biodegrad. Polym.* **2013,** (1), 56-65.

20. Bhardwaj, N.; Kundu, S. C., Electrospinning: A fascinating fiber fabrication technique. *Biotechnol. Adv.* **2010,** *28* (3), 325-347.

21. Bailey, A. G., Electrostatic Spraying of Liquids. *Phys. Unserer Zeit* **1989,** *20* (5), 160-160.

22. Rutledge, G. C.; Fridrikh, S. V., Formation of fibers by electrospinning. *Adv. Drug Deliv. Rev.* **2007,** *59* (14), 1384-1391.

23. Taylor, G., Disintegration of Water Drops in an Electric Field. *Proc. Roy. Soc. Lond. A.* **1964,** *280* (1382), 383-397.

24. Li, Z.; Wang, C., Introduction of Electrospinning. In *One-Dimensional nanostructures: Electrospinning Technique and Unique Nanofibers*, Springer Berlin Heidelberg: Berlin 2013; pp 1-13.

25. Yarin, A. L., et al., Bending instability in electrospinning of nanofibers. *J. Appl. Phys.* **2001,** *89* (5), 3018.

26. Greiner, A.; Wendorff, J. H., Electrospinning: a fascinating method for the preparation of ultrathin fibers. *Angew. Chem. Int. Ed. Engl.* **2007,** *46* (30), 5670-703.

27. McGraw, J. D., et al., Plateau-Rayleigh instability in a torus: formation and breakup of a polymer ring. *Soft Matter* **2010,** *6* (6), 1258-1262.

28. Hohman, M. M., et al., Electrospinning and electrically forced jets. I. Stability theory. *Phys. Fluids* **2001,** *13* (8), 2201.

29. Reneker, D. H.; Yarin, A. L., Electrospinning jets and polymer nanofibers. *Polymer* **2008,** *49* (10), 2387-2425.

30. Koombhongse, S., et al., Flat polymer ribbons and other shapes by electrospinning. *J. Polym. Sci. Part B: Polym. Phys.* **2001,** *39* (21), 2598-2606.

31. Garg, K.; Bowlin, G. L., Electrospinning jets and nanofibrous structures. *Biomicrofluidics* **2011,** *5* (1), 013403.

32. Huebner, A. L.; Chu, H. N., Instability and breakup of charged liquid jets. *J. Fluid Mech.* **2006,** *49* (02), 361.

33. Sill, T. J.; von Recum, H. A., Electrospinning: applications in drug delivery and tissue engineering. *Biomaterials* **2008,** *29* (13), 1989-2006.

34. Ramakrishna, S., *An Introduction to Electrospinning and Nanofibers*. World Scientific: Singapore, 2005.

35. Wannatong, L., et al., Effects of solvents on electrospun polymeric fibers: preliminary study on polystyrene. *Polym. Int.* **2004,** *53* (11), 1851-1859.

36. Wang, X., et al., Needleless Electrospinning of Uniform Nanofibers Using Spiral Coil Spinnerets. *J. Nanomater.* **2012,** *2012*, 1-9.

37. Niu, H. T.; Lin, T., Fiber Generators in Needleless Electrospinning. *J. Nanomater.* **2012,** *2012*, 10-23.

38. Theron, S. A., et al., Multiple jets in electrospinning: experiment and modeling. *Polymer* **2005,** *46* (9), 2889-2899.

39. Ding, B., et al., Fabrication of blend biodegradable nanofibrous nonwoven mats via multi-jet electrospinning. *Polymer* **2004,** *45* (6), 1895-1902.

40. Teo, W. E.; Ramakrishna, S., A review on electrospinning design and nanofibre assemblies. *Nanotechnol.* **2006,** *17* (14), R89-R106.

41. Zander, N., Hierarchically Structured Electrospun Fibers. *Polymers* **2013,** *5* (1), 19.

42. Li, D., et al., Electrospinning of Polymeric and Ceramic Nanofibers as Uniaxially Aligned Arrays. *Nano Lett.* **2003,** *3* (8), 1167-1171.

43. Ki, C. S., et al., Characterization of gelatin nanofiber prepared from gelatin–formic acid solution. *Polymer* **2005,** *46* (14), 5094-5102.

44. Shenoy, S. L., et al., Role of chain entanglements on fiber formation during electrospinning of polymer solutions: good solvent, non-specific polymer–polymer interaction limit. *Polymer* **2005,** *46* (10), 3372-3384.

45. Graessley, W. W., In *The Entanglement Concept in Polymer Rheology*, Springer Berlin Heidelberg: Berlin, 1974; pp 1-179.

46. Gaylord, N. G.; Gibbs, J. H., Physical chemistry of macromolecules. C. TANFORD. Wiley, New York, 1961. *J. Polym. Sci.* **1962,** *62* (173), S22-S23.

47. Rai, P.; Rosen, S. L., An empirical relation between the Mark–Houwink–Sakurada constants. *J. Polym. Sci. B Polym. Phys.* **1997,** *35* (12), 1985-1987.

48. Krause, W. E., et al., Rheology of Sodium Hyaluronate under Physiological Conditions. *Biomacromolecules* **2001,** *2* (1), 65-69.

49. Gupta, P., et al., Electrospinning of linear homopolymers of poly(methyl methacrylate): exploring relationships between fiber formation, viscosity, molecular weight and concentration in a good solvent. *Polymer* **2005,** *46* (13), 4799-4810.

50. Eda, G.; Shivkumar, S., Bead structure variations during electrospinning of polystyrene. *J. Mater. Sci.* **2006,** *41* (17), 5704-5708.

51. Li, Z.; Wang, C., Effects of Working Parameters on Electrospinning. In *One-Dimensional nanostructures: Electrospinning Technique and Unique Nanofibers*, Springer Berlin Heidelberg: Berlin, 2013; pp 15-28.

52. Zong, X., et al., Structure and process relationship of electrospun bioabsorbable nanofiber membranes. *Polymer* **2002,** *43* (16), 4403-4412.

53. Haghi, A. K.; Akbari, M., Trends in electrospinning of natural nanofibers. *Phys. Status Solidi A* **2007,** *204* (6), 1830-1834.

54. Dumitriu, S.; Popa, V. I., *Polymeric Biomaterials: Structure and function*. CRC Press: Boca Raton, 2013.

55. Hayati, I., et al., Investigations into the mechanisms of electrohydrodynamic spraying of liquids: I. Effect of electric field and the environment on pendant drops and factors affecting the formation of stable jets and atomization. *J. Colloid Interface Sci.* **1987,** *117* (1), 205-221.

56. Chen, J.-P., et al., Electrospun collagen/chitosan nanofibrous membrane as wound dressing. *Colloids Surf., A* **2008,** *313–314*, 183-188.

57. Kim, T. G., et al., Controlled protein release from electrospun biodegradable fiber mesh composed of poly(ε-caprolactone) and poly(ethylene oxide). *Int. J. Pharm.* **2007,** *338* (1–2), 276-283.

58. Ma, Z., et al., Surface engineering of electrospun polyethylene terephthalate (PET) nanofibers towards development of a new material for blood vessel engineering. *Biomaterials* **2005,** *26* (15), 2527-2536.

59. Maretschek, S., et al., Electrospun biodegradable nanofiber nonwovens for controlled release of proteins. *J. Controlled Release* **2008,** *127* (2), 180-187.

60. Verreck, G., et al., Incorporation of drugs in an amorphous state into electrospun nanofibers composed of a water-insoluble, nonbiodegradable polymer. *J. Controlled Release* **2003,** *92* (3), 349-360.

61. Pillay, V., et al., A Review of the Effect of Processing Variables on the Fabrication of Electrospun Nanofibers for Drug Delivery Applications. *J. Nanomater.* **2013,** *2013*, 22-44.

62. Gibson, P., et al., Transport properties of porous membranes based on electrospun nanofibers. *Colloids Surf., A* **2001,** *187–188*, 469-481.

63. Li, X., et al., Electrospun Superhydrophobic Organic/Inorganic Composite Nanofibrous Membranes for Membrane Distillation. *ACS Appl. Mater. Interfaces* **2015,** *7* (39), 21919-21930.

64. Albetran, H., et al., Characterization and optimization of electrospun TiO2/PVP nanofibers using Taguchi design of experiment method. *J. Asian Ceram. Soc.* **2015,** *3* (3), 292-300.

65. Both Engel, A., et al., Electrospun Carbon Fibers: Promising Electrode Material for Abiotic and Enzymatic Catalysis. *J. Phys. Chem. C* **2015,** *119* (29), 16724-16733.

66. Canesi, E. V., et al., n-Type Semiconducting Polymer Fibers. *ACS Macro Lett.* **2012,** *1* (3), 366-369.

67. Miao, J., et al., Electrospinning of Nanomaterials and Applications in Electronic Components and Devices. *J. Nanosci. Nanotech.* **2010,** *10* (9), 5507-5519.

68. Wenguo, C., et al., Electrospun nanofibrous materials for tissue engineering and drug delivery. *Sci. Technol. Adv. Mater.* **2010,** *11* (1), 014108-014119.

69. Salehi, S., et al., Characterization of structural, mechanical and nano-mechanical properties of electrospun PGS/PCL fibers. *RSC Adv.* **2014,** *4* (33), 16951-16957.

70. Kim, K., et al., Incorporation and controlled release of a hydrophilic antibiotic using poly(lactide-co-glycolide)-based electrospun nanofibrous scaffolds. *J. Controlled Release* **2004,** *98* (1), 47-56.

71. Nasouri, K., et al., Thermodynamic Studies on Polyvinylpyrrolidone Solution Systems Used for Fabrication of Electrospun Nanostructures: Effects of the Solvent. *Adv. Polym. Techn.* **2015,** *34* (3), 21495-21513.

72. Luo, C. J., et al., Mapping the Influence of Solubility and Dielectric Constant on Electrospinning Polycaprolactone Solutions. *Macromolecules* **2012,** *45* (11), 4669-4680.

73. Wu, X.-F., et al., Modeling of solvent evaporation from polymer jets in electrospinning. *Appl. Phys. Lett.* **2011,** *98* (22), 223108-223111.

74. Reneker, D. H., et al., Electrospinning of Nanofibers from Polymer Solutions and Melts. In *Adv. Appl. Mech.*, Hassan, A.; Erik van der, G., Eds. Elsevier: 2007; Vol. Volume 41, pp 43-346.

75. Pisignano, D., et al., *Polymer Nanofibers: Building Blocks for Nanotechnology*. Royal Society of Chemistry: Cambridge, 2013.

76. Casper, C. L., et al., Controlling Surface Morphology of Electrospun Polystyrene Fibers: Effect of Humidity and Molecular Weight in the Electrospinning Process. *Macromolecules* **2004,** *37* (2), 573-578.

77. Demir, M. M., Investigation on glassy skin formation of porous polystyrene fibers electrospun from DMF. *Express Polym. Lett.* **2009,** *4* (1), 2-8.

78. Richard-Lacroix, M.; Pellerin, C., Molecular Orientation in Electrospun Fibers: From Mats to Single Fibers. *Macromolecules* **2013,** *46* (24), 9473-9493.

79. Ritchie, R. O., The conflicts between strength and toughness. *Nat. Mater.* **2011,** *10* (11), 817-822.

80. Papkov, D., et al., Simultaneously strong and tough ultrafine continuous nanofibers. *ACS Nano* **2013,** *7* (4), 3324-31.

81. Ji, Y., et al., Confinement-induced super strong PS/MWNT composite nanofibers. *Europh. Lett.* **2008,** *84* (5), 56002-56008.

82. Gururajan, G., et al., Molecular orientation evolution and solvent evaporation during electrospinning of atactic polystyrene using real-time Raman spectroscopy. *Appl. Spectrosc.* **2011,** *65* (8), 858-865.

83. Richard-Lacroix, M.; Pellerin, C., Orientation and Partial Disentanglement in Individual Electrospun Fibers: Diameter Dependence and Correlation with Mechanical Properties. *Macromolecules* **2015,** *48* (13), 4511-4519.

84. Greenfeld, I., et al., Stiffness, Strength, and Toughness of Electrospun Nanofibers: Effect of Flow-Induced Molecular Orientation. *Macromolecules* **2016,** *49* (17), 6518-6530.

85. Camposeo, A., et al., Local mechanical properties of electrospun fibers correlate to their internal nanostructure. *Nano Lett.* **2013,** *13* (11), 5056-62.

86. Stachewicz, U., et al., Size dependent mechanical properties of electrospun polymer fibers from a composite structure. *Polymer* **2012,** *53* (22), 5132-5137.

87. Dhanalakshmi, M.; Jog, P., Preparation and characterization of electrospun fibers of Nylon 11. *Express Polym. Lett.* **2008,** *2* (8), 540-545.

88. Wang, W.; Barber, A. H., Measurement of size-dependent glass transition temperature in electrospun polymer fibers using AFM nanomechanical testing. *J. Polym. Sci. B Polym. Phys.* **2012,** *50* (8), 546-551.

89. Baji, A., et al., Effect of fiber diameter on the deformation behavior of self-assembled carbon nanotube reinforced electrospun Polyamide 6,6 fibers. *Mater. Sci. Engineer. A* **2011,** *528* (21), 6565-6572.

90. Ji, Y., et al., Structure and Nanomechanical Characterization of Electrospun PS/Clay Nanocomposite Fibers. *Langmuir* **2006,** *22* (3), 1321-1328.

91. Ma, J., et al., Thermal conductivity of electrospun polyethylene nanofibers. *Nanoscale* **2015,** *7* (40), 16899-908.

92. Zhong, Z., et al., Structure-induced enhancement of thermal conductivities in electrospun polymer nanofibers. *Nanoscale* **2014,** *6* (14), 8283-91.

93. Lee, K. H., et al., The change of bead morphology formed on electrospun polystyrene fibers. *Polymer* **2003,** *44* (14), 4029-4034.

94. Wang, C., et al., Scaling Laws in Electrospinning of Polystyrene Solutions. *Macromolecules* **2006,** *39* (22), 7662-7672.

95. Liu, W., et al., Electrospinning of Grooved Polystyrene Fibers: Effect of Solvent Systems. *Nanoscale Res. Lett.* **2015,** *10*, 237-247.

96. Fong, H., et al., Beaded nanofibers formed during electrospinning. *Polymer* **1999,** *40* (16), 4585-4592.

97. Jarusuwannapoom, T., et al., Effect of solvents on electro-spinnability of polystyrene solutions and morphological appearance of resulting electrospun polystyrene fibers. *Europ. Polym. J.* **2005,** *41* (3), 409-421.

98. Pai, C.-L., et al., Morphology of Porous and Wrinkled Fibers of Polystyrene Electrospun from Dimethylformamide. *Macromolecules* **2009,** *42* (6), 2102-2114.

99. Megelski, S., et al., Micro- and Nanostructured Surface Morphology on Electrospun Polymer Fibers. *Macromolecules* **2002,** *35* (22), 8456-8466.

100. Valiquette, D.; Pellerin, C., Miscible and Core−Sheath PS/PVME Fibers by Electrospinning. *Macromolecules* **2011,** *44* (8), 2838-2843.

101. McGrath, K. J., et al., Chain configuration of polystyrene arising from freeze-drying dilute solutions. *Macromolecules* **1993,** *26* (22), 6127-6128.

102. Sasaki, T., et al., Fourier transform infra-red study on the structure of freeze-dried atactic polystyrene from dilute solutions. *Polymer* **1997,** *38* (18), 4765-4768.

103. Tretinnikov, O. N.; Zbankov, R. G., FTIR Spectroscopic Evidence of Lowered Chain Interpenetration in Thin Polymer Films. *Macromolecules* **2004,** *37* (10), 3543-3545.

104. Greenfeld, I., et al., Polymer dynamics in semidilute solution during electrospinning: a simple model and experimental observations. *Phys. Rev. E Stat. Nonlin. Soft Matter. Phys.* **2011,** *84* (4 Pt 1), 041806-041821.

105. Guenthner, A. J., et al., Dynamics of Hollow Nanofiber Formation During Solidification Subjected to Solvent Evaporation. *Macromol. Theory Simul.* **2006,** *15* (1), 87-93.

106. Richard-Lacroix, M.; Pellerin, C., Partial Disentanglement in Continuous Polystyrene Electrospun Fibers. *Macromolecules* **2015,** *48* (1), 37-42.

107. Verdonck, E., et al., A discussion of the principles and applications of Modulated Temperature DSC (MTDSC). *Int. J. Pharm.* **1999,** *192* (1), 3-20.

108. Simon, S. L., Temperature-modulated differential scanning calorimetry: theory and application. *Thermochim. Acta* **2001,** *374* (1), 55-71.

109. Dazzi, A., et al., AFM-IR: combining atomic force microscopy and infrared spectroscopy for nanoscale chemical characterization. *Appl. Spectrosc.* **2012,** *66* (12), 1365-1384.

110. Gabbott, P., A Practical Introduction to Differential Scanning Calorimetry. In *Principles and Applications of Thermal Analysis*, Blackwell Publishing Ltd: Hoboken, 2008; pp 1-50.

111. Hutchinson, J. M., Relaxation processes and physical aging. In *The Physics of Glassy Polymers*, Haward, R. N.; Young, R. J., Eds. Springer Netherlands: Dordrecht, 1997; pp 85-153.

112. Heijboer, J., Secondary Loss Peaks in Glassy Amorphous Polymers. *Int. J. Polym. Mater.* **1977,** *6* (1-2), 11-37.

113. Prest, W. M.; Roberts, F. J., Enthalpy Recovery in Pressure-Vitrified and Mechanically Stressed Polymeric Glasses. *Ann. N. Y. Acad. Sci.* **1981,** *371* (1), 67-86.

114. Petrie, S. E. B., Thermal behavior of annealed organic glasses. *J. Polym. Sci. A-2: Polym. Phys.* **1972,** *10* (7), 1255-1272.

115. Berens, A. R.; Hodge, I. M., Effect of Annealing and Prior History on Enthalpy Relaxation in Glassy Polymers. 1. Experimental Study of Poly(vinyl chloride). *Macromolecules* **1982,** *15 (3)*, 756-761.

116. Brown, I. G., et al., Glass transition and thermodynamic state of densified polymeric glasses. *Polymer* **1978,** *19* (6), 659-663.

117. Yourtee, J. B.; Cooper, S. L., Properties of densified amorphous polystyrene. *J. Appl. Polym. Sci.* **1974,** *18* (3), 897-912.

118. Hodge, I. M.; Huvard, G. S., Effects of annealing and prior history on enthalpy relaxation in glassy polymers. 3. Experimental and modeling studies of polystyrene. *Macromolecules* **1983,** *16* (3), 371-375.

119. Krause, S., et al., Glass temperatures of some acrylic polymers. *J. Polym. Sci. A General Papers* **1965,** *3* (10), 3573-3586.

120. Fox, T. G.; Flory, P. J., Second-Order Transition Temperatures and Related Properties of Polystyrene. I. Influence of Molecular Weight. *J. Appl. Phys.* **1950,** *21* (6), 581-593.

121. Markovitz, H., Thomas G. Fox 1921–1977. *Rheol. Acta* **1978,** *17* (3), 207-209.

122. Boyer, R. F., The Relation of Transition Temperatures to Chemical Structure in High Polymers. *Rubber Chem. Technol.* **1963,** *36* (5), 1303-1421.

123. Pellerin, C., et al., Influence of the Reference Temperature on the Orientation and Relaxation of Miscible Polystyrene/Poly(vinyl methyl ether) Blends. *Macromolecules* **2003,** *36* (1), 153-161.

124. Clark, J. N., et al., Small-angle neutron scattering studies of phase equilibria in blends of deuterated poly(methyl methacrylate) with solution chlorinated polyethylene. *Macromolecules* **1993,** *26* (22), 5897-5907.

125. Brunacci, A., et al., Enthalpy relaxation in glassy polystyrenes: 1. *Polymer* **1997,** *38* (4), 865-870.

126. Turnbull, D.; Cohen, M. H., Free-Volume Model of the Amorphous Phase: Glass Transition. *J. Chem. Phys.* **1961,** *34* (1), 120-125.

127. Agrawal, A., Effect of temperature and molecular weight on enthalpy relaxation in polystyrene. *J. Polym. Sci. B Polym. Phys.* **1989,** *27* (7), 1449-1461.

128. Tsen, W. C.; Chuang, F. S., Phase transition and domain morphology of siloxane-containing hard-segmented polyurethane copolymers. *J. Appl. Polym. Sci.* **2006,** *101* (6), 4242-4252.

129. Fraga, F., et al., Kinetic analysis of relaxation process for the epoxy network diglycidyl ether of bisphenol A/m-xylylenediamine. *J. Appl. Polym. Sci.* **2005,** *96* (5), 1591-1595.

130. Gong, L., et al., Discovery of β-Form Crystal Structure in Electrospun Poly[(R)-3-hydroxybutyrate-co-(R)-3-hydroxyhexanoate] (PHBHx) Nanofibers: From Fiber Mats to Single Fibers. *Macromolecules* **2015,** *48* (17), 6197-6205.

131. Sperling, L. H., Crosslinked Polymers and Rubber Elasticity. In *Introduction to Physical Polymer Science*, John Wiley & Sons, Inc.: Hoboken, 2005; pp 427-505.

132. Onogi, S., et al., Rheological Properties of Anionic Polystyrenes. I. Dynamic Viscoelasticity of Narrow-Distribution Polystyrenes. *Macromolecules* **1970,** *3* (2), 109-116.

133. Nielsen, L. E., *Mechanical Properties of Polymers and Composites*. Marcel Dekker Incorporated: New York, 1974; Vol. 1.

134. Liu, W., et al., Tailoring the grooved texture of electrospun polystyrene nanofibers by controlling the solvent system and relative humidity. *Nanoscale Res. Lett.* **2014,** *9* (1), 350-350.

135. Liu, W., et al., Electrospinning of Grooved Polystyrene Fibers: Effect of Solvent Systems. *Nanoscale Res. Lett.* **2015,** *10* (1), 1-10.

136. Huang, C., et al., Needleless Electrospinning of Polystyrene Fibers with an Oriented Surface Line Texture. *J. Nanomater.* **2012,** *2012*, 1-7.

137. Nezarati, R. M., et al., Effects of humidity and solution viscosity on electrospun fiber morphology. *Tissue Eng. C Methods* **2013,** *19* (10), 810-819.

138. Breath Figures Caught in Polymers. *Science* **2001,** *292* (5514), 1-9.

139. Lu, P.; Xia, Y., Maneuvering the internal porosity and surface morphology of electrospun polystyrene yarns by controlling the solvent and relative humidity. *Langmuir* **2013,** *29* (23), 7070-7078.

140. Celebioglu, A.; Uyar, T., Electrospun porous cellulose acetate fibers from volatile solvent mixture. *Mater. Lett.* **2011,** *65* (14), 2291-2294.

141. Lefebvre, D., et al., Fourier transform infra-red study of uniaxially oriented poly(2,6-dimethyl 1,4-phenylene oxide)-atactic polystyrene blends. *Polymer* **1981,** *22* (12), 1616-1620.